9th Croatian-Slovenian-Serbian Symposium on Zeolites

PROCEEDINGS

Editors

Ivona Nuić
Matjaž Mazaj
Aleksandra Daković

Split, 2021

Proceedings of the 9th Croatian-Slovenian-Serbian Symposium on Zeolites
Proceedings of the 9th Slovenian-Serbian-Croatian Symposium on Zeolites
Proceedings of the 9th Serbian-Croatian-Slovenian Symposium on Zeolites

Publisher
Croatian Zeolite Association (CROZA)

Editors

Ivona Nuić
Matjaž Mazaj
Aleksandra Daković

Split, 2021

PROCEEDINGS OF THE
9th CROATIAN-SLOVENIAN-SERBIAN
SYMPOSIUM ON ZEOLITES

September 23-25, 2021
Split, Croatia

Organizers
CROATIAN ZEOLITE ASSOCIATION
SLOVENIAN ZEOLITE ASSOCIATION
SERBIAN ZEOLITE ASSOCIATION

Under the auspices of
Federation of European Zeolite Association (FEZA)

All articles in the Proceedings were reviewed.

Organizing Committee

Chairs:

Assis. Prof. Ivona Nuić, Faculty of Chemistry and Technology, Split, Croatia
Prof. Jasna Hrenović, Faculty of Science, Zagreb, Croatia

Members:

Prof. Nediljka Vukojević Medvidović, Faculty of Chemistry and Technology, Split, Croatia
Prof. Marina Trgo, Faculty of Chemistry and Technology, Split, Croatia
Assis. Prof. Mario Nikola Mužek, Faculty of Chemistry and Technology, Split, Croatia
Prof. Sandra Svilović, Faculty of Chemistry and Technology, Split, Croatia
PhD Josip Bronić, Ruđer Bošković Institute, Zagreb, Croatia
Prof. Nataša Zabukovec Logar, National Institute of Chemistry, Ljubljana, Slovenia
Prof. Nataša Novak Tušar, National Institute of Chemistry, Ljubljana, Slovenia
Assis. Prof. Jelena Dikić, Innovation Center of the Faculty of Technology and Metallurgy, Belgrade, Serbia
Assoc. Prof. Vladislav Rac, Faculty of Agriculture, Belgrade, Serbia

Scientific and Program Committee

Prof. Darko Tibljaš, Faculty of Science, Zagreb, Croatia
Assoc. Prof. Tomislav Ivanković, Faculty of Science, Zagreb, Croatia
PhD Tatjana Antonić Jelić, Ruđer Bošković Institute, Zagreb, Croatia
PhD Sanja Bosnar, Ruđer Bošković Institute, Zagreb, Croatia
Prof. Vesna Tomašić, Faculty of Chemical Engineering and Technology, Zagreb, Croatia
Prof. Xuesen Du, Chongqing University, China
Prof. Qiang Wang, Beijing Forestry University, China
PhD Matjaž Mazaj, National Institute of Chemistry, Ljubljana, Slovenia
PhD Petar Djinović, National Institute of Chemistry, Ljubljana, Slovenia
PhD Andraž Krajnc, National Institute of Chemistry, Ljubljana, Slovenia
PhD Aleksandra Daković, Institute for Technology of Nuclear and Other Mineral Raw Materials, Belgrade, Serbia
Prof. Ljiljana Damjanović-Vasilić, Faculty of Physical Chemistry, Belgrade, Serbia
Prof. Vladimir Simić, Faculty of Mining and Geology, Belgrade, Serbia

This page intentionally left blank.

9th Croatian-Slovenian-Serbian Symposium on Zeolites

23rd-25th September 2021, Split, Croatia

Time	**Thursday, 23. 09. 2021**	Time	**Friday, 24. 09. 2021**	Time	**Saturday, 25. 09. 2021**
8:30-9:00	Registration				
9:00-9:30	Opening				
	chair Bronić		*chair Rakić*		*chair Vukojević Medvidović*
9:30-10:15	PL Mintova	9:00-9:45	PL Giordano	9:00-9:45	PL Migliori
10:15-10:45	IL Byrne	9:45-10:15	IL Žerjav	9:45-10:15	IL Ugrina
		10:15-10:30	OP Kalebić	10:15-10:30	OP Labtim d.o.o.
10:45-11:15	☕ *Coffee break*	10:30-11:00	☕ *Coffee break*	10:30-10:45	CP Jasika d.o.o.
	chair Novak Tušar		*chair Bosnar*	10:45-11:00	CP Alumina d.o.o.
11:15-11:20	CP Labtim d.o.o.	11:00-11:15	OP Hrenović	11:00-11:15	Closing remarks and *Coffee break* ☕
11:20-11:35	OP Bosnar	11:15-11:30	OP Ivanković		
11:35-11:50	OP Škrjanc	11:30-11:45	OP Dikić		
11:50-12:05	OP Medak	11:45-12:00	OP Vukojević Medvidović		
12:05-12:20	OP Palčić	12:00-12:15	OP Vukojević Medvidović		
12:20-12:35	OP Rac	12:15-12:30	OP Mužek		
		12:30-12:45	OP Nuić		
12:35-14:00	🍽 *Lunch*	12:45-14:00	🍽 *Lunch*		
	chair Zabukovec Logar				
14:00-14:45	PL Valtchev				
14:45-15:15	IL Markiv				
15:15-15:30	OP Vu				
15:30-15:45	☕ *Coffee break*				
	chair Trgo				
15:45-16:00	OP Stojanović				
16:00-16:15	OP Pavlović				
16:15-16:30	OP Smiljanić				
16:30-16:45	OP Dimitrijević	16:00-18:00	*Diocletian Palace walking tour*		
16:45-17:00	OP Novaković	19:00-	*Conference dinner*		
17:00-17:15	OP Dib				

PL = plenary lecture
IL = invited lecture
OP = oral presentation
CP = company presentation

Boris Subotić: 75th anniversary of life and 52 years of scientific work

Dr. sc. Boris Subotić is a retired senior scientist at the Ruđer Bošković Institute. He is a well-known and internationally recognized scientist in the field of microporous and mesoporous materials, especially zeolites.

Dr. sc. Boris Subotić was born on December 02, 1946. in Dugo Selo, near Zagreb, Croatia. He achieved the BS degree at the Faculty of Science, University of Zagreb, and was employed in the Laboratory for Colloid Chemisty of the Ruđer Bošković Institute in 1969. In 1976 he obtained the Ph.D degree in Chemistry at the Ruđer Bošković Institute and the University of Zagreb. In 1988 he became a co-founder and member of the Laboratory for the Synthesis of New Materials, and from 1995 to 2011 he was the head of the same laboratory. He was also a member of the Institute’s Scientific Council for a long time, and from 2005 to 2009 he was a member of director's advisory team and President of the Institute’s Commission for Innovation. He was also co-founder of the Croatian Zeolite Association and the first president of the Association.

Dr. sc. Boris Subotić

During his long scientific work, he established the research of zeolites at the Ruđer Bošković Institute (synthesis, characterization and application) with a special emphasis to investigation of mechanisms of crystallization and transformation of zeolites. In this context, he established theoretical basis of the model of autocatalytic nucleation of zeolites, and together with co-workers, experimentally proved validity and significance of the model. In the meantime, together with the coworkers, he developed the model of crystallization of zeolites based on the population balance all relevant sub-processes (mechanism and kinetics of precipitation amorphous aluminosilicate precursor, its dissolution as well as nucleation and crystal growth of zeolites). The results of more recent investigations showed that crystallization of zeolites in heterogeneous systems (aluminosilicate hydrogels) occur via formation/transformation three different aluminosilicate precursors (gel, worm-like particles and condensed aggregates), and that crucial importance in the process of crystallization play the core-shell nano-precursors (3–20 nm in size) formed at the very early stage of the crystallization process. For this reason his very recent and present investigations are focused on the investigation of chemical and structural properties of the core(amorphous silica)@shell(TAA-polysilicates) and their influence on the course of crystallization and properties of products (zeolites).

Besides the main directions of investigation, dr. Boris Subotić and co-workers also studied solution-mediated transformations of thermodynamically less stable types of zeolites (mainly zeolite A) and some other materials (orthombic barium fluoride) to more stable ones (zeolite P, hydroxysodalite, cubic zeolite P), thermodynamics and kinetics of exchange of cations from solution with the host ions from zeolites, mechanochemical transformations of zeolites to amorphous phase, high-temperature transformations of zeolites and amorphous aluminosilicates to ceramics, and others.

Dr. sc. Boris Subotić is still very active scientist publishing regularly in prestigious world journals. He has published more than two hundred scientific papers, and between them more than hundred are included in Web of Science Core Collection. The number of citations of dr. sc. Boris Subotić is about 3000, and his h-index is 29. He is the author of five chapters in books and four patents. He has been the supervisor of one postdoctoral fellowship, ten Ph.D thesis and four master's theses. He participated at more than 80 international and national scientific meetings and held many invited lectures and seminars at conferences and universities.

At the end of this presentation, we extend our warmest congratulations to dr. sc. Boris Subotić on the occasion 75th anniversary of his life and 52nd anniversary of his scientific work with gratitude for all he has done on improvement and development of zeolites in our country and for a great contribution to establishing cooperation with world scientists, which in addition to scientific results often amazed by the rich knowledge of the native and world culture and art. We wish him more many years of good health and fruitful work.

Congratulations are joined by the Slovenian Zeolite Association and the Serbian Zeolite Association

Tatjana Antonić Jelić (*Croatian Zeolite Association*)

CONTENTS

OPPORTUNITIES IN DEFECTS ENGINEERING AND HEALING IN ZEOLITES

Izabel C. Medeiros-Costa[1,2] *Eddy Dib,*[1] *Nikolai Nesterenko,*[2] *Jean-Pierre Dath,*[2] *Jean-Pierre Gilson,*[1] *Svetlana Mintova*[1]
[1]Laboratoire Catalyse et Spectrochimie (LCS), Normandie University, ENSICAEN, CNRS, 6 boulevard du Marechal Juin, 14050 Caen, France
[2]Total Energies, Research & Technology Feluy, B-7181 Seneffe, Belgium
E-mail: mintova@ensicaen.fr

Zeolites have been game-changing materials in oil refining and petrochemistry over the last 60 years and have the potential to play the same role in the emerging processes of the energy and environmental transition. Although zeolites are crystalline inorganic solids, their structures are not perfect and the presence of defects sites – mainly Brønsted acid sites and silanols - influences their thermal and chemical resistance as well as performances in key areas such as catalysis, gas and liquid separations and ion-exchange.

In this presentation I will review the type of defects in zeolites and the characterization techniques used for their identification and quantification. Emerging and powerful techniques are now available to locate defects and their further development will most probably add rich information how to tune the properties and performances of zeolites. More specifically, I will focus on silanol (Si-OH) defects located within the micropore structure and/or on the external surface of zeolites. The main approaches applied to engineer and heal defects and their consequences on the properties and applications of zeolites in catalysis and separation processes will be presented. The metal healing where the defects act as ports of entry for novel isomorphous substitution (Mo, W, V…) producing new active sites in zeolites working outside of the comfort zone will be presented.

Defects in zeolites need further exploration, explanation and exploitation as they belong to the "Zeolite Crystal Engineering" toolbox to design the new catalysts and adsorbents required in the energy transition and in applications in emerging fields (biomedical, sensors, nanotechnology).

EXAMINING ZEOLITIC IMIDAZOLATE FRAMEWORKS (ZIFs) FOR ETHANOL ADSORPTION

Ciara Byrne
Department of Inorganic Chemistry and Technology, National Institute of Chemistry, Hajdrihova 19, SI-1000 Ljubljana, Slovenia
E-mail: ciara.byrne@ki.si

ABSTRACT

Zeolitic imidazolate frameworks (ZIFs) are comprised of transition metal ions (Zn) and imidazolate linkers. Due to their properties (large surface areas, suitable pore size distribution and structure stability), ZIFs have great potential for adsorptive separation and storage applications. Four different ZIF structures have been investigated for heat storage application, with ethanol as the adsorbate. The two main criteria for selecting ZIF structures for selected application are the pore entrance size and the pore/cage but structure stability, hydrophilicity/hydrophobicity and pore accessibility should also be considered. This research shows that ZIF-93 has the highest % ethanol uptake while ZIF-90 had the highest specific surface area and desorption entropy. The % uptake of ethanol is affected by pore/cage entrance and capacity, functional groups of linkers and crystallite size.

Key words: ZIFs, ethanol uptake, DSC.

INTRODUCTION

The increasing demand of heating/cooling is of grave concern due to the ever increasing population. Since energy for heating and cooling represents up to 50% of the world's final energy consumption, there has been an increased interest in finding environmentally friendly methods for the optimization of heat supply/demand. One method that addresses this issue and uses renewable energy is Thermal Energy Storage (TES), which uses the reversible chemical reactions and/or sorption processes of gases in solids or liquids. One major benefit of using this method is that it only shows an insignificant amount of heat loss while reaching a considerably higher energy storage density.

Sorption thermal energy can be examined using traditional adsorbents (*e.g.* zeolites) or innovative adsorbents (*e.g.* metal-organic frameworks) [1,2]. As they have the potential for many application (such as catalysis and gas capture/storage), there has been an increased interest in metal-organic frameworks (MOFs) [3]. One of the subgroups of MOFs is Zeolitic imidazolate frameworks (ZIFs), which are comprised of transition metal ions (Zn, Co, etc.) and imidazolate linkers [3]. ZIFs are structured similarly to zeolites, with the metal ion replacing the Si/Al and the imidazolate linker replacing the O atoms. ZIFs are considered to be highly stable. Due to their properties, including ordered porous structures and possibility to shape them in glass-like monoliths, ZIFs also have been proposed as supports for adsorptive separation applications [4]. In spite of a great potential, the reports on the optimization of ZIF for heat storage and allocations applications are scarce and majority focusing on water as working fluid. On the other hand, using ethanol instead of water is reportedly advantageous, which can be seen in a study by De Lange *et al.* (2015) [5]. The use of ethanol as an adsorbate has seldom been explored for this purpose but may prove to be beneficial for applications at lower temperatures when compared to water [6,7].

The ZIFs studied were selected based on their reported pore sizes and pore capacities [8]. ZIF-8, ZIF-90 and ZIF-93 were selected as they have large pore entrances and pore/cage capacities. For comparison purposes ZIF-74, which has a significantly lower reported porosity, was studied [8].

Table 1. Pore entrance size, the pore/cage capacity and topology for the ZIFs examined [8,9].

ZIF	Pore entrance [Å]	Pore capacity [Å]	Topology
ZIF-8	3.5	11.6	SOD
ZIF-74	1.2	2.6	GIS
ZIF-90	3.5	11.2	SOD
ZIF-93	3.6	17.9	RHO

Based on the encouraging result by De Lange et al. (2015), this study will examine four different ZIFs for heat storage and allocation applications, using ethanol as the adsorbate.

EXPERIMENTAL

ZIF-8, ZIF-90 and ZIF-93 were synthesised using optimised methods based on literature. ZIF-74 was synthesised by significantly modifying the method published by Banerjee *et al.* (2008) [10]. The samples used zinc nitrate hexahydrate (ZIF-8 and ZIF-74) or zinc acetate dehydrate (ZIF-90 and ZIF-93) as the zinc-containing precursor. The linkers used were 2-methylimidazole (ZIF-8), Nitroimidazole (ZIF-74), 5,6-dimethylbenzimidazole (ZIF-74), 2-Hydroxyisocaproic acid (ZIF-90) and 4-methyl-5-imidazolecarboxaldehyde (ZIF-93). TG of the as-synthesized sample showed that ZIF-74 did not require activation. The activation of the three other ZIFs was achieved *via* drying in a vacuum over at 150°C overnight (ZIF-8), soaking in methanol for 6-8 hours followed by drying in vacuum oven at 150°C overnight (ZIF-90) and heating in a vacuum oven at 85°C overnight. All ZIFs were characterised using XRD, TG, SEM and Nitrogen physisorption. The % ethanol uptake was examined using an IGA-100 gravimetric analyser (Hiden Isochema Ltd.). The isotherms were collected at two different temperatures (25°C and 30°C) in the relative pressure range from 0 – 0.9. Finally, the ZIFs were analysed with DSC to determine the desorption entropy. The ZIFs were soaked in a desiccator with ethanol for 7 days prior to DSC analysis.

RESULTS AND DISCUSSION

Structural properties were examined using XRD, TG, and nitrogen physisorption, which revealed phase pure products. The crystalline structures of the three ZIFs were confirmed using XRD and comparing to the simulated XRD pattern (Figure 1).

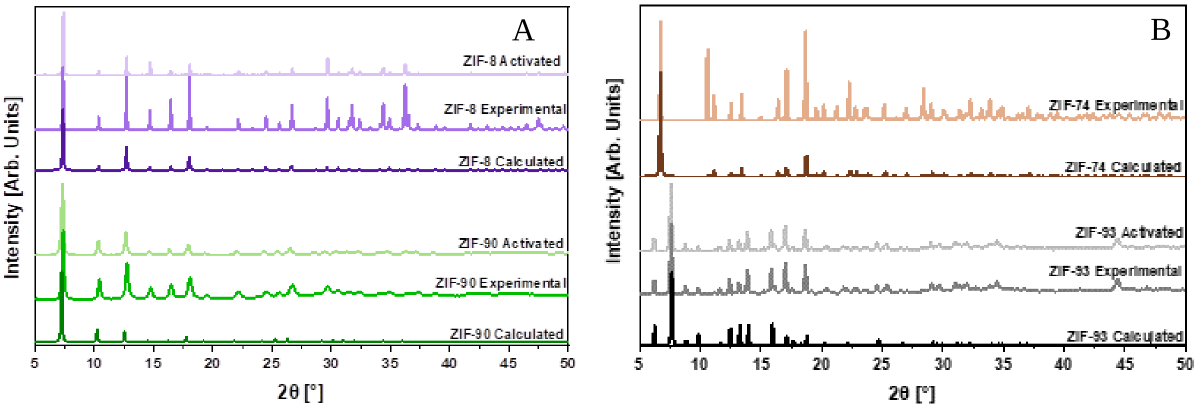

Figure 1. X-ray diffraction patterns of as-synthesized and activated ZIFs. Calculated patterns are also shown. A: ZIF-8 (purple) and ZIF-90 (green). B: ZIF-74 (brown) and ZIF-93 (black/grey).

XRD analysis was repeated after the activation method to ensure that crystalline structure had remained intact (Figure 1). TG analysis was completed prior and after the activation of ZIF structures to ensure that any solvents present were removed during activation but the remaining structure had not collapsed. SEM was performed on the as-synthesised ZIFs to examine the morphology of the materials and the size of the crystals. As it can be seen in Figure 2, ZIF-8 and ZIF-74 products are made up of large crystals while ZIF-90 and ZIF-93 show significantly smaller crystals.

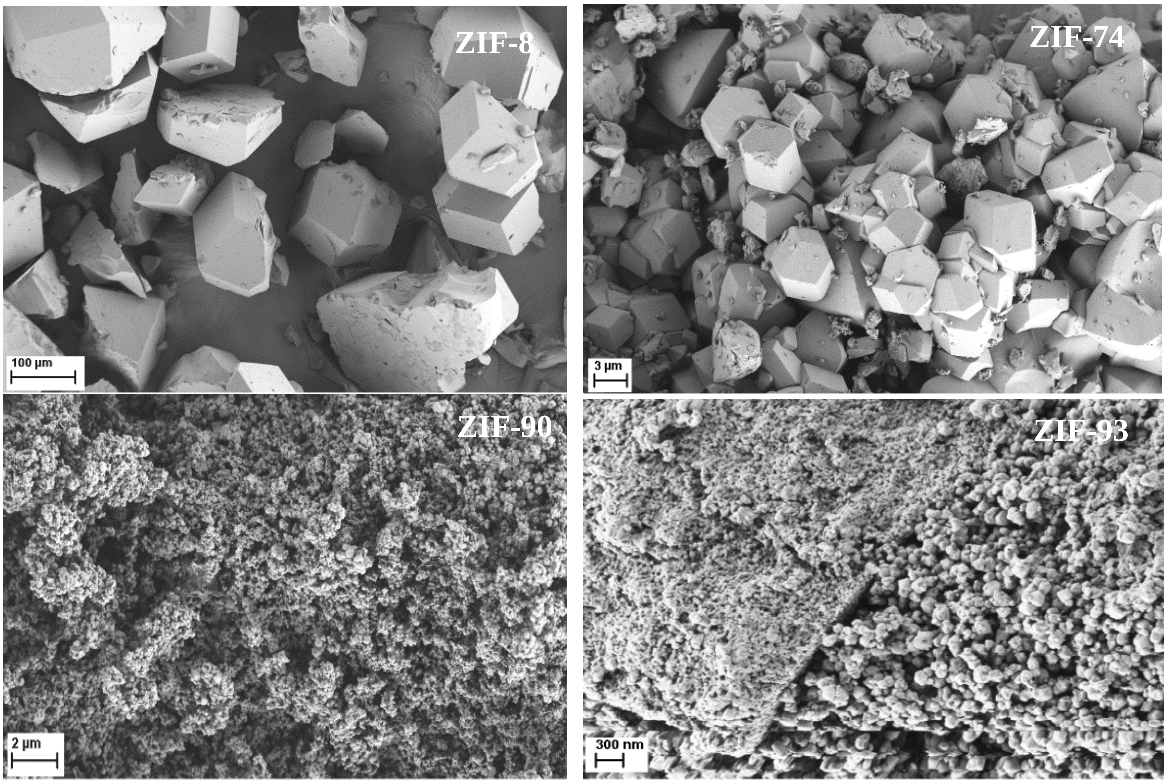

Figure 2. SEM images of as-synthesized ZIF-8, ZIF-74, ZIF-90 and ZIF-93.

Nitrogen physisorption showed that the ZIFs had a specific surface area of up to 1119 m^2/g (Table 2). The ethanol uptake results (Table 2) showed that the capacity up to 37 wt. % ethanol could be reached and that mechanism of sorption of ethanol in selected ZIFs were dominated by diffusion limitations of the molecules through the pores. The structures remained crystalline after the analysis. Based on the all the results for the three ZIFs, the pore capacity and pore size has a direct impact on the surface area and the % ethanol uptake. ZIF-8, ZIF-90 and ZIF-93, which have the larger pore size and pore capacity, showing significantly higher ethanol uptake in comparison to ZIF-74.

Table 2. The specific surface area (S_{BET}), ethanol uptake and DSC analysis for all ZIFs studied.

ZIF	S_{BET} [m^2/g]	Ethanol uptake [%]	DSC [J/g]
ZIF-8	621	19.9	158.4
ZIF-74	6	0.6	58.9
ZIF-90	1119	25.5	260.3
ZIF-93	1058	37.6	206.2

Despite ZIF-8 and ZIF-90 having similar or the same pore entrance, pore/cage capacity and topology, they showed significant differences in the crystal size, specific surface area, % ethanol uptake and DSC results (Figure 2 and Table 2). This difference, at least for ethanol uptake, is likely due to the hydrophobic linker used for ZIF-8 while ZIF-90 has a slightly hydrophilic linker. DSC analysis (Table 2) showed that the ZIFs had a desorption entropy of up to 260.3 J/g (ZIF-90). DSC analysis showed that there was a 101.9 J/g difference between ZIF-8 and ZIF-90.

CONCLUSION

In this study, the evaluation of four ZIFs as sorbents for sorption based energy storage by using ethanol as sorbate revealed a stable system suitable for potential use in TES. The ZIFs were synthesized using simplified methods. The samples were phase pure and fully activated. ZIF-93 shows the highest % of ethanol uptake while ZIF-90 had the highest specific surface area and desorption entropy. ZIF-74 showed to have the lowest % of ethanol uptake, specific surface area and desorption entropy. Finally, ZIF-90 and ZIF-93 showed that there is not always a direct correlation between % ethanol uptake and desorption entropy.

ACKNOWLEDGMENTS

This research was funded by Slovenian Research Agency Research programme P1-0021. The author would like to thank Edi Kranjc for XRD measurements, Mojca Opresnik for SEM imaging, Alenka Ristić for DSC training, Suzana Mal for help with DSC measurements and finally Nataša Zabukovec Logar for providing guidance and discussion of the results.

REFERENCES

[1] A. Ristić and N.Z. Logar, *Nanomaterials,* 2019, **9**, 27-43.

[2] S.K. Henninger, S.J. Ernst, L. Gordeeva, P. Bendix, D. Fröhlich, A.D. Grekova, L. Bonaccorsi, Y. Aristov and J. Jaenchen, *Renew. Energy*, 2017, **110**, 59-68.

[3] Y. Ban, Y. Peng, Y. Zhang, H. Jin, W. Jiao, A. Guo, P. Wang, Y. Li and W. Yang, *Micropor. Mesopor. Mater.,* 2016, **219**, 190-198.

[4] C. Zhou, L. Longley, A. Krajnc, G.J. Smales, A. Qiao, I. Erucar, C.M. Doherty, A.W. Thornton, A.J. Hill, C. W. Ashling, O.T. Qazvini, S.J. Lee, P.A. Chater, N.J. Terrill, A.J. Smith, Y. Yue, G. Mali, D.A. Keen, S.G. Telfer and T.D. Bennett, *Nat. Commun.,* 2018, **9**, 1-9.

[5] M.F. De Lange, B.L. Van Velzen, C.P. Ottevanger, K.J.F.M. Verouden, L.C. Lin, T.J.H. Vlugt, J. Gascon and F. Kapteijn, *Langmuir,* 2015, **31**, 12783-12796.

[6] H. Wu, F. Salles and J. Zajac, *Molecules,* 2019, **24**, 945-995.

[7] B.R. Pimentel, M.L. Jue, E.K. Zhou, R.J. Verploegh, J. Leisen, D.S. Sholl and R.P. Lively, *J. Phys. Chem. C,* 2019, **123**, 12862-12870.

[8] A. Phan, C.J. Doonan, F.J. Uribe-Romo, C.B. Knobler, M. Okeeffe and O.M. Yaghi, *Acc. Chem. Res.,* 2010, **43**, 58-67.

[9] W. Morris, C.J. Doonan, H. Furukawa, R. Banerjee and O.M. Yaghi, *J. Am. Chem. Soc.,* 2008, **130**, 12626-12627..

[10] R. Banerjee, A. Phan, B. Wang, C. Knobler, H. Furukawa, M. O'Keeffe and O.M. Yaghi, *Science,* 2008, **319**, 939-943.

SYNTHESIS AND CHARACTERIZATION OF BORON MODIFIED ZEOLITE WITH MFI STRUCTURE

Sanja Bosnar[1], *Vladislav Rac*[2], *Ljiljana Damjanović-Vasilić*[3], *Vladimir Pavlović*[2], *Steva Lević*[2], *Josip Bronić*[1], *Vesna Rakić*[2]

[1]Ruđer Bošković Institute, Division of Materials Chemistry, Zagreb, Croatia

[2]University of Belgrade, Faculty of Agriculture, Department of Chemistry and Biochemistry, Serbia

[3]University of Belgrade, Faculty of Physical Chemistry, Serbia

E-mail: sbosnar@irb.hr

ABSTRACT

In this work MFI type zeolite samples with different amount of boron were prepared. Obtained samples were characterized by X-ray diffraction (XRD), scanning electron microscopy (SEM), energy dispersive spectroscopy (EDS) and Fourier transform infrared spectroscopy (FTIR). Results of characterization showed that presence of boron in the reaction mixture influences size and morphology of synthesized zeolite crystals. The amount of boron in the reaction mixture, as well as presence of aluminium, has influence on the extent of boron loss during calcination of the final zeolite product. However, the incorporation of boron into the zeolite structure did not affect the crystallinity - the MFI structure was preserved in all obtained samples.

Key words: boron, borosilicate, MFI type structure, hydrothermal treatment.

INTRODUCTION

Zeolites are porous crystalline aluminosilicates. Because of specific properties related to their structure, zeolites are promising materials for many different applications in industry and everyday life. They are well known as adsorbents, ion exchangers, catalysts, etc.

In the basis of complex zeolite structure are tetrahedra of silicon and aluminium oxide connected through common oxygen atoms [1]. Presence of aluminium brings framework charge which is counterbalanced by different exchangeable cations. If cations are exchanged by proton, Brønsted acid sites of different strength form, which is important for acid catalytic applications. By isomorphous substitution of silicon and/or aluminium atom by other elements (i.e. boron, gallium, germanium, titanium, zinc, iron, etc.), it is possible to modify zeolite porosity and acidity, and in that way, tune zeolite properties for specific applications [2].

Hence, by introduction of boron into zeolite MFI structure, materials with different properties could be obtained. Brønsted acid sites formed are weaker in comparison to the aluminium containing counterpart [3]. Since B-O bonds are shorter than Si-O and Al-O bonds, a size of crystal unit of boron modified zeolites is reduced [3]. Post synthesis treatment of boron containing zeolite can substitute boron by other cations and in that way metallosilicate structures can be obtained which cannot be obtained easily by usual hydrothermal treatment [4]. Additionally, deboronation can also increase number of defects, i.e., silanol nests, H-bonded silanols, in high silica MFI zeolites, which can increase their catalytic activity [5].

In this work, we present preliminary results of our study of boron containing zeolite synthesis with the aim of their possible application in catalysis and adsorption. Therefore, we have hydrothermally synthesized several zeolite samples with different amount of boron in the starting reaction mixture. Obtained samples were characterized by XRD, SEM, EDS and FTIR, to study boron influence on the properties of the final zeolite product.

EXPERIMENTAL

Chemicals used in preparation of the reaction mixtures were boric acid (H_3BO_3, Sigma Aldrich), sodium hydroxide (NaOH, 98%, Kemika), tetrapropyl ammonium bromide (TPABr, 98%, Sigma Aldrich), fumed silica (SiO_2, Sigma Aldrich), aluminium hydroxide ($Al(OH)_3$, Kemika) and deionized water. All chemicals were used as obtained. The molar composition of the reaction mixtures was $60SiO_2 \cdot 2.5\ Na_2O \cdot x\ B_2O_3 \cdot y\ Al_2O_3 \cdot 8\ TPABr \cdot 800\ H_2O$, where x and y=0 for sample 1; x=1, y=0 for sample 2; x=2 and y=0 for sample 3 and x and y=2 for sample 4. Reaction mixtures were prepared by dissolving appropriate amount of TPABr in water solution of NaOH. Then, fumed silica was added, and white thick gel was obtained. In reaction mixtures, which contained both B and Al, boric acid and aluminium hydroxide were added to the solution of NaOH and TPABr, before adding fumed silica. Four reaction mixtures/gels were prepared. The gels were transferred into Teflon-lined metal autoclaves and heated at 150°C for 5 days. After synthesis, obtained samples were washed with water, dried, and calcined at 550° C for 5 hours. In this way obtained samples were used for further characterization by XRD, SEM, EDS and FTIR.

XRD was done using Rigaku Ultima IV diffractometer in Bragg-Braentano geometry, with Ni filtered CuKα radiation (λ=1.54178 Å). Diffraction data were acquired over the scattering angle 2θ from 2° to 70° with a step of 0.02° and acquisition rate of 1°/min. Elemental analysis was done using EDS (JEOL JSM-6390LV equipped with energy dispersive X-ray spectrometer, Oxford Aztec X-max). The morphology of samples was investigated by scanning electron microscopy (SEM, JEOL JSM-6390LV). Prior to the SEM observations, the powders were coated with gold to minimize charging. FTIR spectra were collected using IRAffinity-1 (SHIMADZU) spectrophotometer; 2 mg of sample was pelletized in 200 mg of KBr (Fisher Scientific); for each spectrum 100 scans were collected with 4 cm^{-1} resolution.

RESULTS AND DISCUSSION

XRD diffractograms in Figure 1 show that all samples are fully crystalline zeolites with MFI type of structure. The peaks of other crystalline phases were not detected in the diffractograms suggesting that boron, when present in the sample, is dispersed in the zeolite structure [6].

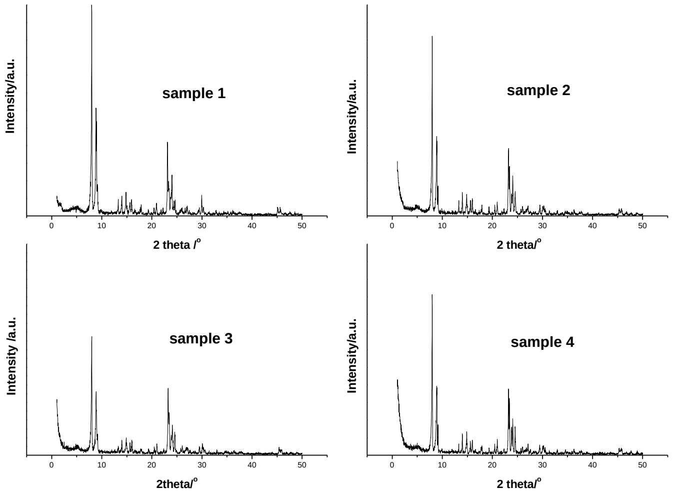

Figure 1. X-ray diffraction patterns of samples 1-4.

SEM micrographs in Figure 2 show the morphology of the obtained samples. In sample 1 (Fig 2a), obtained from the reaction mixture without boron and aluminium present in the reaction mixture, particles have characteristic intergrown structure with crystal size of about 6 µm. By addition of boron into reaction mixture (Si/B=30), in obtained sample 2 (Fig 2b) particles become more rounded, but their sizes remain quite similar. With further increase of the boron amount in the reaction mixture (Si/B=15), particles of obtained sample 3 are large polycrystalline spheres with size of about 17 µm, as visible in the Fig 2c. When both aluminium and boron were present in the reaction mixture (Si/B=15, Si/Al=15) obtained sample 4 has large and rounded particles with size of about 16 µm, with surface morphology (Fig 2d) resembling intergrown structure. It was shown that by simple change of Si/B ratio in the reaction mixture is possible to influence the size and shape of the obtained zeolite particles, which is in agreement with literature data [7].

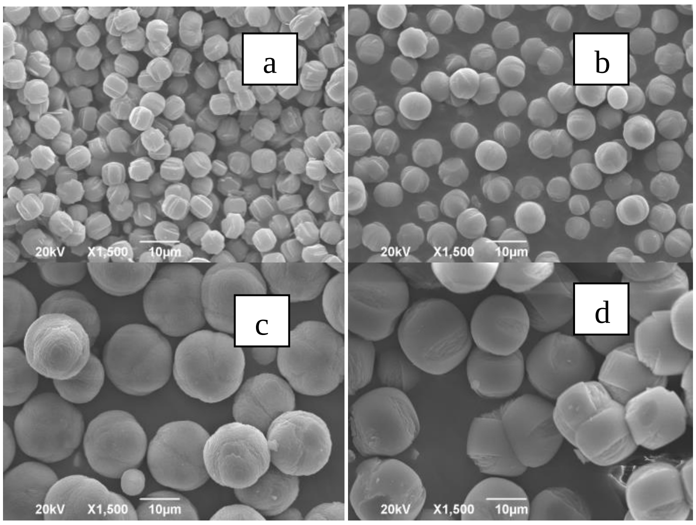

Figure 2. SEM of samples: a) sample 1, b) sample 2, c) sample 3, d) sample 4.

EDS results show that after calcination of the samples the amount of boron in the sample 2, although present in the reaction mixture, is not present in the calcined material. On the other side in the samples 3 and 4, where amount of boron is present in the reaction mixture in double amount, boron is still present also in the calcined samples: 4.73 wt% in sample 3 and 5.37 wt% in sample 4.

FTIR results presented in Figure 3 corroborate EDS results, and in spectra of samples 3 and 4 it is possible to notice bands that suggest presence of boron in the zeolite structure, which are not found in the samples 1 and 2.

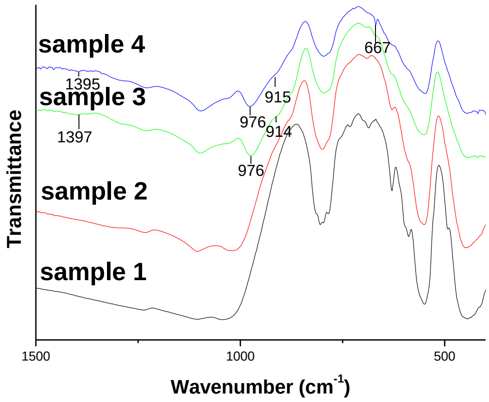

Figure 3. FT-IR spectra of samples 1-4.

The weak shoulder and band at about 660 cm^{-1}, for samples 3 and 4, respectively, are attributed to the bending vibrations of B-O-Si [7]. For the samples 3 and 4, presence of wide shoulders at about 920 cm^{-1} are connected to symmetric stretching B-O-Si modes and presence of tetracoordinated boron**,** while small shoulders at about 1090 cm^{-1} are due to stretching modes of BO_4 units [8]. Bands at about 970 cm^{-1} are connected to Si-OH stretching vibration of bridging hydroxyls but could also be connected to the Si-O-B vibrations [9]. Band at about 1400cm^{-1} is ascribed to asymmetric B-O stretching of the $[B(OSi)_3]$ units in calcined samples [10,11]. Its weak intensity in our samples 3and 4 is probably due to the strong interaction of boron in trigonal coordination with water [11].

CONCLUSION

Results obtained in this work showed that incorporation of boron in MFI zeolite structure brings changes of the morphology of zeolite particles, from intergrowth structure of pure MFI structure to polycrystalline spherical particles. Size of borosilicate crystals depend on the Si/B ratio in the reaction mixture. In FTIR spectra of boron modified zeolites, besides characteristic bands for MFI structure, additional bands can be noticed, indicating incorporation of boron atoms in the MFI structure. In calcined samples the amount of boron is lower than expected from reaction mixture composition. This finding could be partly ascribed to the deboronation process during calcination but also to the possible lower incorporation of boron during synthesis. It seems that amount of boron in starting reaction mixture and presence of aluminium has important influence on the range of the abatement.

ACKNOWLEDGMENTS

The authors acknowledge the financial supports by the Croatian Science Foundation (project IP-2016-06-224), by the Ministry of Science and Education of the Republic of Croatia (bilateral Croatian-Serbian project for 2019-2021: Energy storage in metal-organic structures obtained by mechanochemical process), and by the Ministry of Education, Science and Technological Development of Republic of Serbia (Contract numbers: 451-03-9/2021-14/200146 and 451-03-9/2021-14/200116, and bilateral Serbian-Croatian project for 2019-2021: Energy storage in metal-organic structures obtained by mechanochemical process, project number: 337-00-205/2019-09/20).

REFERENCES

[1] D.W. Breck, *Zeolite Molecular Sieves*, Wiley, New York, 1974.

[2] R.M. Barrer, *Hydrothermal Synthesis of Zeolites*, Academic Press, London, 1982.

[3] R. Millini, G. Perego and G. Bellusi, *Topics in Catalysis*, 1999, **9**, 13-34.

[4] R. de Ruiter, A.P.M.Kentgens, J. Grootendorst, J.C. Jansen and H. van Bekkum, *Zeolites*, 1993, **13**, 611-621.

[5] L. Forni, G. Fornasari, F. Trifirò, A. Aloise, A. Katović, G. Giordano and J.B. Nagy, *Micropor.Mesopor.Mater*., 2008, **101**, 161-168.

[6] R. Lü, H. Tangbo, Q. Wang and S. Xiang, *J. Nat. Gas Chem*., 2003, **12**, 56-62.

[7] A. Cichocki, J. Parasiewicz-Kaczmarska, M. Michalik and M. Bus, *Zeolites*, 1990, **10,** 5**77-**582.

[8] G. Coudurier and J.C. Védrine, *Pure Appl. Chem*., 1986, **58**, 1389-1396.

[9] Y.Han, H. Kim, J. Park, S.Lee and J. Kim, *Int.J.Hydr.Energy*, 2012, **37**, 14240-14247.

[10] R. Bandyopadhyay, Y. Kubota, N. Sugimoto, Y. Fukushima and Y. Sugi, *Micropor. Mesopor. Mater*., 1999, **32**, 81-91.

[11] L. Regli, S. Bordiga, C. Lamberti, K.P. Lillerud, S.I. Jones and A. Zecchina, *J.Phys.Chem*., 2007, **111,** 2992-2999.

GREEN SYNTHESIS OF ZIF-90 AND ITS MIXED METAL ANALOGUES

Aljaž Škrjanc[1,2], *Ciara Byrne*[1], *Matjaž Mazaj*[1], *Nataša Zabukovec Logar*[1,2]
[1]National Institute of Chemistry, Hajdrihova 19, SI-1001 Ljubljana, Slovenia
[2]Graduate School, University of Nova Gorica, Vipavska cesta 13, SI-5000 Nova Gorica, Slovenia
E-mail: aljaz.skrjanc@ki.si

ABSTRACT

In this study, a new green solvent-based synthesis of Zeolitic Imidazolate Framework - 90 (ZIF-90) is investigated. Two biobased aprotic dipolar solvents Cyrene™ and γ-valerolactone (GVL) successfully replaced DMF in the synthesis of ZIF-90 at room temperature with a comparable product yield. After thermal treatment, PXRD showed that the Cyrene™-based product exhibited reduced porosity while the GVL-based products preserved its crystallinity and porosity after thermal burst activation. The primary particles of 30 nm to 60 nm in all products further form agglomerates of different sizes and interparticle mesoporosity, depending on the type and molar ratios of solvents used. The optimal solvent ratio was then used to synthesize mixed-metal ZIF-90 with Mg, Cu, Co, and Ni. The synthesized ZIFs were characterised using PXRD, TGA, N_2 physisorption and SEM-EDX. For all mixed-metal samples, a decrease in the specific surface area was observed. Finally, preliminary adsorption tests were completed on the optimal solvent ratio ZIF-90 and its mixed metal analogues.

Key words: mixed-metal ZIF, ZIF-90, green synthesis, GVL.

INTRODUCTION

Zeolitic imidazolate frameworks (ZIFs) are a subgroup of metal-organic frameworks (MOFs), which have shown promising results as functional materials for different applications, mainly in adsorption and catalysis. Of the wide array of known ZIFs, the largest portion of articles is on ZIF-8, ZIF-67, and ZIF-90. While ZIF-8 and ZIF-67 synthesis already use more environmentally friendly solvents, ZIF-90 synthesis still mainly relies on DMF.

A water based ZIF-90 synthesis has already been reported [1]. However, due to the lower surface area and large particle size of the products, it has yet to be widely used. Another approach towards greener synthesis was reported [2] using the mixed solvent system of DMF/MeOH, where the amount of DMF was halved compared to the typical ZIF-90 synthesis. Overview of biobased DMF alternatives that have already been used in MOF chemistry narrowed down the list of possible alternatives to dihydrolevoglucosenone with commercial name Cyrene™, and gamma-valerolactone (GVL).

After successful substitution of DMF, we investigated the impact of mixed metal(MM) systems on the various ZIF-90 properties, as MM ZIF-67 with Co/Zn was shown to exhibit increased stability [3].

EXPERIMENTAL

The green synthesis method was adapted from *Brown*[2], where a volumetric substitution of DMF was done with both pure and Methanol diluted green solvents, as described for single-metal ZIF-90 [4].

In a 100 mL beaker, 1.93 g (19 mmol) of 2H-imidazole carbaldehyde (HICA) was added to 50 mL linker solvent (Table 1). The mixture was stirred at room temperature until either fully suspended or fully dissolved in the solvent. A separate solution of 1.46 g (6.5 mmol) of $Zn(AcO)_2 \cdot 2H_2O$ in 50 mL of metal precursor solvent (Table1) was prepared in a 150 mL beaker. The HICA suspension was then slowly poured into the zinc solution and was stirred for 1 h.

The product was isolated by centrifuging at 9000 rpm for 35 min, washed with MeOH, and centrifuged again. The precipitate was left to air-dry overnight at room temperature in the centrifuge bottle.

The MM ZIF-90 were prepared using the same method as ZIF-90-GM, with 20 mol. % of $Zn(AcO)_2{\cdot}2H_2O$ substituted with Mg, Co, Cu and Ni acetates hydrates. Unlike the pure ZIF-90-GM, which was activated by heating at 200 °C for 1.5 h, the MM samples were activated by soaking in methanol and then heated at 150 °C overnight. The as-synthesised green ZIF-90's were characterized using PXRD, TGA, SEM and N_2 physisorption.

Table 1. Solvent composition for the synthesised zeolitic imidazolate frameworks (ZIF)-90 samples.

Product	Linker Solvent	Metal Precursor Solvent
ZIF-90-C	Cyrene^{TM} (481 mmol)	MeOH (1250 mmol)
ZIF-90-G	GVL (525 mmol)	MeOH (1250 mmol)
ZIF-90-2G	GVL (263 mmol) + MeOH (625 mmol)	GVL (263 mmol) + MeOH (625 mmol)
ZIF-90-GM	GVL (263 mmol) + MeOH (625 mmol)	MeOH (1250 mmol)
ZIF-90-G2M	GVL (179 mmol) + MeOH (825 mmol)	MeOH (1250 mmol)

RESULTS AND DISCUSSION

The as-synthesised green ZIF-90's were characterised using PXRD, TGA, SEM and N_2 physisorption. Using the Scherrer equation, the particulate size of the prepared ZIFs were calculated to be in the range of 30 – 60 nm. SEM imaging showed that larger agglomerates formed in the case of ZIF-90-D, ZIF-90-GM, and ZIF-90-G2M with the latter’s SEM (Figure 1) also showing a large amount of impurities.

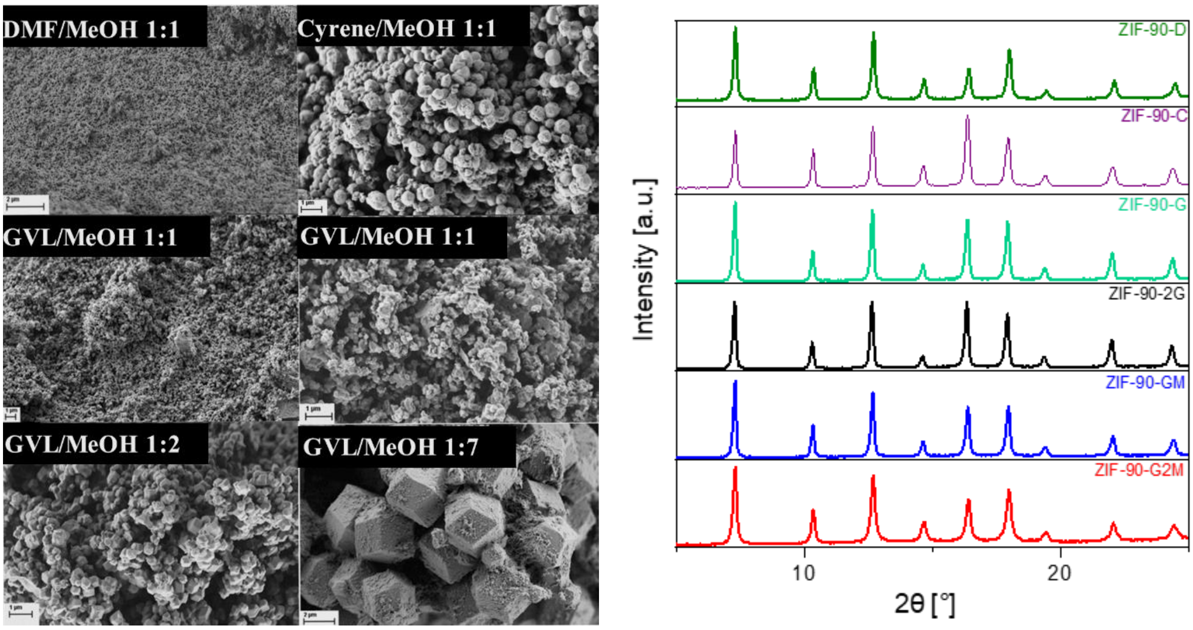

Figure 1. Left - SEM images of ZIF-90 prepared with different solvent ratios; Right - XRD patterns of synthesized ZIF-90.

As a result of its higher specific surface area and higher thermal stability, the ZIF-90-GM procedure was selected for the synthesis of the MM samples.

All as synthesized ZIF-90 PXRD showed similar crystallinity of MM samples if compared to a single-metal analogue. The calculated particle sizes ranged from 40 to 70 nm. Dopant metal ion concentration in MM ZIFs was detected using SEM-EDX on palletized samples. All dopant ions except Mg were detected in significant amounts. The determined dopant concentration showed that from the initial 20% in the metal precursor mixture around 9.7 – 11.4 % remained.

The activated MM samples were also analysed using SEM-EDX for metal ion ratio in the product with no significant change observed. The activated samples were then analysed using N_2 physisorption to determine surface area and porosity followed by preliminary gas sorption tests with CO_2, CH_4, and N_2 at room temperature.

Table 2. Gas sorption test results for ZIF-90-GM and MM ZIF-90-GM samples.

Product	Dopant amount (%) *	S_{BET} (m^2/g)	CO_2 uptake at 1 bar (mmol/g)	Selectivity** CO_2/N_2	Selectivity** CO_2/CH_4
ZIF-90-GM	N/A	1044	2.03	17.8	6.8
ZIF-90-GM-Mg	2.6	1003	1.92	14.6	5.8
ZIF-90-GM-Ni	11.3	959	1.92	17.9	6.0
ZIF-90-GM-Co	11.4	949	1.37	6.4	3.8
ZIF-90-GM-Cu	9.7	967	1.18	21.7	6.1

*Percent of dopant metal determined from M/M+Zn ratio, ** calculated from individual isotherms at 1 bar

While metal incorporation had less of an impact on specific surface area, it did have a detrimental effect on CO_2 uptake in the case of Cu and Co MM ZIF-90 (Table 2). With Co doped showing extreme decrease in selectivity for both CO_2/N_2 and CO_2/CH_4, while the Cu showed a significant increase in CO_2/N_2 selectivity compared to ZIF-90-GM. While the Ni doped sample showed almost no change in uptake or selectivity, the opposite effect was observed in the Mg MM ZIF, which despite the very small amount of Mg in the sample showed a large decrease in selectivity for N_2. The pure ZIF-90-GM and Ni modified sample showed similar selectivity as observed in literature [5], with a slightly higher uptake.

CONCLUSION

This study showed that we have successfully implemented the use of a green biobased solvent to synthesise ZIF-90 nanoparticles, with a comparably high surface area. The synthesis was then used to prepare different mixed metal ZIF-90. The ZIFs were characterised, and preliminary adsorption tests were carried out, in all cases the MM showed reduced surface area, which consequently led to slightly reduced CO_2 uptake in Ni and Mg MM ZIF. Most metals did have a significant impact on CO_2/N_2 selectivity, with the Co presence having a significant impact on selectivity for both gasses tested.

REFERENCES

[1] F.K. Shieh, S.C. Wang, S.Y. Leo and K.C.W. Wu, *Chem. - A Eur. J.* **2013**, 19, 11139–11142.

[2] A.J. Brown, J.R. Johnson, M.E. Lydon, W.J. Koros, C.W. Jones and S. Nair, *Angew. Chemie - Int. Ed.* **2012**, 51, 10615–10618.

[3] X. Qian, Q. Ren, X. Wu, J. Sun, H. Wu and J. Lei, *ChemistrySelect* **2018**, 3, 657–661.

[4] A. Škrjanc, C. Byrne and N. Zabukovec Logar, *Molecules* **2021**, 26, 1573.

[5] M. Ghahramaninezhad, F. Mohajer and M. Niknam Shahrak, *Front. Chem. Sci. Eng.* **2020**, 14, 425–435.

EFFECT OF METAL CATIONS IN FAU TYPE ZEOLITE ON ACID SITES

Glorija Medak, Josip Bronić, Andreas Puškarić, Nina Popov
Ruđer Bošković Institute, Bijenička cesta 54, 10 000 Zagreb, Croatia
E-mail: gmedak@irb.hr

ABSTRACT

Faujasite type zeolite isolated from the gel with a composition of $4Na_2O:Al_2O_3:10SiO_2:158H_2O$ after 48 h at 100°C was modified during synthesis using cetrimonium bromide (CTAB), or post-syntheticaly treated with sodium hydroxide aqueous solution in order to create mesopores. This way prepared material was then wet impregnated using metal salts of magnesium(II), cobalt(II), nickel(II) or zinc(II). The effect of exchanged metal cation on Brønsted and Lewis acid sites was observed using adsorption of deuterated acetonitrile in vacuum IR.

Keywords: FAU, wet impregnation, vacuum IR, mesopores.

INTRODUCTION

Faujasite type zeolite is one of the most widely used types of zeolite. Its 12-member ring cage makes it one of the best catalysts for fluid catalytic cracking (FCC) and support for platinum or palladium in a hydrocracking process. Depending on the Si/Al ratio synthetic FAU is classified as X, if the ratio is between 2 and 3, or Y if the ratio is 3 or higher. High aluminum content in X type zeolite results in a large number of Brønsted's acid sites which often leads to unwanted cyclic byproducts and the formation of coke. In order to avoid this problem, post-synthetic modifications to the zeolite structure are needed. One of the most important factors for solid-state catalysts is the rate of diffusion of molecules through the crystal. Large pores enable easy access of reactants but also the fast removal of products from the active site which reduces a possibility for byproduct formation.

Formation of mesopores is most commonly achieved by etching with alkaline water solution or using mesoporosity template such as CTAB. This way prepared zeolites can then be further modified by wet impregnation with various metal salts. The type of metal and it's coordinational preferences can have a huge effect on acid sites in the zeolite framework.

EXPERIMENTAL

The zeolite for post-synthetic treatment (HF2-2) was isolated from a gel with following composition $4Na_2O:Al_2O_3:10SiO_2:158H_2O$ [1]. The aluminate (A) and silicate (B) components of reaction gel were prepared separately. Component B was prepared by mixing Ludox-HS 30 and sodium hydroxide (Kemika, aq, 33%). To prepare component A, sodium aluminate was dissolved in a sodium hydroxide solution and water. Component A was then added in component B while stirring vigorously. A hydrothermal crystallization was conducted at 100°C for 48 hours after aging the reaction gel for 18 hours at room temperature. The resulting product was then washed, dried and calcined at 550°C for 6 hours. To get **HF2-2 des30** thus synthesized product was treated with 0.2 mol dm^{-3} sodium hydroxide water solution at 65°C for 30 minutes [2]. The ratio of solid phase to water solution was 1:30. For the synthesis of **HF2-2 24a** the reaction mixture was cooled down after 24 hours and slurry of CTAB in alkaline water (mass ratio $CTAB:H_2O=1:1$, and pH of the solution same as the one of the reaction gel) was mixed with synthesis gel in the molar ratio $SiO_2:0.4CTAB$. After that reaction mixture was returned to the oven for another 24 hours. The product was washed with distilled water, dried and calcined for 10 hours at 550°C.

Wet impregnation: Prepared FAU type zeolites **HF2-2 des30** and **HF2-2 24a** were wet impregnated with the nitrate salts of magnesium(II) (1 mol dm^{-3}), cobalt(II) (1 mol dm^{-3}), nickel(II) (0.5 mol dm^{-3}) and zinc(II) (1 mol dm^{-3}) two times for 40 minutes after which they were thoroughly washed with redistilled water, dried and calcined at 550°C for 6 hours.

RESULTS AND DISCUSSION

The XRD patterns of parent samples were compared and no significant differences were observed (Figure 1). Diffraction patterns of samples after wet impregnation were compared with those of parent samples and the peaks of corresponding metal oxides were not observed.

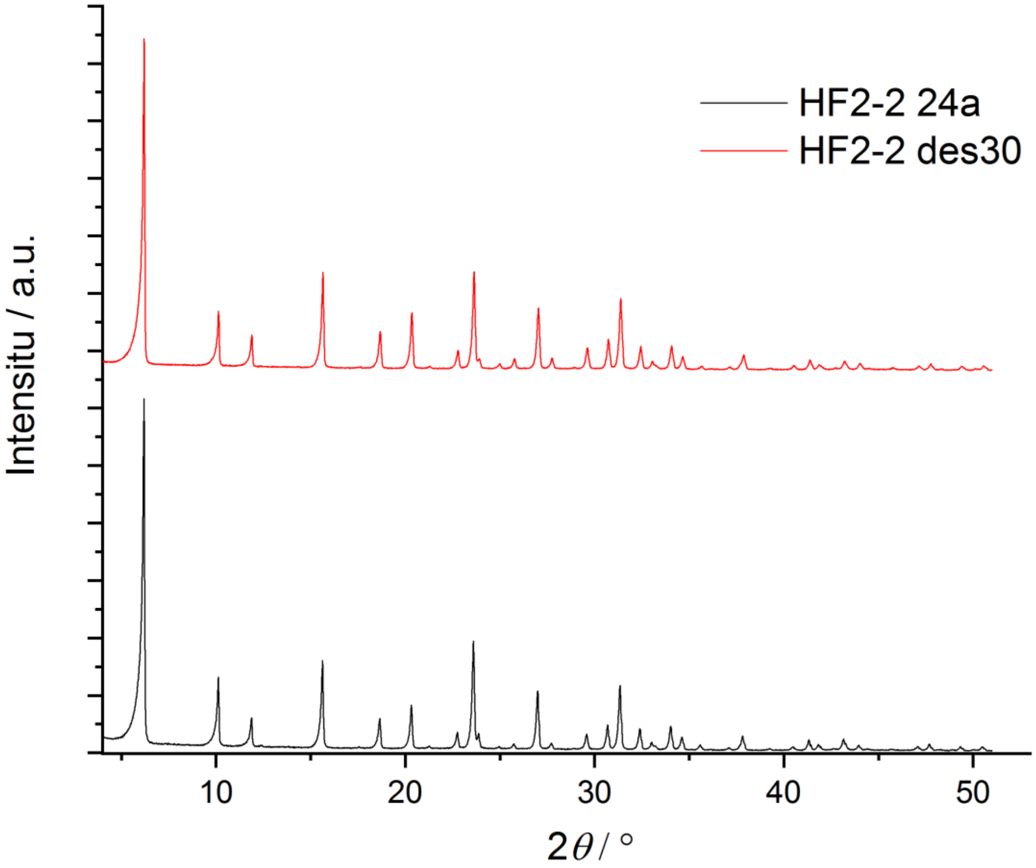

Figure 1. X-ray diffraction patterns of parent samples.

The effect of synthesis with the addition of CTAB compared to post-synthetic treatment with NaOH solution on zeolite morphology was observed using SEM (Figure 2). The difference in morphology after wet impregnation was not observed.

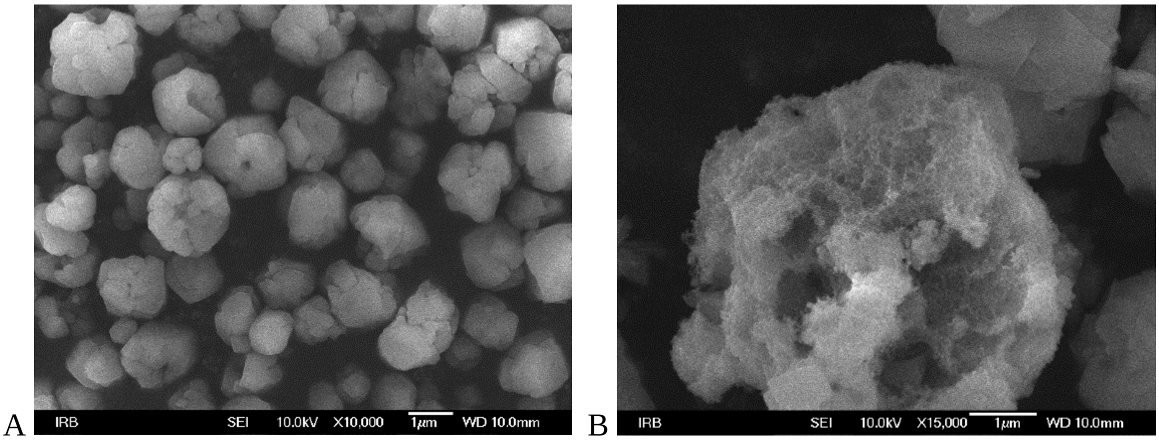

Figure 2. SEM images of HF2-2 24a (A) and HF2-2 des30 (B).

Vacuum IR spectra after adsorption of deuterated acetonitrile (Figure 3) show that in 24a series Co(II) sample has the highest intensity of peak at 2306 cm^{-1} (Lewis acid sites) followed by Mg(II).

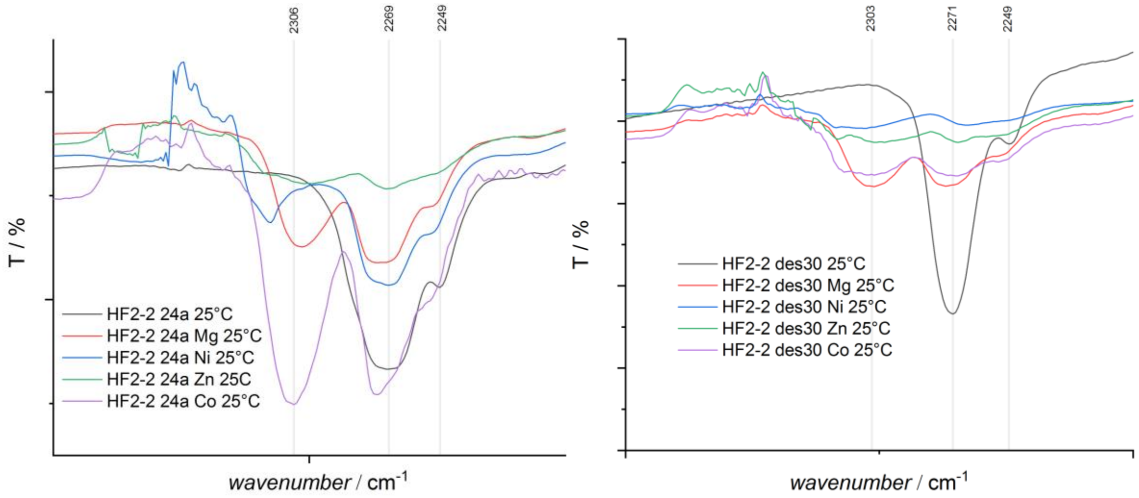

Figure 3. Vacuum IR spectra of deuterated acetonitrile adsorbed on parent and wet impregnated FAU type samples at 25°C.

The sample wet impregnated with Ni(II) shows a shifted peak at 2316 cm^{-1} which indicates a different type of Lewis acid sites compared to other metals. The intensity of a peak at 2269 cm^{-1} (silanol acid sites) is similar for parent and Co(II) sample, while those of Ni(II) and Mg(II) are a bit lower. Sample wet impregnated with Zn(II) has low intensity of both acetonitrile adsorption peaks.

All samples in des30 series show decrease in the intensity of peak at 2271 cm^{-1} after wet impregnation. The peaks at 2303 cm^{-1} are relatively weak in the case of Co(II) and Mg(II) and extremely weak for Ni(II) and Zn(II).

CONCLUSION

In all samples the differences in vacuum IR spectra after deuterated acetonitrile adsorption were observed, while XRD patterns and SEM images don't indicate any structural or morphological differences. The intensity of Lewis' acid site peaks for 24a series of samples follows in order Co>Mg>Ni>Zn, while for the des30 series it is Mg>Co>Zn>Ni. This indicates that the method of sample preparation partially also contributes to the integration of the cations in the framework after wet impregnation.

ACKNOWLEDGEMENTS

This work was supported by Croatian Science Foundation, project IP-2016-06-2214.

REFERENCES

[1] S. Bosnar, D. Bosnar, N. Ren, N, Rajić, B. Gržeta and B. Subotić, *J. Porous Mater.*, 2013, **20**, 1329-1336.

[2] D. Verboekend, G. Vile and J. Perez-Ramirez, *J. Cryst. Growth Des.*, 2012, **12**, 3123-3123.

DISTRIBUTION OF Al SITES IN SSZ-13 ZEOLITES

Katarina Kopljar[1], *Karen Janella Ardila Fierro*[2], *Andraž Krajnc*[3], *Matjaž Mazaj*[3], *Ana Palčić*[2]
[1]Department of Chemistry, Faculty of Science, University of Zagreb, Horvatovac 102a, 10000 Zagreb, Croatia
[2]Laboratory for the Synthesis of New Materials, Division of Materials Chemistry, Ruđer Bošković Institute, Bijenička 54, 10000 Zagreb, Croatia
[3]Department of Inorganic Chemistry and Technology, National Institute of Chemistry, Hajdrihova 19, PO Box 660, 1001 Ljubljana, Slovenia
E-mail: ana.palcic@irb.hr

ABSTRACT

CHA-type zeolites are commercially employed materials in the exhaust gas treatment for the selective catalytic reduction of nitrogen oxides and as the main catalyst in the methanol to olefin conversion technology. In line with general trends of modern society, there is a demand to develop more environment-friendly synthesis routes and improve their performance in the mentioned applications as well as in the other potential fields of usage. For this reason, numerous studies with the aim to meet these requirements are conducted. Acidic properties and particularly the distribution of Al species represent some of the crucial features that determine the efficiency of zeolite materials. Herein is investigated the correlation between the synthesis conditions of a series of SSZ-13 zeolite materials and their respective properties are evaluated by a range of characterization techniques.

Key words: CHA-type zeolites, SSZ-13 zeolite, Al distribution, acid sites, paired sites.

INTRODUCTION

The CHA zeolite framework is built of 4-, 6-, and 8-membered rings arranged to form a tridimensional system of channels perpendicular to each other. There are many CHA-type materials such as natural chabazite mineral, low-silica synthetic chabazite, high-silica (SSZ-13) and silicoaluminophosphate (SAPO-34) chabazites. They are applied in several commercial processes: SAPO-34 is an archetype catalyst in commercial Dalian methanol to olefins process (DMTO) [1]. Na,Ca-CHA is applied for drying of acidic gases in the industry [2] and Cu-CHA materials (Cu-SSZ-13 and Cu-SAPO-34) are highly effective in selective catalytic reduction of nitrogen oxides (NOx), so they are applied for the removal of NOx in transportation diesel-powered engines [3,4]. The synthesis of alumosilicate chabazite materials is usually performed by employing zeolite Y (FAU-type) as both Si and Al source and the most commonly used organic structure directing agent (OSDA) is N,N,N-trimethyl-1-adamantammonium hydroxide (TMADAOH) [5]. Still, there is a demand to develop more environment-friendly synthesis routes and improve their performance in the mentioned applications as well as in the other potential fields of usage. For this reason, numerous studies with the aim to meet these requirements are conducted.

The acidic properties of zeolites (quantity and strength of Brønsted and Lewis acid sites, Al location and distribution, presence of framework defect sites and extra-framework species) affect the overall performance of zeolites as catalysts, sorbents and ion-exchangers [6]. For instance, in methanol dehydration reaction, the samples with paired Al sites accelerate the turnover rates by order of magnitude compared to SSZ-13 material with isolated sites [7]. It seems that the paired acid sites stabilize the surface methoxy species involved in an alternate dehydration mechanism. Further, CHA-type zeolites prepared from systems with different proportions of Al-comprising chemicals ($Al(OH)_3$ and FAU-type zeolite) have similar amount of acid sites, yet differ in the distribution of Al atoms [8]. Herein, CHA-type zeolites will be prepared from reaction mixtures with varying amounts of the OSDA. The Si environment, presence of various OH groups and diverse Al species will be identified in order to be able to prepare CHA-type zeolite materials of controllable acidic properties.

EXPERIMENTAL

A series of SSZ-13 zeolite materials was prepared using commercial FAU-type zeolite material CBV760 obtained from Zeolyst, KOH or NaOH, TMADAOH and doubly distilled water. The initial synthesis mixtures were obtained by admixing the appropriate amount of the chemicals and were subsequently heated at 150 °C. The respective molar oxide composition of the preparation systems as well as the corresponding heating period of time is listed in the Table 1. The obtained powders have been washed, dried, calcined at 600 °C and afterwards ion-exchanged with $[Co(H_2O)_6]^{2+}$ according to the procedure reported in [9]. The features of the prepared materials were characterized by powder X-ray diffraction (XRD), scanning electron microscopy (SEM), dynamic light scattering (DLS), thermogravimetric analysis (TGA), UV–VIS spectroscopy, nitrogen adsorption/desorption, as well as nuclear magnetic resonance (NMR), atomic absorption (AAS) and infrared spectroscopy (IR).

RESULTS AND DISCUSSION

The XRD patterns of the studied materials demonstrates they all present chabazite structure (Figure 1). The samples present Si/Al ratios of rather similar values that lie in the range of 12 to 19 (Table 1). The nitrogen adsorption/desorption experiments show the initial CHA samples exhibit high specific surface areas and micropore volumes as well as maximums of pore width distribution curves at about 0.73 nm that corresponds to the dimensions of the *cha* cage-defining ring [10].

Table 1. Molar oxide compositions of the initial synthesis mixtures, the period of heating time at 150 °C and the Si/al ratio of the end product of each reaction.

system	molar ratio of chemicals used for SSZ-13 synthesis	*t* / d	Si/Al
A1	1 SiO_2 : 0.005 Al_2O_3 : 0.25 KOH : 0.25 TMADAOH : 15 H_2O	6	12
A2	1 SiO_2 : 0.005 Al_2O_3 : 0.25 KOH : 0.125 TMADAOH : 15 H_2O	6	18
A3	1 SiO_2 : 0.005 Al_2O_3 : 0.2 KOH : 0.125 TMADAOH : 15 H_2O	10	19
A4	1 SiO_2 : 0.005 Al_2O_3 : 0.3 KOH : 0.125 TMADAOH : 15 H_2O	5	14
B1	1 SiO_2 : 0.005 Al_2O_3 : 0.25 NaOH : 0.25 TMADAOH : 15 H_2O	6	14
B2	1 SiO_2 : 0.005 Al_2O_3 : 0.25 NaOH : 0.125 TMADAOH : 15 H_2O	6	17
B3	1 SiO_2 : 0.005 Al_2O_3 : 0.2 NaOH : 0.125 TMADAOH : 15 H_2O	10	18
B4	1 SiO_2 : 0.005 Al_2O_3 : 0.3 NaOH : 0.125 TMADAOH : 15 H_2O	5	14

According to the TG results displayed in the Figure 2, the average content of the OSDA in the as-prepared materials is about 22 wt%. Laser light scattering data indicate the majority of the crystals in all systems is smaller than 1 μm. Based on the SEM micrographs, the morphology of the harvested crystals in all systems is found to be cubic, with a few intergrown particles. The analysis of IR spectra of the samples in the silanols band region indicates that the studied samples present isolated silanol groups. In the samples A1, A2 and A4 is observed a band at 3669 cm^{-1}. It is attributed to Lewis acid sites that could be correlated with extra-framework aluminium connected to the zeolite structure. Besides, these samples exhibit band assigned to internal silanols and a very broad band arising due to the silanol nests. On the other hand, only in the spectrum of the sample A3 are found the bands associated with Brønsted acid sites. In ^{27}Al magic angle spinning (MAS) NMR spectra of the studied series of the samples are observed both tetrahedral and octahedral Al species. Interestingly, there are two kinds of octahedral Al entities. A range of Si moieties (Q^4, Q^3, Q^2) was detected in the ^{29}Si MAS NMR spectra. Furthermore, the enhanced signals in ^{29}Si {^{1}H} CP MAS NMR spectra indicate the presence of the Q^3 Si(OH) groups as well as silanol nests defects.

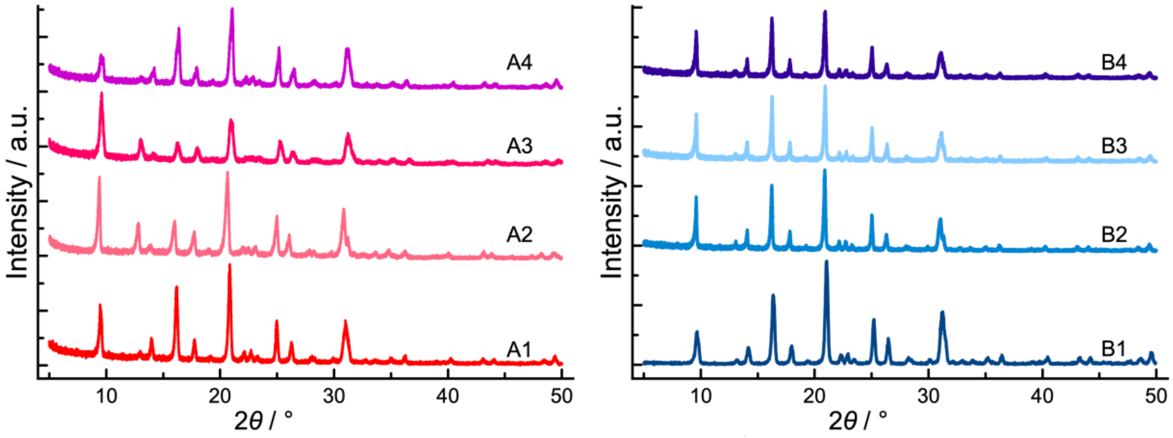

Figure 1. Powder X-ray diffraction patterns of the studied series of SSZ-13 materials.

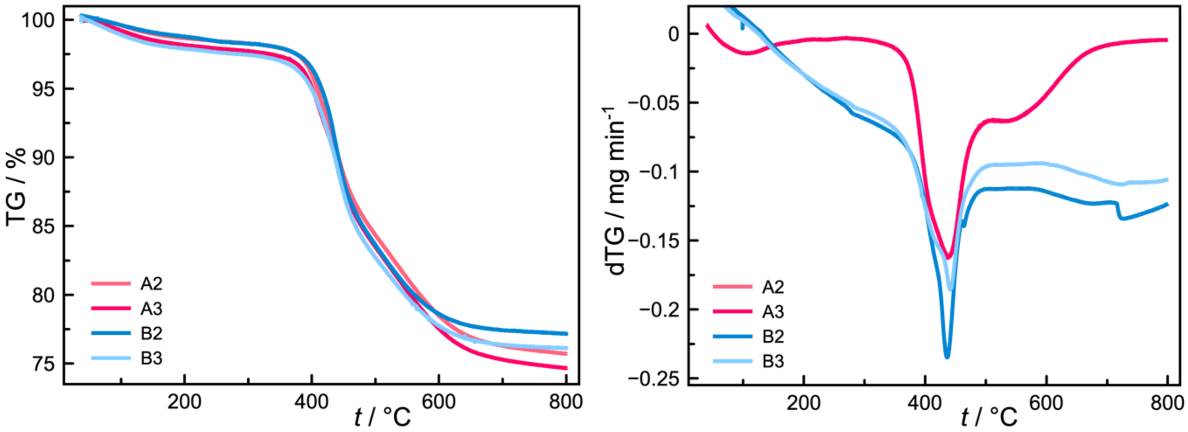

Figure 2. TGA and dTG curves of the selected studied SSZ-13 materials.

UV-VIS spectra confirm the presence of octahedrally coordinated Co entities in the samples. High weight fraction of Co in the exchanged samples suggests that there are paired Al sites (sequences Al−O(−Si−O)$_x$−Al, x = 1, 2, in the six-membered rings of the CHA framework) in the studied samples [11].

CONCLUSION

A series of nanosized high-silica SSZ-13 materials has been prepared employing TMADAOH as OSDA. Their properties have been modified via varying the alkali cation added to the initial synthesis mixture (K^+ or Na^+) as well as by changing the ratios K^+/TMADAOH and Na^+/TMADAOH. The impact of these parameters on the harvested CHA-type materials was investigated in terms of their phase, framework and chemical composition, morphological and textural features, acidic properties as well as structural defects. The results indicate that the present preparation method enables control of the Al distribution in the zeolite framework and consequently facilitated preparation of catalysts with predetermined performance.

ACKNOWLEDGEMENTS

This work has been supported by the Croatian Science Foundation under the project UIP-2019-04-4977.

REFERENCES

[1] P. Tian, Y. Wei, M. Ye and Z. Liu, *ACS Catal.*, 2015, **5**, 1922-1938.

[2] S. Sircar and A.L. Myers, in: "*Handbook of Zeolite Science and Technology*", S.M. Auerbach, K.A. Carrado, and P.K. Dutta (Eds.), Marcel Dekker Inc., New York – Basel, 2003, 1063-1102.

[3] J. Wang, H. Zhao, G. Haller and Y. Li, *Appl. Catal. B*, 2017, **202**, 346-354.

[4] M. Moliner, C. Martínez and A. Corma, *Chem. Mater.*, 2014, **26**, 246-258.

[5] S.I. Zones, US patent US2008007565.

[6] A. Palčić and V. Valtchev, *Appl. Catal. A*, 2020, **606**, 117795.

[7] J.R. Di Iorio, C.T. Nimlos and R. Gounder, *ACS Catal.*, 2017, **7**, 6663-6674.

[8] T. Nishitoba, N. Yoshida, J.N. Kondo and T. Yokoi, *Ind. Eng. Chem. Res.*, 2018, **57**, 3914-3922.

[9] C. Li, A. Vidal-Moya, P.J. Miguel, J. Dedecek, M. Boronat, and A. Corma, *ACS Catal.*, 2018, **8**, 7688-7697.

[10] J.H. Kang, F.H. Alshafei, S. Zones and M.E. Davis, *ACS Catal.*, 2019, **9**, 6012-6019.

[11] J.R. Di Iorio, S. Li, C.B. Jones, C.T. Nimlos, Y. Wang, E. Kunkes, V. Vattipalli, S. Prasad, A. Moini, W.F. Schneider and R. Gounder, *J. Am. Chem. Soc.*, 2020, **142**, 4807-4819.

Fe AND Ce EXCHANGED ZSM-5 ZEOLITES AS ELECTROCATALYSTS FOR ORR AND OER REACTIONS

Jadranka Milikić[1]*, Biljana Šljukić*[1]*, Ivana Stojković Simatović*[1]*, Ljiljana Damjanović-Vasilić*[1]*,*
Srna Stojanović[1]*, Vladislav Rac*[2]*, Vesna Rakić*[2]
[1]*University of Belgrade - Faculty of Physical Chemistry, Studentski trg 12-16, 11000 Belgrade, Serbia*
[2]*University of Belgrade - Faculty of Agriculture, Nemanjina 6, 11080 Zemun- Belgrade, Serbia*
E-mail: vladarac@agrif.bg.ac.rs

ABSTRACT

Samples of zeolite ZSM-5, containing Ce and Fe, were tested as electro-catalysts for oxygen evolution reaction and oxygen reduction reaction, respectively, which play significant roles in energy conversion systems, such as fuel cells, rechargeable metal-air batteries and water electrolyzers. Metallic species were introduced by ion-exchange. Zeolite ZSM-5 was used in its conventional microporous form, but also in a hierarchical, mesopore-containing form, obtained by alkaline-induced demetallation. The samples were characterized by chemical analysis, low-temperature nitrogen adsorption, X-ray diffraction and diffuse reflectance UV-Vis spectroscopy. Electro-catalytic activity studies were performed by cyclic/linear sweep voltammetry in alkaline media. Among the investigated samples, the hierarchical ZSM-5 exchanged with Fe was shown to possess the best properties/performance, for both oxygen evolution and oxygen reduction reaction. In the case of oxygen reduction, the hierarchical sample exhibited the highest onset potential, while in the oxygen evolution reaction, its use resulted in the highest current density, as well as the lowest onset potential. No direct correlation between electro-catalytic activity and the amount of the metallic species in the zeolites were found. The superior behavior of the hierarchical sample could be related to the high degree of dispersity of iron species, as it was detected by diffuse reflectance UV-Vis spectroscopy.

Key words: bifunctional electro-catalysts, oxygen evolution reaction, oxygen reduction reaction, ion-exchanged zeolites.

INTRODUCTION

Due to many adverse environmental issues, related to the use of fossil fuels, there is an urgent need for efficient “green” energy conversion systems. In the domain of electrochemical conversion pathways, several systems, most notably water electrolysers, fuel cells and metal-air batteries have been extensively studied [1]. A series of electrochemical reactions lie at the core of these systems, including oxygen evolution reaction (OER) and oxygen reduction reaction (ORR). Both reactions demand a suitable catalyst and can be performed in alkaline or acidic media, with alkaline electrolytes being regarded as more favourable [2].

The OER reaction in alkaline conditions can be summarized as:

$$4OH^- \leftrightarrow 2H_2O + O_2 + 4e^- \qquad E^0 = +0.40\ V \qquad (1)$$

The ORR reaction can proceed via a “direct” reaction:

$$O_2 + 2H_2O + 4e^- \rightarrow 4OH^- \qquad E^0 = +0.401\ V \qquad (2)$$

or a multistep pathway:

$$O_2 + H_2O + 2e^- \rightarrow HO_2^- + OH^- \quad E^0 = -0.065\ V \qquad (3)$$

$$HO_2^- + H_2O + 2e^- \rightarrow 3OH^- \qquad E^0 = +0.867\ V \qquad (4)$$

$$2HO_2^- \rightarrow 2OH^- + O_2 \qquad (5)$$

Typically, noble metal-based catalysts are the most efficient for ORR and OER. However, due to the inherent differences of the reactions themselves, especially different electric potentials, only a small number of them have been proven to be applicable for both reactions Hence, formulating highly active and durable electro-catalysts, notably bifunctional ones, is still a challenge. Among various materials, zeolite-based catalysts have been probed with some success [3,4]. In this paper, the applicability of Ce and Fe exchanged zeolite ZSM-5 for OER and ORR is considered, including the influence of the porosity alteration.

EXPERIMENTAL

Starting from zeolite ZSM-5 (Zeolyst; [SiO_2/Al_2O_3] = 23), ion-exchanged samples were prepared by ion exchange, at room temperature Cerium was introduced using $Ce(NO_3)_3{\bullet}6H_2O$ (Aldrich, 0.003 M, 5g zeolite/L) and iron using $Fe_2(C_2O_4)_3{\bullet}6H_2O$ (Sigma, 0.01 M, 3g/50 mL). The mixtures were stirred for 7 days and subsequently washed with deionized water, dried at 120 °C and calcined in air at 500 °C for 5h. For ion exchange with Fe, a hierarchical form of the starting zeolite was also used. The hierarchical ZSM-5 was prepared prior to ion-exchange, using demetallation with NaOH (0.2 M, 90 ^{0}C, 30 min), followed by an acid wash (0,1 M HCl, 25 ^{0}C, 6 h). The obtained samples were labelled as Ce-ZSM-5, Fe-ZSM-5 and Fe-ZSM-5H (hierarchical sample). All samples were characterized using low temperature N_2 adsorption (Micromeritics 2010, pre-treatment at 400 °C, 4 hours), X ray diffraction (Rigaku Ultima IV diffractometer. Cu Kα radiation, λ=1.54178 Å, from 4° to 50° 2θ, 0.020° step, 1°/min), diffuse reflectance UV-Vis spectroscopy (Agilent Cary 5000 UV-Vis-NIR) and elemental chemical analysis.

Catalytic inks were prepared by ultrasonically dispersing 5 mg of the corresponding electro-catalyst and 0.6 mg Vulcan XC72R in 40 μL of 2 wt. % polyvinylidene difluoride solution in N-methyl 2-pyrrolidone, for 30 min. The working electrodes were prepared by pipetting 10 μL of each catalytic ink onto glassy carbon (GC) supports and leaving it to dry at room temperature. Current densities were calculated using the geometric area of GC supports. All electrochemical measurements were done using Ivium Potentiostat/Galvanostat in a one–compartment glass cell of 40 mL volume with Pt foil and saturated calomel electrode (SCE), serving as counter and reference electrodes, respectively. All potentials within this paper are given relative to the reversible hydrogen electrode (RHE) reference. For ORR studies, the cyclic voltammograms (CV) were recorded in 1 M KOH (analytical reagent grade, Fisher Chemicals) solution saturated with O_2 (>99.999%, Messer), scanning the potential from 1.1 to 0.3 V at scan rate of 20 mV/s. Linear sweep voltammograms (LSV) with RDE were recorded at scan rate of 5 mV/s and rotation rates ranging from 200 to 1800 rpm set by Pine AFCPRB rotator. For OER studies, LSVs were run in 1 M KOH electrolyte solution from the open circuit potential (OCP) up to 2 V at scan rate of 5 mV/s.

RESULTS AND DISCUSSION

ORR at different samples was systematically studied in O_2-saturated 1 M KOH. Control CVs of all three materials, recorded in deaerated 1 M KOH solutions, showed only small redox peaks corresponding to Ce or Fe reduction (not shown). However, upon saturation of the solution with O_2, a notable increase of current density could be seen, with the appearance of a well-defined peak corresponding to the oxygen reduction (Figure 1A).

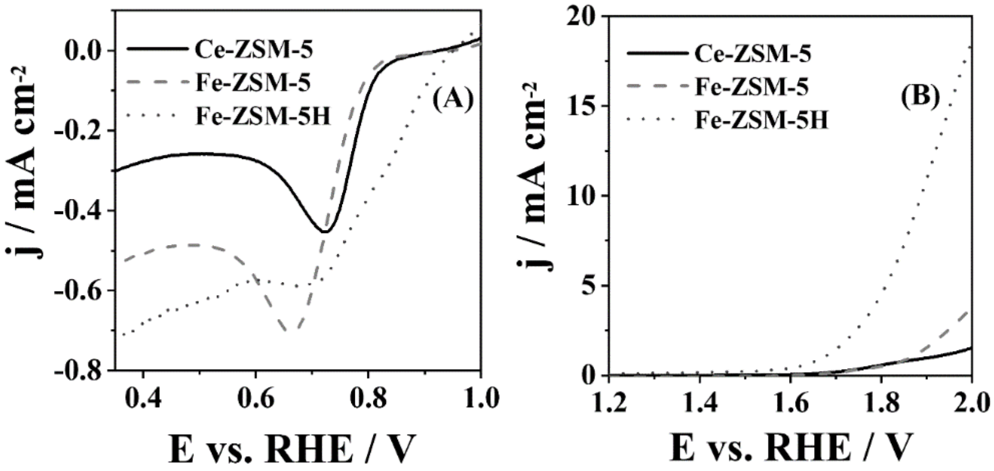

Figure 1. Voltammetric responses of three studied zeolites under ORR (A) and OER (B) polarization conditions.

One of the key parameters for evaluating the performance of ORR catalysts is the onset potential (the more positive onset potential, the better the activity for the ORR). CV of the Fe-ZSM-5H in O_2-saturated 1 M KOH solution showed the ORR onset potential of 0.93 V. ORR onset potentials in case of Ce-ZSM-5 and Fe-ZSM-5 were found to be similar and less positive (Figure 1A, Table 1). In the case of OER (Figure 1B), lower values of the onset potential are favourable. Among the investigated samples, the lowest onset potential (defined as the potential to reach the current density of 1 mA/cm^2) was detected in case of Fe-ZSM-5H, indicating its highest activity. This was further confirmed by the highest current density at the overpotential of 400 mV recorded using this sample.

Table 1. Comparison of parameters for evaluating the performance of ORR and OER catalysts.

	Ce-ZSM-5	Fe-ZSM-5	Fe-ZSM-5H
ORR			
E_{onset} (V)	0.83	0.82	0.93
E_p (V)	0.72	0.66	0.68
j_p (mA/cm^2)	-0.46	-0.71	-0.59
OER			
E_{onset} (V)	1.86	1.86	1.74
j_{400} (mA/cm^2)	0.06	0.06	0.67

It is interesting that the electro-catalytic results did not necessarily correlate with the amounts of Ce or Fe present in the samples (1.0 % Ce, 0.26 % Fe in Fe-ZSM-5 and 0.35 % Fe in FeZSM-5H). Rather, the superior performance of the hierarchical sample Fe-ZSM-5H could be attributed to the high dispersity of Fe species in the zeolite, which was evidenced by DR UV-Vis spectra (Figure 2). The spectra of the conventional microporous Fe-ZSM-5 revealed the presence of a large amount of Fe oxide species (> 400 nm), which could lower the amount of actually active Fe species. On the other hand, in Fe-ZSM-5H mostly isolated Fe ions (< 300 nm) and small oligoclusters (300 - 400 nm) were detected [5]. The difference in Fe dispersity in Fe-ZSM-5 and Fe-ZSM-5H can be related to the existence of mesopores in the hierarchical sample (pore size distribution not shown here), and the related increase of mesoporous/external surface (≈ 80 m^2), measured by nitrogen adsorption.

To further investigate the electro-catalytic activity of Fe exchanged zeolites, OER reaction was conducted in the presence of H_2O_2 [6]. The addition of peroxide (results not shown here) significantly enhanced the activities of both samples; the superior behaviour of the hierarchical sample was even more pronounced, in terms of both onset potential and current density.

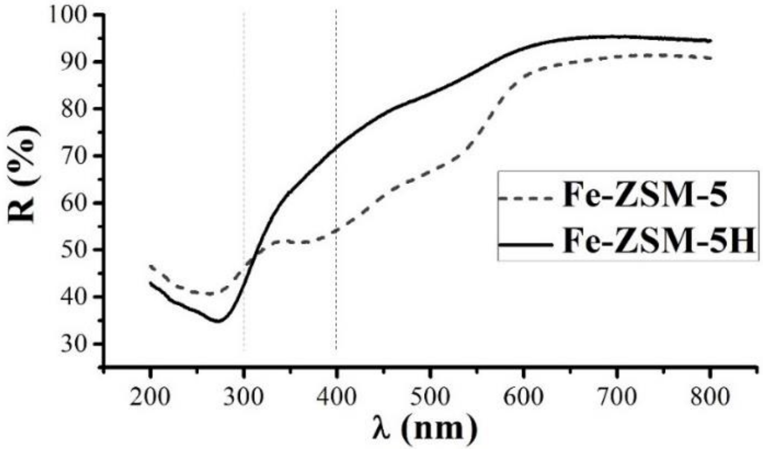

Figure 2. DR UV-Vis spectra of Fe-ZSM-5 and Fe-ZSM-5H.

CONCLUSION

Transition metal-exchanged ZSM-5 zeolite samples were successfully applied as electro-catalysts for oxygen evolution and oxygen reduction reactions. Although the presented results can only be considered as preliminary, they clearly show that the modifications of the zeolitic porous structures prior to ion exchange can significantly improve their electrochemical performance. The overall highest activity, as judged by the values of onset potentials and current densities, was measured for the hierarchical Fe-ZSM-5H sample. It is very probable that its favourable properties were due to the induced mesoporosity, which altered the form of the introduced iron species. Hence, in order to further improve zeolite-based electrocatalysts for ORR and OER, special attention should be paid to the nature of metallic species in the zeolitic framework (isolated ions, small oxide clusters, large oxide particles) and the related porosity variations of the starting zeolitic materials.

REFERENCES

[1] S. Ghosh and R.N. Basu, *Nanoscale*, 2018, **10**, 11241-11280.

[2] S. Li, X. Hao, A. Abudula and G. Guan, *J. Mater. Chem. A*, 2019, **7**, 18674-18707.

[3] J. Milikić, M. Vasić, L. Amaral, N. Cvjetićanin, D. Jugović, R. Hercigonja and B. Šljukić, *Int. J. Hydrog. Energy*, 2018, **43**, 18977-18991.

[4] J. Milikić, R.C.P. Oliveira, I. Stoševski, J. Krstić, R. Hercigonja, Š. Miljanić, D.M.F. Santos and B. Šljukić, *New J. Chem.*, 2019, **43**, 14270-14280.

[5] M.S. Kumar, M. Schwidder, W. Grunert, U. Bentrup and A. Bruckner, *J. Catal.*, 2006, **239**, 173-186.

[6] H. Dotan, K. Sivula, M. Gratzel, A. Rothschild and S.C. Warren, *Energy Environ. Sci.*, 2011, **4**, 958–964.

PAST AND FUTURE OF ZEOLITE MATERIALS

Valentin Valtchev[1,2]
[1]Laboratoire Catalyse et Spectrochimie, Normandie University, ENSICAEN, UNICAEN, CNRS, F-14050 Caen, France
[2]The ZeoMat Group, Qingdao Institute of Bioenergy and Bioprocess Technologies, CAS, Laoshan District, CN-266101 Qingdao, China
E-mail: valentin.valtchev@ensicaen.fr

The zeolite materials have been diligently serving society almost 60 years. However, after serving more than half a century as heterogeneous catalysts, molecular sieves, and ion exchangers in a variety of industrial (Oil refining, Petro- and Fine- chemicals production, etc.) and environmental (exhaust gas treatment, heavy and radioactive ion sequestration, water purification) applications the molecular sieve zeolites face new challenges. These new challenges come with the societal demand for cleaner, safer, and sustainable technology.

The present lecture is devoted to the prospects of zeolites in light of the societal and energy challenges of the current time. Recent advances in the *in situ* and *post-synthesis* control of zeolite properties, with examples based on industrial relevant materials, will be revised. The advantages, disadvantages, and limits of the *in situ* and *post-synthesis* methods of zeolite properties control will be discussed. Amongst the objectives of the lecture is to anticipate future developments in the field of crystalline microporous materials and the place of zeolite in the energy transition.

THE DURABILITY PROPERTIES OF CONCRETE INCORPORATING ZEOLITIC TUFF

Zinoviy Blikharskyy [1], Khrystyna Sobol[1], Taras Markiv[1], Oksana Pozniak[1], Wojciech Franus[2]
[1]Lviv Polytechnic National University, Bandera str.12, 79000, Lviv, Ukraine
[2]Lublin University of Technology, Nadbystrzycka 40, 20-618 Lublin, Poland
E-mail: taras.y.markiv@lpnu.ua

ABSTRACT

The corrosion resistance of concrete containing zeolitic tuff in different aggressive environment was investigated in the article. Objective of this work was investigation of the behaviour of concretes incorporating 10% by mass of zeolitic tuff and superplasticizer, as well as 10% by mass of the zeolitic tuff, a superplasticizer and an air-entraining agent as well as concretes without zeolitic tuff, which contain only a superplasticizer and an air-entraining agent in Na_2SO_4 and $MgCl_2$ solutions. The chemical composition of the zeolitic tuff and Portland cement used in this research was determined using X-ray spectrometer ARL 9800 XP. The results of the research show that fresh concrete mixture incorporating zeolitic tuff due to its porous structure and high surface area demands a higher amount of superplasticizer to obtain the targeted slump flow. The results also reveal the effectiveness of the zeolitic tuff use to improve corrosion resistance of concretes exposed to Na_2SO_4 and $MgCl_2$ solutions.

Key words: zeolitic tuff, pozzolanic reaction, corrosion resistance, durability.

INTRODUCTION

The durability properties of concrete structures play an important role in the infrastructure of cities. The properties of concrete depend on different factors, such as type of Portland cement, correctness of concrete mix design, placement and curing. It is well known that the use of pozzolans instead of cement results in an increase of the concrete durability in different aggressive environments depending on the exposure classes [1,2].

Zeolitic tuff as a natural pozzolanic material possesses unique properties, which makes it possible to use it in some regions of the world in the construction industry, because of its lower cost and accessibility. In spite of the zeolitic tuff being crystalline, it is characterised by proper pozzolanic activity [3,4]. The lime reactivity of the zeolitic tuff (clinoptilolite type) is comparable to silica fume (SF) and higher than fly ash (FA) [3-5]. Calcium hydroxide, which has been produced during period of cement hydration reacts with the reactive SiO_2 and Al_2O_3 of zeolitic tuff producing calcium hydrosilicates. Therefore, concretes containing zeolitic tuff become more durable due to higher resistance to the expansion caused by sulphate attack and lime leaching by flowing waters as a result of the reduction of free $Ca(OH)_2$ in the hardened concrete [6,7]. Many researchers concluded that zeolitic tuff improves the compressive strength of concrete if its content is less than approximately 10% by mass [8,9]. A higher amount of zeolitic tuff can result in the reduction of the compressive strength. The particle size distribution also plays very important role [10].

Some researchers also reported that concrete incorporating zeolitic tuff has improved durability properties such as higher resistance to freezing/thawing cycles, drying shrinkage and water penetration depth, but various types, structures and purities can have different influence on the concrete strength and durability [11-13].

The aim of the article is to study the influence of zeolitic tuff (Sokyrnytsia, Ukraine) on the behaviour of concrete exposed to different aggressive environments.

EXPERIMENTAL

The zeolitic tuff of clinoptilolite type and Portland cement CEM I 42.5R were used in this study. The chemical composition of the zeolitic tuff and Portland cement was determined using X-ray spectrometer ARL 9800 XP and presented in Fig. 1. Zeolitic tuff in comparison with Portland cement has a higher content of silica, alumina and iron oxides. Namely these oxides are responsible for the pozzolanic activity of zeolitic tuff.

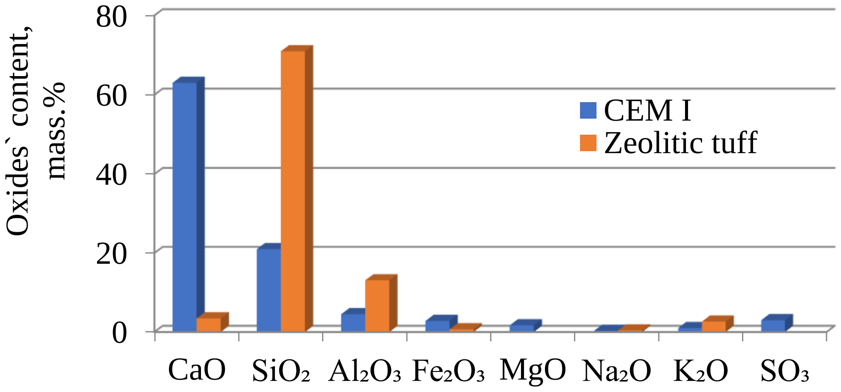

Figure 1. Chemical composition of Portland cement (CEM I) and natural zeolitic tuff.

The properties of Portland cement were determined according to EN 196. The specific surface of Portland cement was 425 m^2/kg. The water demand was 27%, initial and final setting time were 200 and 260 min, respectively. The compressive strength of cement CEM I 42.5R after 2 and 28 days was 30.5 and 55.0 MPa, respectively.

The properties of aggregates were tested according to PN-EN 1097 and conform to the requirements of European norms. Polycarboxylate-based superplasticizer and an air-entraining agent, based on abietate salts, were used in this study. Four concrete mixtures, as in previous research [11], were prepared, namely the control concrete mixtures without zeolitic tuff, which contained 1.22% by mass of superplasticizer (Z0P), 1.22% by mass of superplasticizer and 0.3% by mass of air-entraining agent (Z0PA) as well as two mixtures incorporating 10% by mass of the zeolitic tuff instead of Portland cement and 1.64% by mass of superplasticizer (Z10P) and 1.64% by mass of superplasticizer and 0.3% by mass of air-entraining agent (Z10PA).

Nominal mixture proportions of fine-grained concretes were cement:sand = 1:1.88 and (cement + zeolite):sand = 1:1.88, except that coarse aggregate was not used. The use of zeolitic tuff results in a decrease of the workability of the concrete mixture. It was compensated by using an extra amount of superplasticizer. The higher water demand of concrete mixtures containing zeolitic tuff is caused by its porous microstructure. An air-entraining agent was used to increase the durability properties of concretes.

The corrosion resistance was determined using 40x40x160 mm prisms. Three samples for each test were prepared, demolded 24 h after casting, and stored 6 and 12 months in the different environment, namely in a water, Na_2SO_4 solution with a concentration of SO_4^{2-} 10 g/l and $MgCl_2$ solution with a concentration of Mg^{2+} 10 g/l. Then the coefficient of corrosion resistance (CR) was determined as the ratio of the strength of the samples in an aggressive environment to the strength of similar samples in water.

The morphology and chemical composition of main mineral components of the studied materials were determined using scanning electron microscope SEM FEI Quanta 250 FEG, equipped with EDS.

RESULTS AND DISCUSSION

The durability properties of concrete are one of the key factors on the way to the sustainable development of construction industry. Some of them were studied in the previous research [11]. It was established that zeolitic tuff used in an optimal amount (10% by mass) in spite of its pores structure was an effective component of concrete. It results in the increase of the resistance to freezing and thawing damage, the decrease of drying shrinkage and the water penetration depth. The study of corrosion resistance revealed that the coefficient of corrosion resistance of concretes incorporating 10% by mass of zeolitic tuff is higher in both $MgCl_2$ and Na_2SO_4 aggressive environments. The coefficient of CR is higher for concrete specimens exposed to Na_2SO_4 solution by approximately 1.5 times in comparison with concretes exposed to $MgCl_2$ aggressive environment (Fig. 2).

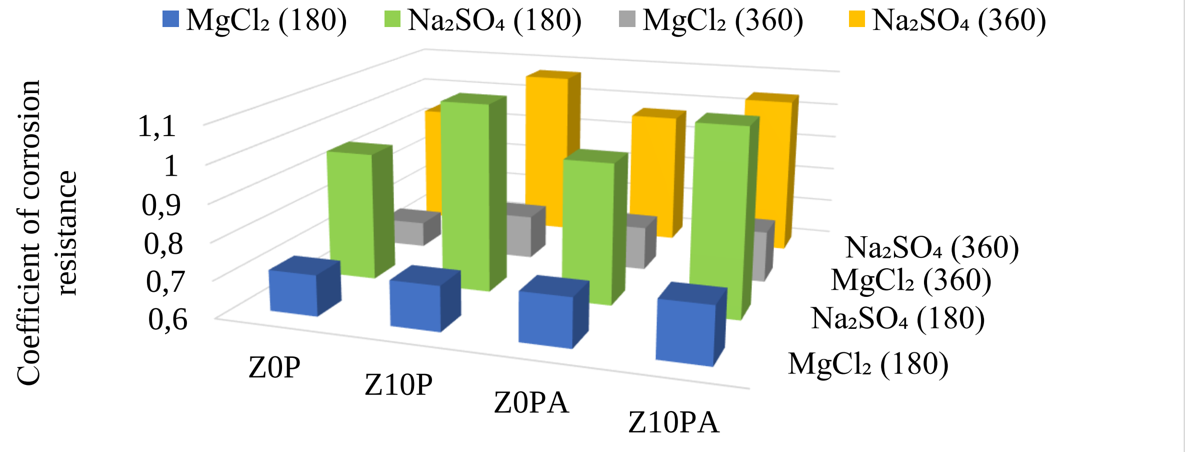

Figure 2. Coefficients of corrosion resistance of fine-grained concrete, determined by the results of compressive strength tests.

According to the scanning electron microscopy data, the microstructure of fine-grained concrete without zeolitic tuff, exposed for 180 days to $MgCl_2$ solution, exhibited a separate polyhedral block shape, which was cemented closely with other hydration products as indicated in Fig. 3 a. Loose formations of $Mg(OH)_2$, which is formed as a result of chemical reaction between calcium hydroxide (Portlandite) and magnesium chloride in an aggressive environment, is observed on the surface of concrete. These formations accumulate in the pores of the fine-grained concrete and do not interfere with the diffusion of Ca^{2+} ions from the deep layers to the surface. As the concentration of $Ca(OH)_2$ decreases, high calcium hydrosilicates and hydroaluminates begin to break down, leading to the loss of concrete durability properties. The microstructure of fine-grained concrete without mineral additions (Fig. 3 c), exposed for 180 days to Na_2SO_4 solution, is characterized by a fine-crystalline structure, long prismatic crystals of the ettringite. The crystallization of the ettringite is accompanied by an increase in volume by 2.5-2.86 times. The rapid growth of ettringite crystals with prolonged exposure to sulphates causes the destruction of the concrete structure. The formation of substances, such as $Mg(OH)_2$, ettringite, which are produced in aggressive environments was confirmed by the results of microprobe analysis. If zeolitic tuff is added, the surplus SiO_2 reacts with calcium hydroxide producing progressively more low calcium C–S–H and as a result more refined and compact structure resulting in the improvement of the concrete durability in both aggressive environments (Fig. 3, b, d).

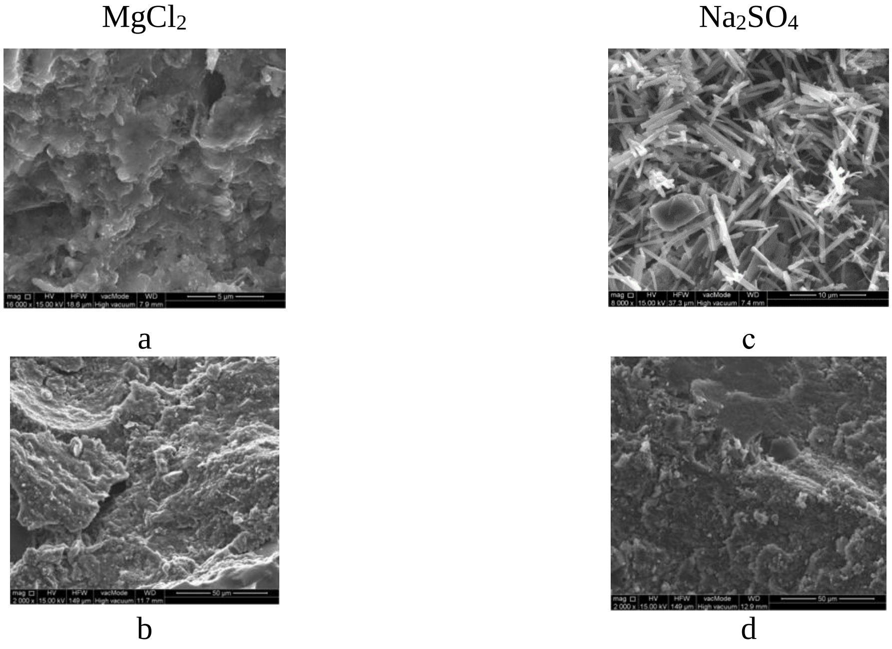

Figure 3. Microstructure of specimens ZOP without mineral additions (a, c) and with 10 % by mass of zeolitic tuff Z10P (b, d), which were exposed to $MgCl_2$ and Na_2SO_4 solutions, respectively.

CONCLUSION

This paper considers the issues of development of effective concrete containing zeolitic tuff. The most important conclusions are that incorporation of cement replacement materials, such as zeolitic tuff in spite of its pores structure allows to improve the resistance of such concrete against aggressive environments such as Na_2SO_4 and $MgCl_2$ solutions improving the durability properties of concretes.

REFERENCES

[1] Y. Kocak, E. Tasci and U. Kaya, *Constr. Build. Mater.*, 2013, **47**, 720–727.
[2] Kh. Sobol, T. Markiv, V. Terlyha and W. Franus, *Bud. Archit.*, 2015, **14(1)**, 105-113.
[3] W. Franus and K. Dudek, *Geol Carpath.*, 1999, **50**, 23-24.
[4] M. Najimi, J. Sobhani, B. Ahmadi and M. Shekarchi, *Constr. Build. Mater.*, 2012, **35**, 1023–1033.
[5] B. Uzal and L. Turanli, *Cem. Concr. Compos.*, 2012, **34**, 101–109.
[6] M. Sanytsky, Kh Sobol and T. Markiv, "*Modified composite cements", Lviv Polytechnic National University Publishing House*, Lviv-Ukranian, 2010, 132.
[7] D. Caputo, B. Liguori and C. Colella, *Cem. Concr. Compos.*, 2008, **30**, 455–462.
[8] D. Jana, *in: Proceedings of the twenty-ninth conference on cement microscopy Quebec City, PQ, Canada*, 2007.
[9] T. Markiv, O. Huniak and Kh. Sobol, *Theory Pract. of Build.*, 2014, **781**, 116-121.
[10] M. Sanytsky, A. Usherov-Marshak, T. Kropyvnytska and I. Heviuk, *Cem. Wapno, Beton.*, 2020, **25(5)**, 416-427.
[11] T. Markiv, Kh. Sobol, M. Franus and W. Franus, *Arch. Civ. Mech. Eng.*, 2016, **16**, 554–562.
[12] F. Sabet, N. Ali and M. Shekarchi, *Constr. Build. Mater.*, 2013, **44**, 175–184.
[13] B. Ahmadi and M. Shekarchi, *Cem. Concr. Compos.*, 2010, **32**, 134–141.

Ni/ZSM-5 AS EFFICIENT CATALYST FOR THE SELECTIVE HYDROGENATION OF LEVULINIC ACID TO γ-VALEROLACTONE IN VAPOR PHASE

Hue-Tong Vu[1], *Andrii Kostyniuk*[1], *Petar Djinović*[1], *Miha Grilc*[1,2], *Blaž Likozar*[1,2], Nataša Zabukovec Logar[1,2], *Nataša Novak Tušar*[1,2]
[1] National Institute of Chemistry, Hajdrihova 19, 1000 Ljubljana, Slovenia
[2] University of Nova Gorica, Vipavska 13, 5000 Nova Gorica, Slovenia
E-mail: tong.vu@ki.si

ABSTRACT

In search for efficient and robust catalysts for the continuous vapor-hydrogenation of biomass-derived levulinic acid (LA) to γ-valerolactone (GVL), Ni supported on ZSM-5 zeolites were investigated. This study provides an insight into the correlations between the catalyst properties and catalytic activity in the LA hydrogenation in a packed-bed reactor. The preliminary results show that the acid properties play a role in the product selectivity of the hydrogenation of LA in *iso*-propanol. The GVL formation is favoured by catalysts with a high fraction of Brønsted acid sites in proximity of the Ni active sites.

Key words: vapor-phase hydrogenation, levulinic acid, GVL, Ni/ZSM-5, packed-bed reactor.

INTRODUCTION

Biomass valorization, i.e., transforming abundant carbon-containing resources into high-value chemicals, has been the topic of a large number of studies [1]. Among these, the hydrogenation of biomass-derived levulinic acid (LA) to γ-valerolactone (GVL) has gained increasing attention [2]. GVL is considered as a platform chemical and can be found in a plethora of industrial applications. The conversion of LA into GVL requires both the acid and redox properties. With respect to acid functionality, ZSM-5 zeolites with their intrinsic and tunable acid properties have been used as solid catalysts in many catalytic applications. Additionally, ZSM-5 zeolites also provide high specific surface area to support active metal sites and great (hydro)thermal stability. The latter is especially crucial for continuous heterogeneously-catalyzed processes in vapor phase. Thus, in the current study, catalysts consisting of zeolite ZSM-5 functionalized with Ni are employed in the vapor-phase hydrogenation of LA in a packed-bed reactor. The tunability of the acid properties of ZSM-5 zeolites by varying n_{Si}/n_{Al}-ratio allows a systematic investigation of their correlation with the catalytic activity of Ni/ZSM-5 catalysts in the hydrogenation of LA. The obtained findings enable the tailoring of product selectivity and thus a higher yield of the target product (GVL) is obtained while maintaining high productivity. With that in mind, a series of ZSM-5 zeolites with different Si-to-Al molar ratios, i.e., 13, 21 and 28, were synthesized using a „green“ template-free method. The obtained zeolites were impregnated with Ni aiming at various Ni content (ω_{Ni} = 1, 3 and 5 wt.%). To unveil the correlations between material properties and catalytic activity, the bifunctional Ni/ZSM-5 catalysts were characterized and tested in the vapor-phase hydrogenation of LA in *iso*-propanol.

EXPERIMENTAL

ZSM-5 zeolites with different n_{Si}/n_{Al} were prepared using a “green” surfactant-template free method, which was published in a previous work [3]. Subsequently, the obtained zeolites were loaded with Ni via incipient-wetness impregnation using $Ni(NO_3)_2.6H_20$ aiming at different Ni content, i.e., 1, 3 and 5 wt.%. The obtained catalysts are labelled as *x*Ni/ZSM-5-*y* with *x* refers to Ni content and *y* is Si-to-Al molar ratio (n_{Si}/n_{Al}).

The catalytic experiments were carried out in a Microactivity Reference reactor (PID Eng&Tech). In a typical experiment, 100 mg of catalyst were mixed with 100 mg of glass beads (both having particle size < 100μm), which were then sandwiched by quartz wool in a tubular reactor. The catalysts were first heated and treated at 400 °C under a N_2 flow (Q_{N_2} = 30 ml min^{-1}) for 1 h. Subsequently, the gas stream was switched to H_2 (Q_{H_2} = 30 ml min^{-1}) for catalyst reduction while holding at 400 °C. The reduction was performed for 2 h. Subsequently, the reactor was cooled down and kept at 250 °C. The reaction solution, i.e., 1 wt.-% LA in *iso*-propanol solvent, was fed at a flow rate of 0.03 g h^{-1} using a Gilson HPLC pump. The liquid products were collected every hour after reaching the reaction steady state (approximately after 120 min). The liquid products were identified and quantified by a GC-MS (Shimadzu, QP 2010) using a ZebronTM ZB–5MSi capillary column (60 m x 0.25 mm x 0.25 μm). The concentrations of the reaction products, i.e., LA, γ-valerolactone (GVL), angelica lactone (AL), *iso*-propyl levulinate (PL), pentanoic acid (PA) and *iso*-propyl pentanoate (PP), were determined using calibration curves of commercial LA, GVL, AL and self-prepared PL, PP via external calibration technique. The relative errors of measured concentrations were below 3% (for LA, GVL, AL and PA) and below 5% (for PL and PP).

RESULTS AND DISCUSSION

A series of ZSM-5 zeolites with different Si-to-Al ratios, i.e., n_{Si}/n_{Al} = 13, 21 and 28 (determined by SEM-EDX), were successfully synthesized. All catalysts exhibit the MFI framework structure as confirmed by XRD. In terms of textural properties, a type I isotherm, which is typical for highly microporous ZSM-5 zeolites, was recorded regardless of Si-to-Al ratios and Ni content. Additionally, the N_2 sorption analysis results show that all employed catalysts possess comparable specific surface area (400 m^2 g^{-1}) and pore width (0.8 nm) despite various Ni content, i.e., ω_{Ni} = 0.8, 1.6 and 3.4 wt.% (determined by SEM-EDX). This suggests a great preservation of the structural and textural properties of Ni/ZSM-5 after the introduction of Ni via incipient-wetness impregnation.

To investigate the catalytic activity, the bifunctional Ni/ZSM-5 catalysts were investigated in the vapor-phase hydrogenation of LA in a fixed-bed reactor under ambient pressure. The hydrogenation of LA into γ-valerolactone (GVL) underwent angelica lactone (AL) formation as suggested by the detection of AL in all catalytic experiments, i.e., Y_{AL} = 1 – 7%, under investigated conditions (T = 250 °C, c_{LA} = 1 wt.-%, Q_{LA} = 0.03 g min^{-1} and Q_{H_2} = 30 ml min^{-1}). In addition to the target product GVL, the detection of *iso*-propyl levulinate (PL) confirms the occurrence of the competitive acid-catalyzed esterification between LA and the solvent *iso*-propanol regardless of the catalyst employed. Furthermore, the hydrogenated products of GVL and PL, i.e., pentanoic acid (PA) and *iso*-propyl pentanoate (PP), respectively, are also present in the products mixture. A proposed reaction pathway is displayed in Figure 1.

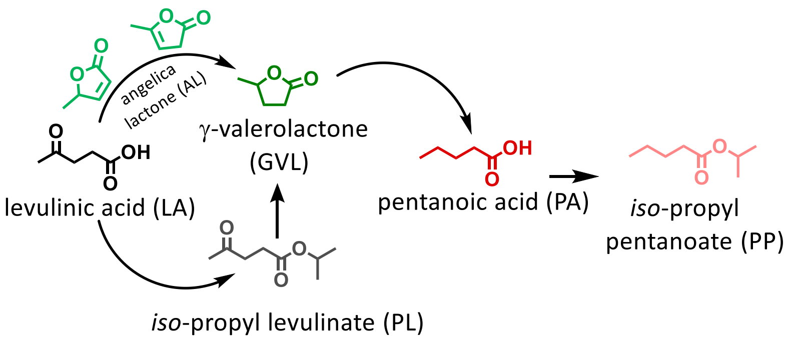

Figure 1. Proposed reaction pathway of the hydrogenation of LA in *iso*-propanol.

The catalytic results are depicted in Figure 2. With increasing the Ni content, a gradual gain in the yield of the target product GVL, i.e., from 2% to 37% and 43%, was obtained due to the higher hydrogenation activity (Figure 2, left). Additionally, no GVL was recorded in the hydrogenation of LA using ZSM-5-21 under identical conditions. These observations confirm the key role of Ni active sites, which is proportional to the hydrogenation activity of the catalysts, in the conversion of LA into GVL.

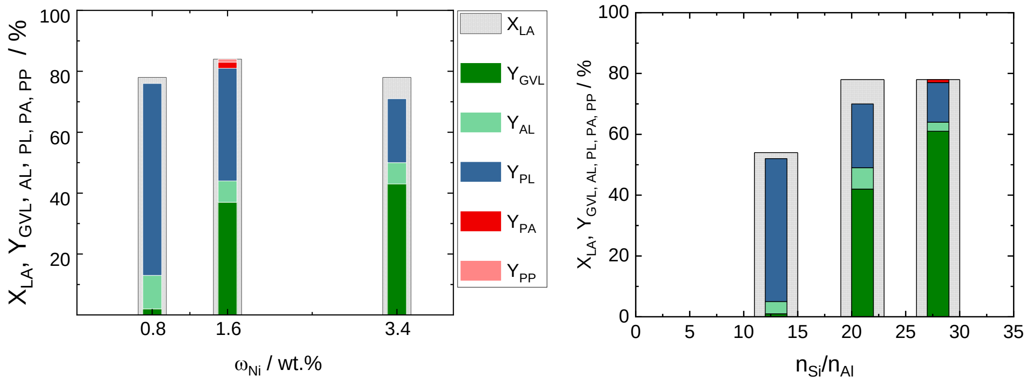

Figure 2. LA conversion (X_{LA}), yield (Y) of products (GVL, AL, PL, PA and PP) over the bifunctional catalysts *x*-ZSM-5-21 with $x = \omega_{Ni}$ = 0.8, 1.6 and 3.4 wt.% (left) or 3.4 wt.% Ni supported on ZSM-5-*y* with $y = n_{Si}/n_{Al}$ = 13, 21 and 28 (right). Reaction conditions: m_{cat} = 100 mg, Q_{H_2} = 30 ml min^{-1}, c_{LA} = 1 wt.-%, Q_{LA} = 0.03 g min^{-1}, 250 °C, 4 h.

To investigate the influence of acid properties in the hydrogenation of LA, a series of the bifunctional Ni/ZSM-5 catalysts with comparable Ni content (ω_{Ni} = 3.4 wt.%) and importantly with different Si-to-Al molar ratios, i.e., 13, 21 and 28. Upon increasing the Si-to-Al molar ratios from 13 to 28, both LA conversion and GVL yield increase from 54% to 78% and from 1% to 61%, respectively. In addition to the gradual gain in the GVL formation, the yield of propyl levulinate (PL), the esterification product between LA and i-propanol solvent, decreases from 47% to 21% and further to 13%, respectively. It is noted that GVL can be formed via the hydrogenation of LA and PL via AL and propyl-3-hydroxyvalerate, respectively (Figure 2). The observed increase in the catalytic activity might be associated with the difference in the acid properties of the catalysts. At first, the increase in the hydrogenation activity seems to be associated with the gradual decrease in the acid site density of the catalysts from 518 to 448 and further to 329 μmol g^{-1} as a result of increasing the Si-to-Al molar ratios from 13 to 21 and to 28, respectively. Further investigation in the acid site types reveals that the increased catalytic activity is proportional with the ratios of Brønsted acid sites-to-Lewis acid sites (n_{BAS}/n_{LAS}), which is 4, 9 and 11, respectively, which were calculated from DRIFTS with pyridine. It is suggested that the combination of surface Ni sites and a large amount of BAS in proximity facilitates the hydrogenation of LA to GVL and even to the further hydrogenated product pentanoic acid (PA). This is in good agreement with a previous study proposed that the LA hydrogenation occurs at the interface between Ni and acid sites of the catalysts [4].

CONCLUSION

The obtained results show that the hydrogenation of levulinic acid (LA) in iso-propanol over the bifunctional Ni/ZSM-5 catalysts entails various reaction pathways. Based on the composition of reaction mixtures, a reaction network was proposed. In addition to the hydrodeoxygenation into γ-valerolactone (GVL), LA also undergoes esterification forming iso-propyl levulinate or/and further hydrogenation of GVL into pentanoic acid. Regarding the catalysts, Ni active sites are crucial in the hydrogenation of LA into GVL. By tailoring the catalyst properties via n_{Si}/n_{Al}, the hydrogenation is selectively driven into forming GVL. The hydrogenation of LA occurs at the interface of Ni and acid sites. The highest GVL yield obtained is 61% (LA conversion of 78%) recorded for Ni/ZSM-5 exhibiting the highest Brønsted acid sites-to-Lewis acid sites ratio ($n_{BAS}/n_{LAS} = 11$). Further investigation focusing on both the Ni and acid sites of catalysts will be conducted to disclose its relations with the catalytic activity in the vapor-phase hydrogenation of LA.

REFERENCES

[1] S.G. Wettstein, D.M. Alonso, E.I. Gürbüz and J.A. Dumesic, *Curr. Opin. Chem. Eng.*, 2012, **1**, 218-224.

[2] R. Xu, K. Liu, H. Du, H. Liu, X. Cao, X. Zhao, et al., *ChemSusChem*, 2020, **13**, 6461-6476.

[3] M. Popova, P. Djinović, A. Ristić, H. Lazarova, G. Dražić, A. Pintar et al., *Front. Chem.*, 2018, **6**, 285-296.

[4] V.V. Kumar, G. Naresh, M. Sudhakar, C. Anjaneyulu, S.K. Bhargava, J. Tardio et al., *RSC Adv.*, 2016, **6**, 9872-9879.

PHOTOCATALYSIS OF BISPHENOL A IN AQUEOUS SOLUTION BY ZEOLITE/TITANIA COMPOSITES

Srna Stojanović[1], Vladislav Rac[2], Vesna Rakić[2], Ljiljana Damjanović-Vasilić[1]
[1]University of Belgrade, Faculty of Physical Chemistry, Studentski trg 12-16, 11000 Belgrade, Serbia
[2] University of Belgrade, Faculty of Agriculture, Nemanjina 6, 11800 Belgrade, Serbia
E-mail: srna@ffh.bg.ac.rs

ABSTRACT

The composites based on TiO_2 nanoparticles, supported on natural zeolite clinoptilolite (Cli) and synthetic beta (β) zeolite were prepared using simple ultrasound assisted solid state dispersion method and tested for photodegradation of bisphenol A (BPA) in aqueous solution. X-ray powder diffraction (XRPD), UV-Vis diffuse reflectance (DR) spectroscopy and Fourier transform infrared (FTIR) spectroscopy were used for characterisation of the obtained composites. The composite based on β zeolite (Si/Al=19) showed photocatalytic efficiency for removal of BPA comparable to efficiency of TiO_2. Furthermore, composite based on low cost natural zeolite clinoptilolite with addition of H_2O_2 also proved to be effective for photodegradation of BPA.

Key words: photocatalysis, TiO_2, zeolite, bisphenol A, emerging contaminant.

INTRODUCTION

Nowadays, various emerging contaminants are being detected in the aquatic environments because application of conventional wastewater treatments is inefficient for their complete removal. The mass production of bisphenol A (BPA), about three million tons annually, and wide spread use, e.g. as a plasticizer in different man-made products, led to its presence in the surface waters, groundwater and wastewater [1]. Numerous harmful effects of BPA to human body have been proven: endocrine disrupting property, carcinogenesis and epigenetic modifications [1]. Regardless of these facts, BPA is still widely used. Canadian government, European Commission and Food and Drug Administration have forbidden the usage of BPA in the production of certain infant products, yet the presence of BPA in the environment raises serious concerns and requires application of different technologies for its efficient elimination [2].

Advanced oxidation process is a very promising technique that relies on the production of highly reactive species such are hydroxyl radicals, which are able to degrade different organic compounds. TiO_2 based photocatalysis gained a significant attention as an effective and environmentally friendly method for pollutants elimination because TiO_2 nanoparticles have high activity, chemical stability, no toxicity and low price. However, their agglomeration and costly filtration process in wastewater systems represent a drawback in the process. The deposition of TiO_2 on high surface area supports such as zeolites could resolve this issue and also prevent leaching of nanoparticles as there are concerns about toxicity of TiO_2 nanoparticles [3]. Zeolites are compatible materials for photocatalysis which possess photochemical stability, high adsorption capacity and transparency to ultraviolet/visible irradiation [4]. Thus, composites where TiO_2 is immobilised on zeolitic support offer a promising solution as the leaching of nanoparticles is prevented, agglomeration reduced and reusability preserved. Moreover, the removal of pollutants can be obtained through synergistic effect of zeolites' adsorption and TiO_2 photocatalysis [5].

In this study, clinoptilolite was used as a support for TiO_2 nanoparticles because it is affordable and abundant natural zeolite with the purpose of developing economical photocatalyst. For comparison, synthetic β zeolite was also used as a support. In order to investigate the influence of Si/Al ratio, β zeolite with Si/Al=19 and Si/Al=180 were used. The aim of this study was to test and compare photocatalytic degradation of BPA using composites based on TiO_2 nanoparticles and different zeolites (Cli, β(19) and β(180)).

EXPERIMENTAL

Natural zeolite clinoptilolite (Cli) (Si/Al = 5, Zlatokop mine, Serbia) and β zeolite (Si/Al = 19 and Si/Al = 180, Alfa Aesar) were used as a supports for Aeroxide® (formerly Degussa) P25 TiO_2 nanoparticles from Evonik (denoted as P25). P25 in amounts of 20 wt% were thoroughly mixed with starting zeolites using ethanol in a 10:1 ratio (ethanol ml/solid powder g) and sonicated for 4 h at 80 °C. Afterwards the composites were dried at 80 °C and calcinated in air at 500 °C for 5 h. The materials were labelled as TCli-20, Tβ(19)-20 and Tβ(180)-20 where T stands for TiO_2, Cli and β indicate the type of used zeolite, number in parentheses labels Si/Al ratio and the other number represent wt% of used TiO_2.

XRPD patterns of composite materials were obtained using Rigaku Ultima IV diffractometer (Cu Kα radiation λ=1.54178 Å) with 4° - 50° 2θ range, 0.020° step and 1°/min acquisition rate. UV–Vis diffuse reflectance (DR) spectra of composite materials were recorded on Agilent Cary UV-Vis-NIR 5000 spectrophotometer equipped with an integration sphere (range: 200 - 800 nm, data interval: 1 nm and scan rate: 600 nm min^{-1}). FTIR spectra of composite materials were acquired on Nicolet 6700 FTIR spectrometer (range: 4000 - 400 cm^{-1}, resolution: 2 cm^{-1} and acquisitions: 32).

Bisphenol A (BPA) (2,2-Bis(4-hydroxyphenyl)propane) was purchased from Sigma Aldrich (≥ 99%). The photocatalytic tests were performed with 40 ml of aqueous solutions of BPA containing 1 gL^{-1} of catalyst at room temperature under constant stirring and illumination. In order to reach adsorption-desorption equilibrium, suspensions were stirred for 30 minutes in the dark. The used initial concentrations of BPA were different: 10, 20 and 50 mgL^{-1}. The lamp (Osram Vitalux 300 W) that simulates sun irradiation was used as a light source. The BPA (λ_{max} = 225 nm) concentration was measured using UV-Vis spectrophotometer (Thermo scientific evolution 220) ranging from 200 to 400 nm.

RESULTS AND DISCUSSION

XRPD patterns of P25, starting zeolites and investigated composite material are shown in Fig. 1. Peaks in diffractogram of natural zeolite Cli correspond to characteristic reflections of clinoptilolite mineral and to photocatalytically inert impurities of quartz (2θ = 20.8°, 26.7°) and feldspar [6].

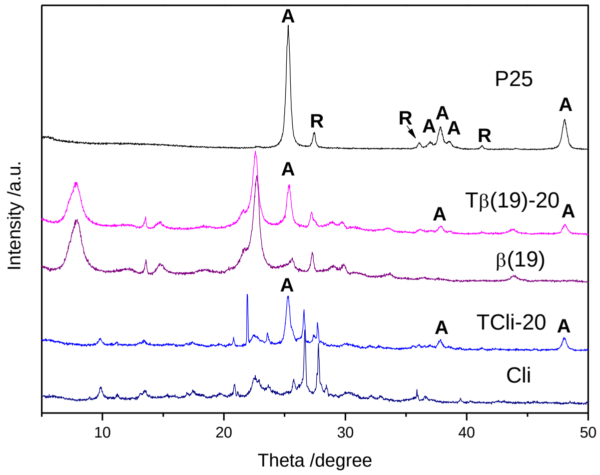

Figure 1. XRPD patterns of P25, starting zeolites (Cli and β(19)) and composite materials (TCli-20 and Tβ(19)-20). Abbreviations: A-anatase and R-rutile.

The diffractograms of composite materials TCli-20 and Tβ(19)-20 exhibit characteristic reflections of starting zeolites (Cli and β(19)) together with reflections originating from TiO_2 anatase phase (2θ = 25.3°, 37.9°, 48.1°) (JCPDS 89-4921). Loading of TiO_2 nanoparticles and preservation of zeolitic structure was confirmed by the XRPD analysis. Similar, UV-Vis DR spectra (data not showed) of composites confirmed loading of TiO_2 nanoparticles and that the preparation procedure did not affect significantly the optical properties of TiO_2. In addition, FTIR spectra (data not showed) also confirmed that the zeolitic structure have not been affected by the TiO_2 loading.

The results of BPA degradation using P25 nanoparticles and composites TCli-20, Tβ(19)-20 and Tβ(180)-20 are shown in Figs 2 and 3. For comparison, the amount of used P25 in photocatalytic experiment was matched to 20 wt% of catalyst loading and denoted as (P25-20). Photolysis test (Fig. 2) revealed that the BPA remains stable in the absence of photocatalyst.

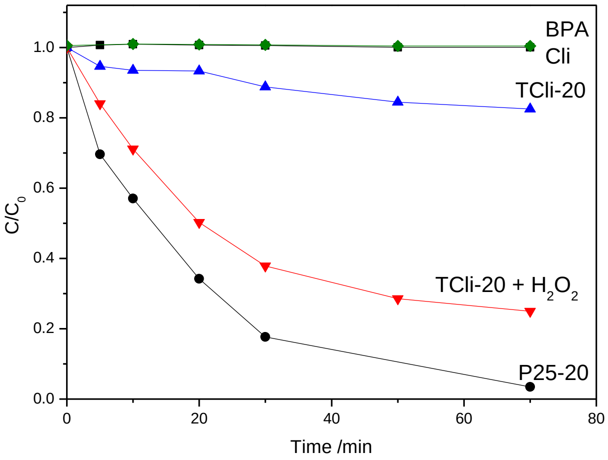

Figure 2. Degradation of BPA (C_0= 10 mgL^{-1}) using: Cli, P25-20, TCli-20 and TCli-20 with addition of 25 µl H_2O_2 (0 min – start of irradiation, C-concentration measured at 225 nm at different irradiation time).

The photocatalytic experiment conducted with TCli-20 (Fig. 2) revealed that after 70 minutes of irradiation only 17.5 % of BPA was degraded, whereas under the same conditions with addition of 25 µl H_2O_2 the degradation rate was significantly improved: 75.1 % of BPA was successfully degraded. Addition of H_2O_2 was beneficial to photocatalytical process as more $^{\bullet}OH$ radicals were formed. For the determination of reaction constant rates, the curves presented in Fig. 2 were used. The pseudo first order rate model was utilized and the rate constant values were determined as 0.003 min^{-1}, 0.027 min^{-1} and 0.050 min^{-1} for TCli-20, TCli-20 + H_2O_2 and P25-20, respectively.

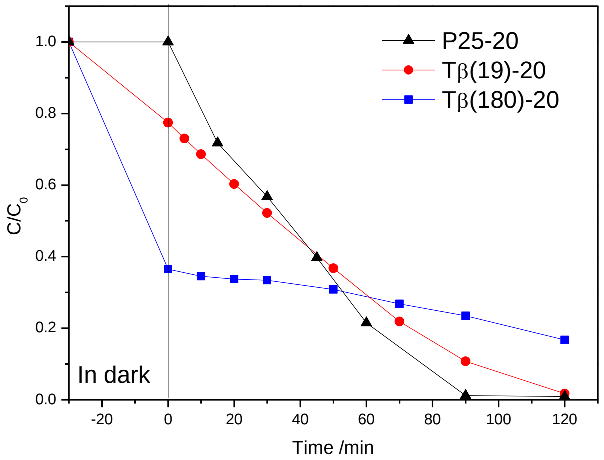

Figure 3. Removal of BPA using: C_0= 20 mgL^{-1} for P25-20 and Tβ(19)-20 and C_0= 50 mgL^{-1} for Tβ(180)-20 (0 min – start of irradiation, C-concentration measured at 225 nm at different irradiation time).

In the experiments conducted with composites based on β zeolite (Fig. 3.) higher concentrations of BPA were used as the removal process is achieved through the adsorption and photocatalytic degradation. The results showed that during experiment in the dark using BPA concentration of 20 mgL^{-1} composite Tβ(19)-20 adsorbed 4.5 mgL^{-1}. In the case of composite Tβ(180)-20, BPA concentration C_0=50 mgL^{-1} was used because of the higher adsorption capacity of this zeolite compared to β(19) in order to achieve similar concentrations of BPA remained in aqueous solutions for photocatalytic tests. The composite Tβ(19)-20 successfully removed BPA after 120 minutes exposure to light, whereas P25-20 was slightly more efficient and completely eliminated BPA after 90 minutes (Fig. 3). However, in the case of Tβ(180)-20 prolonged irradiation is needed for complete elimination of BPA. The calculated pseudo first order constant rates were 0.004 min^{-1}, 0.019 min^{-1} and 0.023 min^{-1} for Tβ(180)-20, Tβ(19)-20 and P25, respectively. The degradation of BPA was followed by UV-Vis spectroscopy, and the UV-Vis spectra (data not shown) revealed that composite Tβ(19)-20 successfully achieved complete elimination of BPA and its potential by-products.

CONCLUSION

This study showed that successful photocatalytic degradation of BPA from aqueous solution can be achieved using low cost TCli-20 composite with addition of H_2O_2. Furthermore, complete removal of BPA was observed using composite material based on P25 and β zeolite with Si/Al = 19. The combined effect of adsorption by β zeolite and TiO_2 photocatalysis was favourable for complete removal of investigated contaminant.

ACKNOWLEDGEMENT

The authors acknowledge the financial support by the Ministry of Education, Science and Technological Development of Republic of Serbia (Contract numbers: 451-03-9/2021-14/200146; 451-03-9/2021-14/200116).

REFERENCES

[1] P. Venkanta Laxma Reddy, K. Kim, B. Kavitha, V. Kumar, N. Raza and S. Kalagara, *J. Environ. Manage*, 2018, **213**, 189-205.

[2] A. Bhatnagar and I. Anastopoulos, *Chemosphere*, 2017, **168**, 885-902.

[3] Y. Wang, X. Zhu, Y. Lao, X. Lv, Y. Tao, B. Huang, J. Wang, J. Zhou and Z. Cai, *Sci. Total Environ.*, 2016, **565**, 818-826.

[4] H. Zhad, K. Abbas, S. Hena and Md. Rabiul Awual, *J. Environ. Chem. Eng.*, 2018, **6**, 218-227.

[5] X. Liu, Y. Liu, S. Lu, W. Guo and B. Xi, *Chem. Eng. J.*, 2018, **350**, 131-147.

[6] Š. Cerjan Stefanović, N. Zabukovec Logar, K. Margeta, N. Novak Tušar, I. Arčon, K. Maver, J. Kovač and V. Kaučič, *Micropor. Mesopor. Mat.*, 2007, **105**, 251-259.

PHOTOCATALYTIC REMOVAL OF DYES FROM WASTEWATER UNDER SOLAR LIGHTS BY NATURAL CLINOPTILOLITE FROM DIFFERENT REGIONS

Jelena Pavlović[1], Andraž Šuligoj[2], Nevenka Rajić[3]
[1]Innovation Centre of the Faculty of Technology and Metallurgy, University of Belgrade, Karnegijeva 4, 11120 Belgrade, Serbia
[2]National Institute of Chemistry, Hajdrihova 19, 1000 Ljubljana, Slovenia
[3]Faculty of Technology and Metallurgy, University of Belgrade, Karnegijeva 4, 11120 Belgrade, Serbia
E-mail: jelena.pavlovic@tmf.bg.ac.rs

ABSTRACT

Due to their structural complexity, chemical stability, and toxicity, organic dyes mostly used in the textile industry, cause serious environmental problems. Advanced Oxidation Processes (AOPs) currently appear to offer a high potential for complete degradation of organic dyes. The present work is focused on natural clinoptilolite (CLI) and its unusual photocatalytic activity. CLI from different regions were studied as photocatalysts in the photodegradation of methylene blue (MB) as a model cationic dye under visible light at room temperature and atmospheric pressure at different pH. For all CLI samples at pH = 6, the total degradation degree of MB varied from 74 to 88 %, thus indicating a high photocatalytic activity of CLI.

Keywords: clinoptilolite, natural zeolites, organic dyes, photocatalyst, photocatalytic degradation.

INTRODUCTION

Removal of the harmful organic dyes from wastewater is an important task for environmental protection. AOPs have been found as an effective and suitable method which enables a complete degradation of organic dyes by converting them into less harmful CO_2, H_2O, and inorganic salts. Catalytic degradation has mainly been ascribed to the formation of highly reactive hydroxyl radicals.

Natural clinoptilolite is the most abundant natural zeolite in many regions around the world. According to various studies, CLI can be used for different purposes, due to its unique structural features and possibility to be modified without loss of crystallinity. Although the catalytic activity of CLI has been reported in different reactions [1,2], however the use of unmodified CLI in photocatalysis has not been studied so far to the best of our knowledge.

In this study, we explored the photocatalytic performance of CLI from different regions for the degradation of MB, frequently used in the textile industry. Photocatalytic tests were performed under a visible-light lamp irradiation.

EXPERIMENTAL

Natural clinoptilolite-rich tuffs, used in this study, were provided from different regions: a) Serbia (Slanci deposit, SCLI), b) Turkey (Gördes deposit, TCLI) c) Iran (Semnam deposit, ICLI), d) Romania (Baia Mare deposit, RCLI) and e) Slovakia (Nižný Hrabovec deposit**,** SKCLI).

Prior to all experiments, the samples were sieved to obtain the a particles population having the size in the range from within 63 and 125 μm mesh, washed with deionized water, and dried at 105 °C overnight. Such samples were then used in photocatalytic tests, without any additional modification.

The mineral composition of the zeolitic tuffs was determined by a powder X-ray diffraction method (PXRD) using an APD2000 Ital Structure diffractometer (CuK_α radiation,

λ=0.15418 nm), generated at 38 kV and 28 mA. Scans were performed in the 2θ range 5–50° with a step of 0.02° per 1 s. Semi-quantitative PXRD analysis was conducted using the Rietveld refinement and the Topas-Academic v.4 software package [3].

Photocatalytic tests: The tests were performed using a photocatalytic reactor system shown in Fig. 1. In a typical experiment, suspension contained water solution of MB (C_0 = 10 mg dm^{-3}) and CLI in the concentration of 0.2 g dm^{-3} at different pH (pH= 3, 6, or 9), was stirred by magnetic stirrer for 30 min to reach an adsorption/desorption equilibrium. Then the suspension was irradiated for 300 min under visible light by using the Osram Ultra Vitalux lamp (300 W), positioned 10 cm above the reactor. The photocatalytic pathway of the MB degradation was followed colorimetrically at λ = 664 nm by using UV/VIS spectroscopy (Lambda 365 spectrophotometer, Perkin Elmer).

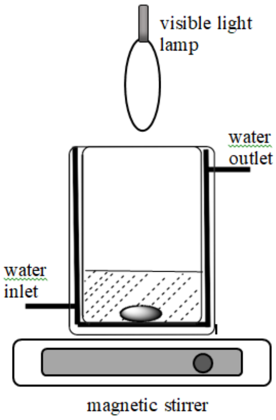

Figure 1. The schematic presentation of the reactor system used in photocatalytic tests.

RESULTS AND DISCUSSION

Fig. 2 shows a representative PXRD diffraction pattern. In all samples, CLI is the major phase with the diffraction peaks at 2θ= 9.8; 11.7; 12.8; 17.2; 19.1; 22.4; 26.0; 29.9 and 32.3° [4]. Results of a quantitative analysis performed by the Rietveld method showed that the tuffs have a high content of CLI which is in the range from 73 to 82 wt.%. The analysis revealed also the presence of a) feldspar and quartz (SCLI); b) anorthite and quartz (TCLI); c) quartz, anorthite and calcite (ICLI); d) biotite and calcite (RCLI), and e) anorthite and quartz (SKCLI).

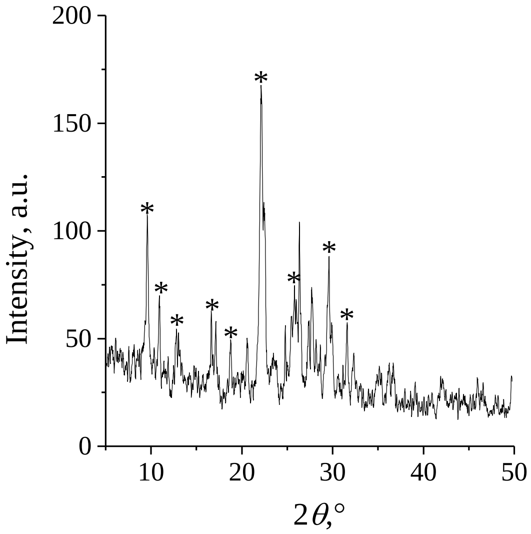

Figure 2. Representative PXRD pattern of the zeolitic tuff (*clinoptilolite phase).

The degradation degree of MB in the absence of catalyst was found to be very low (approx. 10%, not shown). On the other hand, the photocatalytic tests showed that all CLI samples exhibit a high photocatalytic performance (Fig. 3).

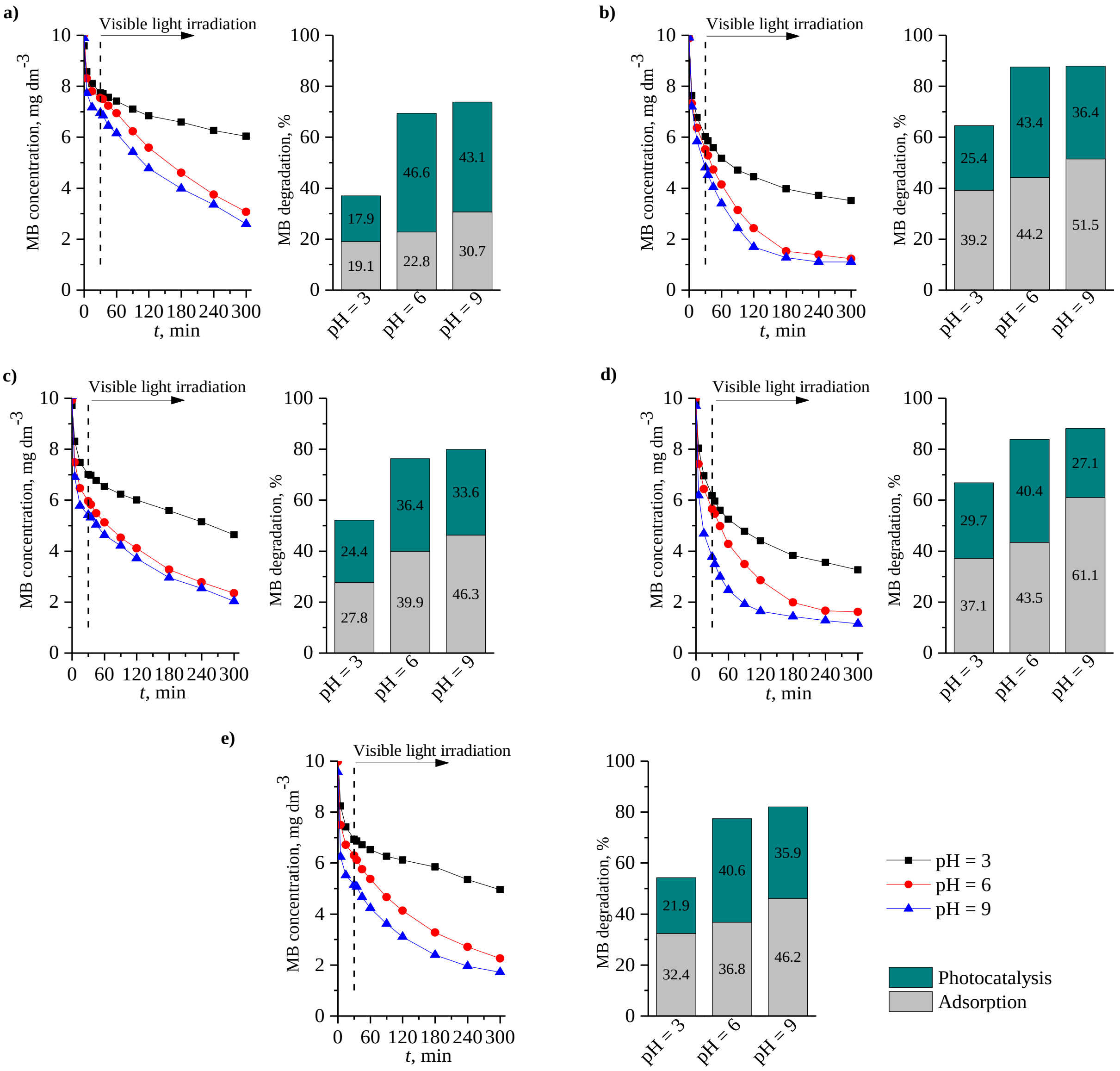

Figure 3. MB photodegradation using as catalyst: a) SCLI, b) TCLI, c) ICLI, d) RCLI and e) SKCLI. The reaction conditions are as follows: C_0= 10 mg dm^3, m_{cat} = 10 mg, V= 50 cm^3, t= 22 °C.

The total degradation degree of MB varies from 74% (SCLI) to 88% (RCLI) within 300 min. For all tested CLI samples, MB adsorption increases with pH. For cationic dyes such as MB, a competition between hydrogen ions and MB cations for adsorption sites occurs resulting in a lower adsorption efficiency in acidic media. Total degradation of MB notably increases by increasing pH from 3 to 6. A slowdown is evident at pH = 9. The best photocatalytic activity for all tested CLI samples was found at pH= 6 (up to 46.6%).

The photocatalytic performance of native CLI samples could be most probably explained by the presence of low content of Fe. The Fe species can photoinduce the species which are responsible for photocatalytic activity [4]. Although Al–O species can also originate active photocatalytic sites, Fe species induce more active photocatalytic species under the applied experimental conditions [4].

MB photodegradation follows the Langmuir–Hinshelwood model, the most commonly used kinetic model for the description of the kinetics of heterogeneous photocatalytic processes. The pseudo-first-order rate constant (k_{app}), calculated from the slopes of the plots $\ln(C_0/C_t)$ *vs* irradiation time (t), are listed in Table 1. It can be seen that the constant significantly increased by increasing pH from 3 to 6. There are no noticeable changes with further increasing of pH up to 9 confirming favorable MB photodegradation at pH= 6.

Table 1. The rate constant (k_{app}) calculated by Langmuir-Hinshelwood model at 22°C.

Sample	pH = 3	pH = 6	pH = 9
	SCLI		
k_{app}, min^{-1}	0.0011	0.0035	0.0036
R^2	0.9613	0.9996	0.9980
	TCLI		
k_{app}, min^{-1}	0.0024	0.0064	0.0066
R^2	0.9344	0.9686	0.9404
	ICLI		
k_{app}, min^{-1}	0.0017	0.0037	0.0038
R^2	0.9678	0.9879	0.9894
	RCLI		
k_{app}, min^{-1}	0.0027	0.0052	0.0054
R^2	0.9451	0.9683	0.9066
	SKCLI		
k_{app}, min^{-1}	0.0014	0.0040	0.0044
R^2	0.9487	0.9937	0.9877

CONCLUSION

Present results show that CLI obtained from different regions can be used as an efficient and environmentally safe photocatalytic material for the photodegradation of organic dyes such as MB under environmentally friendly visible light. Further research will be directed to a detailed study of the photocatalytic decomposition.

ACKNOWLEDGEMENT

This work was supported by the Ministry of Education, Science and Technological Development of the Republic of Serbia (Contract No. 451-03-9/2021-14/200287 and 451-03-9/2021-14/200135).

REFERENCES

[1] J. Pavlović, M. Popova, R.M. Mihalyi, M. Mazaj, G. Mali, J. Kovač, H. Lazarova and N. Rajić, *Micropor. Mesopor. Mat.* 2019, **279**, 10-18.

[2] M. Bahrami and A. Nezamzadeh-Ejhieh, *Mater. Sci. Semicond. Process.* **2015**, 30, 275-284.

[3] A. Coelho, TOPAS Academic 4.1 Coelho Software, Brisbane, Australia, 2007.

[4] E.A. Alvarez-Aguiñaga, M.P. Elizade-González and S.A. Sabinas-Hernández, *RSC Adv.*, 2020, **10**, 39251-39260.

COMPOSITES OF PHILLIPSITE-RICH TUFF AND SURFACTANT – THEIR CHARACTERIZATION AND STABILITY

Danijela Smiljanić[1], Aleksandra Daković[1], Milica Spasojević[1], Milena Obradović[1], Marija Marković[1], Alessio Langella[2], Bruno de Gennaro[3]
[1]Institute for Technology of Nuclear and Other Mineral Raw Materials, Franche D' Epere 86, 11000 Belgrade, Serbia
[2]Department of Earth Sciences, Environment and Resources, Federico II University, Via Cinthia, 80126 Napoli, Italy
[3]DICMAPI, Federico II University, Piazzale V. Tecchio 80, 80125 Naples, Italy
E-mail: d.smiljanic@itnms.ac.rs

ABSTRACT

In this work phillipsite-rich tuff (P) was modified by using amounts of cetylpyridinium chloride (C) equivalent to 70% and 140% of the zeolite external cation exchange capacity (ECEC). Accordingly, composites were denoted as PC-70 and PC-140. Prepared composites were characterized by ATR-FTIR spectroscopy. Additionally, to test the stability of surfactant molecules attached to the tuff surface, composites were extensively washed with distilled water, and zeta potential of unwashed and washed samples was measured. FTIR spectra confirmed presence of C in both composites. Zeta potential measurements showed that composite containing surfactant in the amount below the ECEC value (PC-70) has much higher stability and thus is a more appropriate adsorbent for potential practical application for removal of different pollutants.

Keywords: phillipsite-rich tuff, ATR-FTIR, zeta potential, surfactant stability.

INTRODUCTION

Natural zeolites are abundant, low-cost, and eco-friendly minerals, with high cation exchange capacity, physicochemical stability, and good hydraulic characteristics. For these reasons, natural zeolites were extensively investigated for water treatment - especially for the removal of heavy metal cations. Modification of natural zeolites with cationic surfactants provides adsorbent materials with an increased affinity towards low polar molecules and even anionic species depending on the amount of surfactant at the zeolitic surface. When the amount of surfactant is below or equal to the ECEC, the zeolitic surface charge is changed from negative to neutral (monolayer phase made of hydrophobic surfactant tails with an affinity towards hydrophobic molecules) whereas, when the surfactant amount is above ECEC zeolite surface became more positive (bilayer of surfactant, formed through hydrophobic interactions between surfactant tails, capable for adsorption of anions). Therefore, surfactant modified natural zeolites (SMNZs) with different amounts of surfactants were studied for the removal of different pollutants from water - oxyanions, phenolic compounds, dyes, pesticides, emerging contaminants, etc [1–6]. However, since surfactants are also considered as emerging contaminants, before application of SMNZs for water remediation it is necessary to determine the stability of surfactant bounded to the zeolite surface.

The aim of this work was to prepare composites with the amounts of surfactant cetylpyridinium chloride (C) below and above the ECEC value of the phillipsite-rich tuff and to investigate the stability of adsorbed surfactant molecules at phillipsite surface.

EXPERIMENTAL

The starting material used in this study for the preparation of composites with surfactant was a phillipsite-rich tuff from Campanian region (Marano of Naples, Italy) commercialized in Italy from Italiana Zeoliti – CBC Group. Mineralogical and chemical characterizations for the tuff were previously carried out [7]. The phillipsite-rich tuff had 58 wt% of zeolitic content (44 wt%, 4 wt%, and 10 wt% for phillipsite, chabazite and, analcime, respectively) together with 11 wt% of smectite and 32 wt% of feldspar. The Si/Al ratio and ECEC of the tuff were 2.45 and 0.15 meq/g, respectively.

Phillipsite-rich tuff was treated with two different amounts of cetylpyridinium chloride (CAS: 6004-24-6, M = 358.00 g/mol, Sigma Aldrich, assay: 98.0–102.0%), equivalent to 70% (0.1 meq/g) and 140% (0.2 meq/g) of its ECEC value, and modification was performed according to the procedure given in the literature [6,8]. Furthermore, in order to check the stability of the prepared materials, 1 g of each composite was extensively washed (under vacuum using Büchner funnel and flask) with distilled water (approximately 0.5 L), filtered, and dried at 60 ˚C.

Attenuated Total Reflectance – Fourier Transform Infrared (ATR–FTIR) spectroscopy was used to collect spectra of starting material and composites PC-70 and PC-140, in the spectral range 4000–400 cm^{-1} with resolution 2 cm^{-1} (Bruker Alpha; Opus 7.2 software - Bruker Optik GmbH, Leipzig, Germany). The zeta potentials of P and composites before and after washing were measured using a Zetasizer Nano ZS90, Malvern Instruments. Aqueous suspensions (0.1 mg/mL) for each material were prepared and the average value of 5 measurements was taken. Latex dispersion was used as a calibration standard.

RESULTS AND DISCUSSION

ATR-FTIR spectra of P and composites - PC-70 and PC-140 are presented in Figure 1. Infrared analysis has shown adsorption bands of zeolite-rich tuff associated with internal and external framework vibration of primary and secondary building units [9]. All spectra had a broad peak above 3000 cm $^{-1}$ and a peak at 1635 cm $^{-1}$ from O-H stretching and bending vibration in water molecules, respectively. In the spectra of composites (PC-70 and PC-140) the presence of surfactant was confirmed by: the low-intensity peak at 2956 cm $^{-1}$ that belongs to the CH_3 group, and peaks at 2920 cm $^{-1}$, and 2851 cm $^{-1}$ corresponding to asymmetric and symmetric C-H stretching vibrations of CH_2 groups in the alkyl chain of C molecules. Similarly, low-intensity peaks at 1487 cm $^{-1}$ and 1467 cm $^{-1}$ are from C-H bending vibration in surfactant molecules.

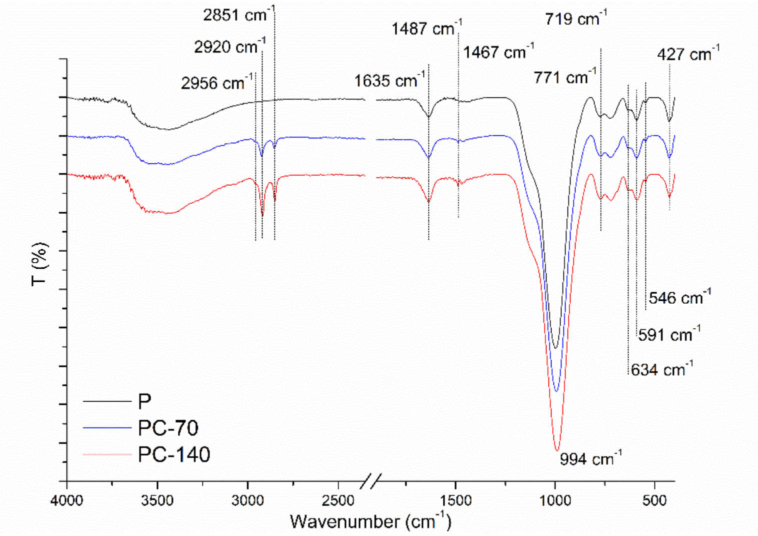

Figure 1. FTIR-ATR spectra of phillipsite-rich tuff before modification and after modification with two different amounts of surfactant.

The vibrations characteristic for silicates were found: at 994 cm $^{-1}$ (with the shoulder on the left side) which belongs to asymmetric stretching of T-O, where T represents Si or Al, and

O is oxygen atom; peaks at 771 cm $^{-1}$ and 719 cm $^{-1}$ are from asymmetric and symmetric stretching of T-O-T, respectively, while peaks at 634 cm $^{-1}$, 591 cm $^{-1}$, 546 cm $^{-1}$, and 427 cm $^{-1}$ are characteristic for T-O-T bending vibrations. These results confirmed presence of C molecules at the zeolitic surface and that modification with surfactant did not change the internal structure of the tuff. Additionally, it is observed that intensities of peaks characteristic for C molecules increased with the increase of the amount of surfactant at the phillipsite surface.

In general, two mechanisms of surfactant adsorption at the zeolitic surface predominate: first, when the amount of surfactant is below or equal to ECEC, a cation exchange of cations at surface with surfactant ions occurs; second, binding of surfactant in excess of the ECEC via hydrophobic interactions between the long tails of the surfactants. It was also reported that desorption of surfactant may occur, especially when the amount of surfactant is above ECEC [10,11].

Zeta potential of P and both composites before and after washing was measured and the change in surface charge was confirmed (Figure 2). According to the literature, when ion exchange of cations with surfactant ions occurs, zeta potential of the SMNZ becomes less negative due to the increased hydrophobicity of the zeolitic surface and approaches zero with amount of surfactant equal to the ECEC value confirming complete hydrophobicity of the zeolitic surface. When amount of surfactant is above ECEC zeta potential becomes positive indicating charge reversal due to the bilayer formation at the zeolite surface.

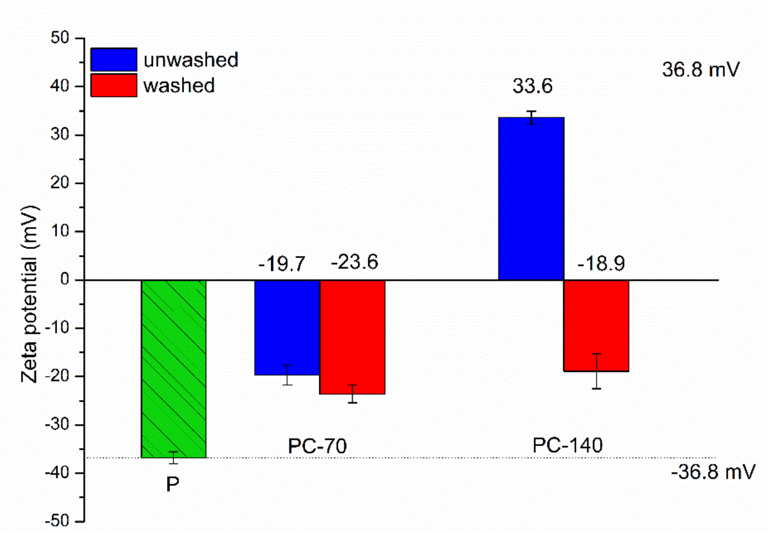

Figure 2. Graphical representation of zeta potential for starting phillipsite-rich tuff, and composites (PC-70 and PC-140) before and after washing.

The zeta potential of P was -36.8 mV, whereas in the case of PC-70, before washing, the zeta potential was less negative (-19.7 mV), confirming that surface is more hydrophobic and that C is tightly bounded at the P surface by ion exchange process. A slightly more negative value of zeta potential (-23.6 mV) was observed after washing, indicating that only a small amount of C was desorbed from the surface of PC-70. At the higher amount of C (sample PC-140), the change in zeta potential value after washing was more visible. Namely, for unwashed composite, the zeta potential was positive (+33.6 mV) confirming charge reversal and presence of C bilayers at P surface. However, after washing, zeta potential became negative (-18.9 mV) indicating desorption of C from bilayers of PC-140. These changes in the zeta potential value of unwashed and washed composite PC-140 suggest that weak hydrophobic interactions between alkyl chains predominate in bilayer. Additionally, after washing, composites had similar values of zeta potential regardless of the initial amount of C.

CONCLUSION

Phillipsite-rich zeolitic tuff was modified with two different levels of surfactant cetylpyridinium chloride (C) – below (70%) and above (140%) zeolite external cation exchange capacity (ECEC). ATR-FTIR analysis has confirmed a successful modification of phillipsite-rich tuff by C molecules. Zeta potential measurement showed that when amount of C was below ECEC value, the surfactant ions was tightly bound to the zeolitic surface, but when the amount of surfactant was above ECEC value, C molecules were adsorbed creating bilayer and was easily desorbed from P surface. Results showed that zeta potential may be a useful tool in the determination of surfactant stability at surface of SMNZ. The composite containing C in amount below the ECEC value (PC-70) may be a more appropriate adsorbent for potential practical application for removal of different pollutants due to the higher stability. The results also suggest that when using the SMNZs for the removal of emerging contaminants the surfactant stability should be tested prior to the application.

ACKNOWLEDGMENT

These experiments were done under the project 451-03-9/2021-14/200023 funded by the Ministry of Education, Science, and Technological Development of Republic of Serbia, and supportof MIUR (Ministero dell’Istruzione, dell’Università e della Ricerca – Italy) Progetti di Ricerca di Interesse Nazionale (PRIN 2010/grant number MKHT9B_006).

REFERENCES

[1] M. Delkash, B. Ebrazi Bakhshayesh and H. Kazemian, *Microporous Mesoporous Mater.*, 2015, **214**, 224–241.

[2] C. Colella, M. de’ Gennaro, A. Langella and M. Pansini, *Sep. Sci. Technol.*, 1998, **33**, 467–481.

[3] P. Misaelides, *Microporous Mesoporous Mater.*, 2011, **144**, 15–18.

[4] S. Wang and Y. Peng, *Chem. Eng. J.*, 2010, **156**, 11–24.

[5] J. Lemić, M. Tomašević-Čanović, M. Adamović, D. Kovačević and S. Milićević, *Microporous Mesoporous Mater.*, 2007, **105**, 317–323.

[6] D. Smiljanić, B. de Gennaro, F. Izzo, A. Langella, A. Daković, C. Germinario, G.E. Rottinghaus, M. Spasojević and M. Mercurio, *Microporous Mesoporous Mater.*, 2020, **298**, 110057.

[7] B. de Gennaro, P. Aprea, C. Colella and A. Buondonno, *J. Porous Mater.*, 2007, **16**, 667–673.

[8] B. de Gennaro, M. Mercurio, P. Cappelletti, L. Catalanotti, A. Daković, A. De Bonis, C. Grifa, F. Izzo, M. Kraković, V. Monetti and A. Langella, *Microporous Mesoporous Mater.*, 2016, **235**, 42-49.

[9] M. Mercurio, F. Izzo, A. Langella, C. Grifa, C. Germinario, A. Daković, P. Aprea, R. Pasquino, P. Cappelletti, F.S. Graziano and B. de Gennaro, *Am. Mineral.*, 2018, **103**, 700–710.

[10] Z. Li, S.J. Roy, Y. Zou and R.S. Bowman, *Environ. Sci. Technol.*, 1998, **32**, 2628–2632.

[11] P.J. Reeve and H.J. Fallowfield, *J. Hazard. Mater.*, 2017, **339**, 208–215.

REMOVAL OF ARSENIC(III) OXYANIONS FROM WASTEWATER USING AMINOSILANE-MODIFIED NATURAL AND SYNTHETIC ZEOLITE

Jelena Dimitrijević[1], *Jelena Petrović*[1], *Dragana Milošević*[2], *Jelena Dikić*[3], *Sanja Jevtić*[4]
[1] Institute for Technology of Nuclear and Other Mineral Raw Materials, 86 Franchet d'Esperey St., 11000 Belgrade, Serbia
[2] Institute of Chemistry, Technology and Metallurgy, Centre for Materials and Metallurgy, Karnegijeva 4, Belgrade, Serbia
[3] Innovation Centre of the Faculty of Technology and Metallurgy, University of Belgrade, Karnegijeva 4, Belgrade, Serbia
[4] Faculty of Technology and Metallurgy, University of Belgrade, Karnegijeva 4, Belgrade, Serbia
E-mail: sanja@tmf.bg.ac.rs

ABSTRACT

Silanization of the natural and synthetic zeolites as well as their use as adsorbents for removing arsenic(III) oxyanions from wastewater are the topic of this paper. Two types of zeolite were used: natural zeolite-clinoptilolite from Zlatokop deposit, Vranjska Banja, Serbia, previously converted to H^+-form and synthetic zeolite, mordenite. The modification was performed with solution (3-aminopropyl) triethoxysilane (APTES). The presence of APTES on the surface of zeolite was confirmed using TG/DSC and FTIR analysis. The results showed that natural aminosilane-modified zeolite has a higher adsorption capacity for arsenic(III) oxyanions compared to mordenite prepared in the same way. The kinetic data follow the Lagergren pseudo-second-order model. This model implies a chemical interaction between AsO_3^{3-}- ions and functional groups on the silanized zeolite surface.

Key words: zeolite, aminosilane, modification, arsenic, wastewater.

INTRODUCTION

Into the environment arsenic comes from various sources, including industrial wastewater, the use of fertilizers and pesticides, the smelting of metal ores and the combustion of fossil fuels [1]. Due to its high toxicity even at low concentrations, it is considered one of the most undesirable metals, so its removal from wastewater is a major environmental challenge [1,2]. Zeolites are good adsorbents for the removal of different metals from aqueous solutions [3,4]. The adsorption mechanism is mainly based on an ion-exchange reaction between cations from zeolite lattice and metal ions from water solutions [5]. In order to improve the adsorption capacity of zeolites various organic compounds, such as amino-silanes are used. Amino-silanes are binding to the surface of the zeolite, whereby amino groups participate in the interaction with metal ions, thus improving the chemisorption's properties of the starting material. In this study, we performed a modification of clinoptilolite and mordenite with (3-aminopropyl) triethoxysilane (APTES) and examined their ability to remove As(III) from water solutions.

EXPERIMENTAL

Natural zeolite-clinoptilolite (Zlatokop, Serbia) and synthetic zeolite-mordenite (CZM20, SiO_2/Al_2O_3 molar ratio 20, Clariant) were chemically modified using (3-aminopropyl)triethoxysilane (APTES, 99%, Acros Organics). Before silanization, clinoptilolite was chemically treated and converted to H^+-form according to the procedure described by Garcia-Basabe *et al.* [6] while mordenite preliminarily was calcined for 30 minutes at 550 ºC in order to remove potentially present moisture. Silanization was performed in a balloon with a reflux condenser in an inert stream of nitrogen in the presence of toluene as a liquid medium. The silanization process was performed for 9 h with continuous stirring on a magnetic stirrer and on a constant temperature of 70 ºC. The APTES was added in drops to the reaction mixture during the whole time of stirring. After the silanization, ethanol was added in drops at 10 min intervals several times. After completion of the silanization process, the modified zeolites were centrifuged and washed to remove toluene from the zeolite surface. The zeolite samples were dried for 24 h at 70 ºC. In the adsorption experiments, the liquid/solid phase ratio was 100:1. The initial concentration of As(III) solution was 10 mg As dm^{-3}. The suspensions were stirred at room temperature for 24 h. After the selected time (0.25, 0.5, 1, 2, 4, 6 and 24 h) aliquots were taken. The suspensions were separated by filtration and the concentration of As(III) before and after adsorption were determined by Perkin Elmer PinAAcle 900T Atomic Absorption Spectrometer (AAS)- Mercury Hydride System (MHS).

Characterization. Powder X-ray diffraction analysis (PXRD) was used to check crystallinity of the H$^+$-form of clinoptilolite after modification. PXRD patterns were recorded in the 2Θ=5-40° at room temperature using an Ital Structure APD2000 diffractometer. APTES content were determined by thermogravimetric analysis using a SDT Q-600 simultaneous TG/DSC instrument (TA Instruments). Interactions of APTES with zeolite surface were studied by Fourier Transform Infrared (FTIR) spectroscopy in the range 4000–450 cm^{-1} at room temperature using MB Bomem 100 Hartmann & Brown spectrometer. All samples were prepared by the KBr method.

RESULTS AND DISCUSSION

The PXRD analysis of the natural zeolite (Clin) and H$^+$-form of this zeolite showed that the clinoptilolite lattice after modification was not affected (Fig. 1).

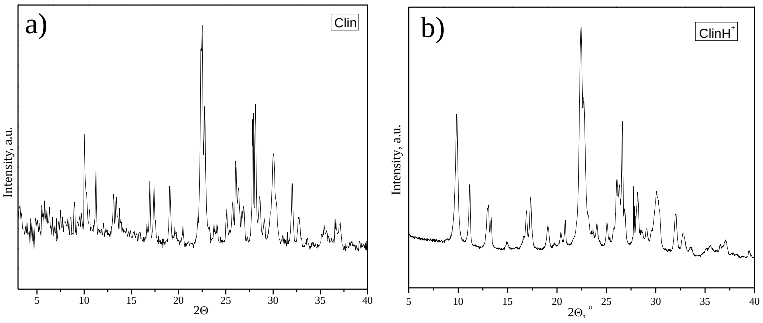

Figure 1. PXRD patterns of Clin (a) and ClinH$^+$ (b).

The results of thermal analysis (TG/DSC) are shown in Fig. 2 and 3. The total weight loss at 800 °C for samples ClinH$^+$ and ClinH$^+$-APTES is 12.4 and 15.3 wt.%, respectively. This confirms that the organic component has bound to the zeolite surface. DSC-curve of ClinH$^+$-APTES shows peak at 310 °C which is a consequence of the degradation of aminosilanes.

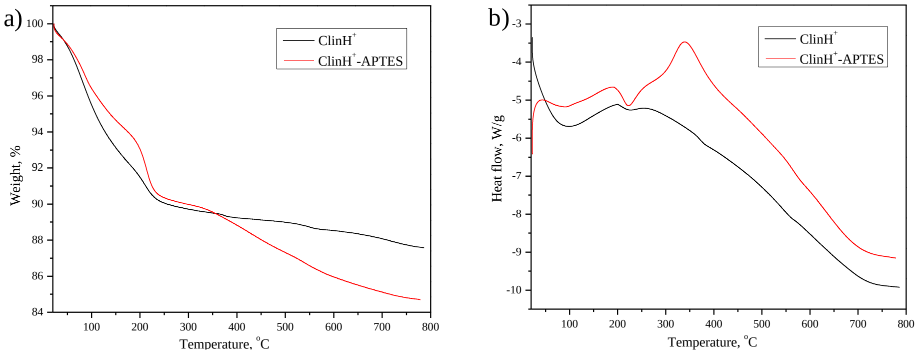

Figure 2. TG (a) and DSC (b) curves of ClinH$^+$ and ClinH$^+$-APTES.

As it can be seen from the Fig. 3, the TG curves of modernite shows that modified mordenite has a greater weight loss (15.4 wt.%) in comparison to the unmodified sample (12.5 wt.%) which confirms the presence of APTES. On the DSC curve of the modified sample a peak at about 320 °C can be observed which can be attributed to the organic component (Fig. 3b).

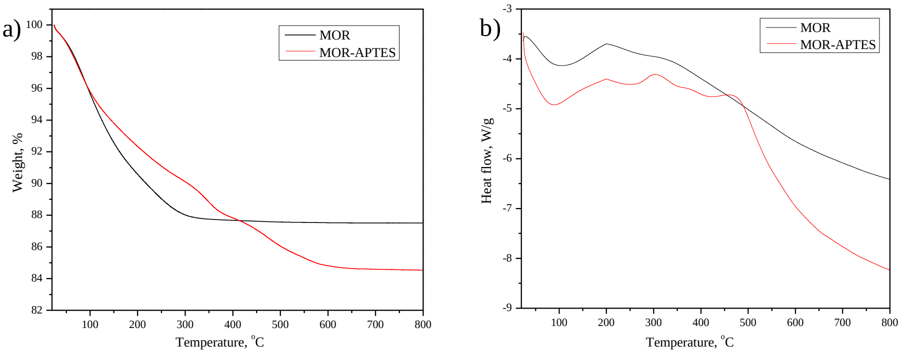

Figure 3. TG (a) and DSC (b) curves of MOR and MOR-APTES.

The FTIR spectra were used to analyse surface functionalities of ClinH+ and MOR, as well as the successfulness of their modification with APTES (ClinH+-APTES and MOR-APTES) (Fig. 4).

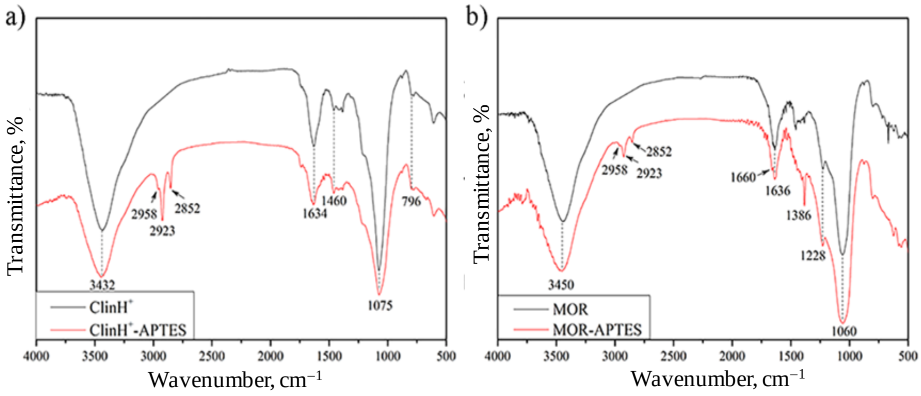

Figure 4. FTIR spectra of: (a) ClinH$^+$ and ClinH$^+$-APTES; (b) MOR and MOR-APTES.

FTIR spectra of all samples (Fig. 4) shows an intense band that occurs in the range between 3400-3500 cm^{-1} assigned with -OH stretching vibrations of surface functional groups, while the peak at 1634 cm^{-1} originates from -OH bending vibration, related with cations located in the structure of zeolite channels. The characteristic band at 1060-1075 cm^{-1} corresponds to the asymmetric stretching vibration of internal Si-O and Al-O bonds in SiO_4 and AlO_4 tetrahedral groups. The band at 796 cm^{-1} is assigned with the stretching vibration mode of O-Si-O and O-Al-O groups in the zeolite structure [7]. Besides the absorption bands of vibration frequencies of -OH, Si-O and Al-O groups, the appearance of new bands at spectra of silan-modified zeolites was observed and is associated with successful APTES modification. The peaks at 2958, 2923 and 2852 cm^{-1} are associated with stretching vibrations of C-H groups. The symmetrical and asymmetrical C-H in-plane bending vibrations of CH_3 groups can be expected in the region 1300-1500 cm^{-1}, as well as, the bands corresponding to N-H in-plane and C-N bond stretching vibration, which is overlapped with C-H vibration. The broad peak between 3300- 3600 cm^{-1} was due to the NH_2 stretch of the amine group overlapped with OH stretching vibration [7].

Adsorption was performed from the solution which contained 10 mg As dm^{-3}. It is evident that ClinH^{+}-APTES was more efficient adsorbent for As(III) ions than MOR-APTES (Fig. 5a). The modified natural zeolite ClinH^{+}-APTES adsorbed 2.5, while the synthetic zeolite prepared in the same way, bound 1.9 mg As/g zeolite.

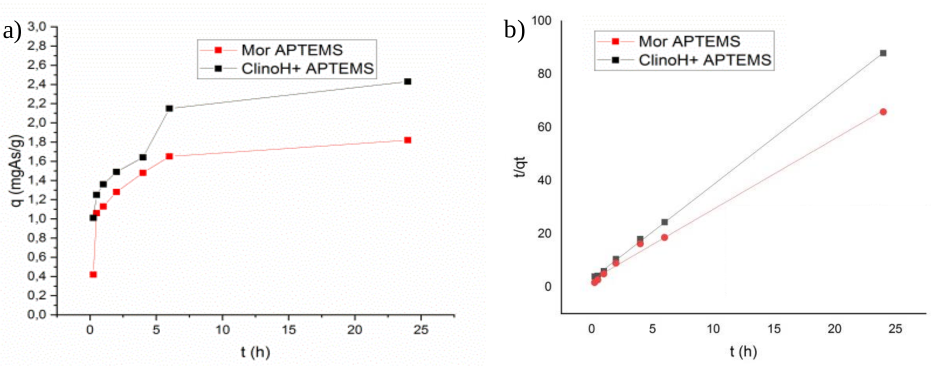

Figure 5. a) As concentration in mg/g on ClinH^{+}-APTES and MOR-APTES; b) Lagergren pseudo-second-order kinetic model applied to the adsorption data for ClinH^{+}-APTES and MOR-APTES.

Different kinetic models were used to describe the obtained experimental data. The correlation factors value (R^2) for both samples of 0.99 confirmed that adsorption kinetics follows the Lagergren pseudo-second order model (Fig. 5b).

CONCLUSION

The modification of natural and synthetic zeolite by (3-aminopropyl)triethoxysilane presents a new approach to the synthesis of efficient adsorbents for arsenic removal from aqueous solutions. This could contribute to resolving the real issues of wastewater treatment from different industries. The adsorbent containing low-cost natural zeolite-clinoptilolite showed a better affinity for As(III) adsorption than synthetic mordenite. The kinetic data follows the Lagergren pseudo-second-order model.

REFERENCES

[1] R. Soni and D.P. Shukla, *Chemosphere*, 2019, **219**, 504-509.

[2] L.K. Wu, H. Wu, Z.Z. Liu, H.Z. Cao, G.Y. Hou, Y.P. Tang and G.Q. Zheng, *J. Hazard. Mater.*, 2017, **347**, 15-24.

[3] N. Rajić, Dj. Stojaković, S. Jevtić, N. Zabukovec Logar, J. Kovač, and V. Kaučič, *J. Hazard. Mater.*, 2009, **172**, 1450-1457.

[4] N. Rajić, Dj. Stojaković, M. Jovanović, N. Zabukovec Logar, M. Mazaj and V. Kaučič, *Appl. Surf. Sci.*, 2010, **257**, 1524-1532.

[5] Š. Cerjan-Stefanović, N. Zabukovec Logar, K. Margeta, N. Novak Tušar, I. Arčon, K. Maver, J. Kovač and V. Kaučič, *Micropor. Mesopor. Mater.*, 2007, **105**, 251-259.

[6] Y. Garcia-Basabe, I. Rodriguez-Iznaga, L. C. De Menorval, P. Llewellyn, G. Maurin, D. W. Lewis, R. Binions, M. Autie, and A. R. Ruiz-Salvador, *Micropor. Mesopor. Mater.*, 2010, **135**, 187-196.

[7] M. Bayat, V. Javanbakht and J. Esmaili, *Int. J. Biol. Macromol.*, 2018, **116**, 607-619.

ZSM-5 AS SORBENT FOR REMOVAL OF LINURON FROM WATER

Ivana Mihajlović, Ali Hgeig, Mladenka Novaković, Nevena Živančev, Maja Petrović
University of Novi Sad, Faculty of Technical Sciences, Department of Environmental Engineering and
Occupational Safety and Health, Trg Dositeja Obradovića 6, 21000 Novi Sad, Serbia
E-mail: mladenkanovakovic@uns.ac.rs

ABSTRACT

Zeolite Socony Mobil-5 (ZSM-5) was used as sorbent to remove linuron pesticide from water. The main parameters of adsorption process such as dosages of adsorbent, contact time and initial concentration of linuron were investigated. Removal efficiencies ranged from 89.50 % to 69.91 % as the initial linuron concentration increased from 2 to 15 mg L^{-1}. Results were modelled by adsorption isotherms: Langmuir, Freundlich and Temkin isotherms. The best correlation was achieved with Temkin adsorption isotherm. Adsorption kinetics of linuron has been studied by the pseudo-first-order model and the pseudo-second-order model. The kinetic studies showed significant correlation for the pseudo- second -order model which indicates that linuron is chemisorbed on analysed zeolite.

Key words: pesticide, water treatment, zeolite, adsorption, separation.

INTRODUCTION

Pesticides as protection agents for plant diseases have an essential role to improve agricultural activities and increase food production. The wide application of pesticides also causes environmental problems related to the distribution of pesticides in the environment, particularly to water ecosystems [1]. Pesticides are often detected at low concentration levels and commonly occur in the form of complex mixtures, which are harmful to life because of their toxicity, carcinogenicity and mutagenicity [2,3]. This is the reason for development efficient remediation techniques to remove pesticides from the water environment [4].

Natural zeolites have a strong ability to adsorb water molecules without the crystal structure of zeolites. The polarity, shape and size of the diffusing molecules present one of the essential characteristics to choose the adsorption relative to the geometry of pores of the zeolites. Zeolite Socony Mobil-5 (ZSM-5) is an aluminosilicate with the chemical formula of $Na_nAl_nSi_{96-n}O_{192}\cdot 16H_2O$ $(0<n<27)$. Zeolite ZSM-5 has a very high temperature and acid stability (>1000 °C and down to pH=3, respectively). It is synthesized at high temperatures and pressures in an autoclave coated with Teflon and is characterized by low water solubility. Zeolite ZSM-5 is a type of a "high-silica"-Zeolite, which is responsible for most of its special properties.

The aim of this paper is to investigate the influence of main parameters such as pH, contact time, mass of adsorbent ZSM-5 and initial concentration of selected pesticide on the removal of linuron from aquatic media. Linuron (3-(3, 4-dichlorophenyl)-1-methoxy-1-methylurea) belongs to the group of herbicides which are widely applied for elimination of weeds bean, wheat, corn, sugarcane and potato.

EXPERIMENTAL

Measurements were conducted at the room temperature (25 ± 2 °C). Zeolite ZSM-5 (manufacturer Acros Organics, Geel, Belgium) was used as adsorbent for removal of linuron. Total surface area (BET) of ZSM-5 is 390 m^2g^{-1}. The batch experiments were carried out by varying pH, concentrations of linuron, contact time and amount of adsorbent. The mixtures were shaken at 140 rpm at room temperature. The analyses of linuron removal were performed using HPLC-DAD (1260, Agilent Infinity). Separation was performed with a reversed phase column Eclipse XDB-C18 (3 x 150 mm, particle size 3.5µm). The operating conditions were:

the flow of 0.8 mL min^{-1}, the temperature of the column was 25 ºC and injection volume of 10 µL. The isocratic separation with the ratio of mobile phases of 50:50 (water and acetonitrile) was used.

Adsorbed amount, q_e (mg g^{-1}), was calculated via the equation:

$$q_e = \frac{(C_0 - C_f)}{m} * V \tag{1}$$

where q_e is the adsorption capacity (mg g^{-1}), C_0 and C_f are the initial and final linuron concentrations, respectively (expressed in mg L^{-1}), V is the solution volume (mL) and m is the adsorbent dosage (g).

The adsorption isotherms models Langmuir, Freundlich and Temkin were applied for the fitting of the experimental data. The kinetic of the adsorption data was analysed using the pseudo-first order and pseudo-second-order model.

RESULTS AND DISCUSSION

The influence of pH value on the removal of linuron by ZSM-5 was studied for values 3,5,6,7,8 and 10. The recoveries varied from 77.2 % to 87.75 % (from pH 10 to pH of 3). It was observed that the optimum pH value is 3 with removal efficiency of 87.75 %. The optimum mass for removal of linuron was 40.00 g L^{-1} at pH 3.00 and contact time of 60 min. The obtained results indicate that the removal percentage of selected pesticide raises with an increment in the adsorbent dosage from 20.00 to 60.00 g L^{-1} for linuron. With increased adsorbent dosage, the available sorption surface and availability of more adsorption sites rise, which results in more adsorbate attributed to the surfaces.

Table 1. Isotherm constants of the Langmuir, Freundlich and Temkin models for removal of linuron by ZSM-5.

	Isotherm model	Parameters
Langmuir	q_{max} (mg g^{-1})	0.880
	K_L (L mg^{-1})	0.125
	r	0.421
	RMSE	0.020
	χ^2	0.072
Freundlich	K_f	0.111
	$1/n$	0.804
	r	0.909
	RMSE	0.021
	χ^2	0.037
Temkin	B (J L^{-1})	0.108
	A	3.404
	r	0.948
	RMSE	0.024
	χ^2	0.036

Influence of initial concentration on separation of linuron from water was studied at optimal experimental conditions pH = 3.00, adsorbent dose 40.00 g L^{-1}, contact time 60 min and temperature 25.0 ± 1 ˚C, respectively. Removal efficiencies ranged from 89.50 % to 69.91 % as the initial linuron concentration increased from 2 to 15 mg L^{-1}. The adsorption capacity values increased continuously with the increase of initial linuron concentration from 0.038 to 0.30 mg L^{-1}. The results were fitted with Langmuir, Freundlich and Temkin models. Isotherm's best fit was chosen based on the largest correlation coefficient (r) value. The results in Table 1. showed that Temkin isotherm fitted better than the other two isotherms.

The removal of linuron as a function of contact time was observed. The removal increased rapidly as the contact time increased from 5.00 to 120 min. The adsorption process took 60 min to reach equilibrium. Hence, the contact time of 60 min was considered as optimum. The initial concentration of linuron in the solution is significant parameter as the pesticides concentration changes over a broad range in industrial effluents. The kinetic of the adsorption data was analysed using the pseudo-first order and pseudo-second-order model (Figure 1 and Figure 2). These results indicate that the pseudo-second order model portrays more properly the sorption kinetic than the pseudo-first order model. According to literature, the pseudo–second-order kinetic model indicates that adsorption mechanism is based on chemical sorption which involves valency forces through sharing or exchanging electrons between a sorbent and sorbate [5,6].

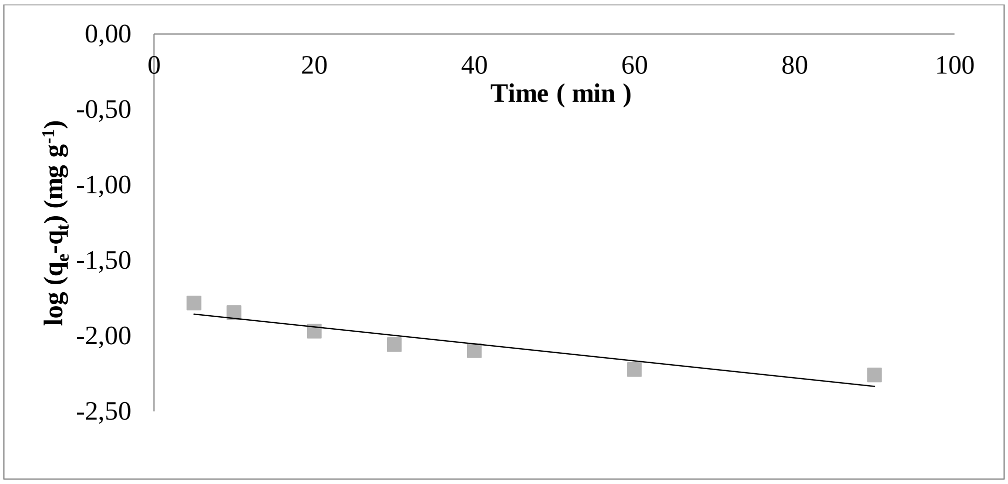

Figure 1. Pseudo-first order kinetics plot of linuron on ZSM-5.

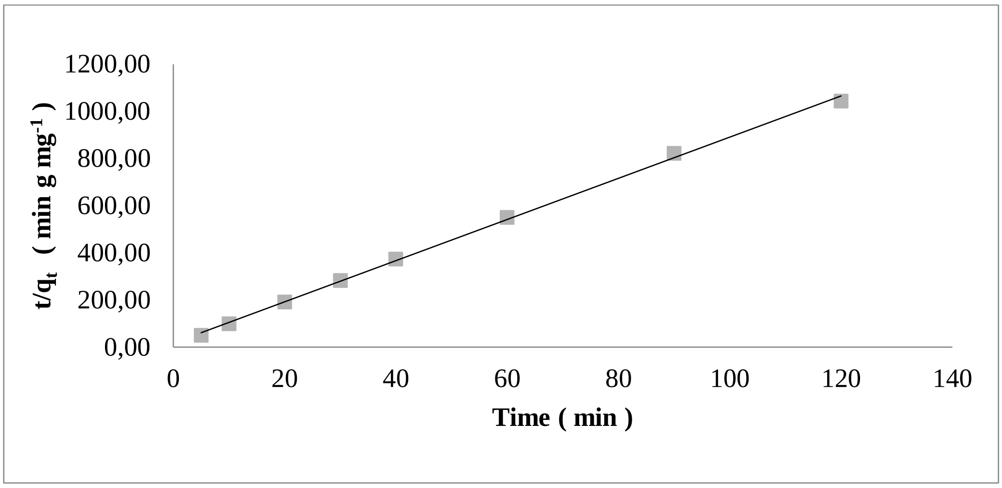

Figure 2. Pseudo-second order kinetics plot of linuron onto ZSM-5.

CONCLUSION

In the current research study, the ZSM-5 zeolite was used as sorbent for separation of linuron from water. The main process parameters such as pH, initial concentration of pesticide, mass of sorbent and contact time were investigated. The equilibrium studies proved that Temkin isotherm model the best describes the adsorption of linuron on zeolite. The kinetic modelling studies showed that kinetics of linuron on zeolite ZSM-5 followed the model of pseudo - second order. The results showed high recovery rates and indicate efficient separation of linuron from water by zeolite ZSM-5.

ACKNOWLEDGMENT

The authors acknowledge for the funding provided by the Ministry of Education, Science and Technological Development through the project no. 451-03-68/2020-14/200156: “Innovative scientific and artistic research from the FTS domain”.

REFERENCES

[1] F.W. Shaarani and B.H. Hameed, *Desalination*, 2010, **255 (1)**, 159-164.

[2] R.J. Gilliom, *Environ. Sci. Technol.* 2007, **41 (10)**, 3408-3414.

[3] C. Zhang, Q. Wang, J. Chen, L. Huang, X. Qiao, X. Li and X. Cai, *Environ. Pollut.* 2011, **159 (2)**, 609-615.

[4] L.H. Mendoza-Huizar, *J. Chem.* 2015, **3**, 1-11.

[5] T.R. Sahoo, B. Prelo, Chapter 7 "*Adsorption processes for the removal of contaminants from wastewater: the perspective role of nanomaterials and nanotechnology*" in: "*Nanomaterials for the Detection and Removal of Wastewater Pollutants*", B. Bonelli, F. Freyria, I. Rossetti and R. Sethi (Eds.), Elsevier Science, Amsterdam, 2020, 162-222.

[6] L. Fu, J. Li, G. Wang, Y. Luan and W. Dai, *Ecotoxicol. Environ. Saf.* 2021, **217**, 112207.

SILANOL NETWORKS IN ZEOLITES INVESTIGATED WITH SOLID-STATE NMR

Eddy Dib[1], *Izabel C. Medeiros-Costa*[1], *Georgi Vayssilo*[2], *Hristiyan Aleksandrov*[2], *Svetlana Mintova*[1]
[1]Laboratoire Catalyse et Spectrochimie (LCS), Normandie University, ENSICAEN, CNRS, 6 boulevard du Marechal Juin, 14050 Caen, France
[2]Faculty of Chemistry and Pharmacy, University of Sofia, 1126 Sofia, Bulgaria
E-mail: dib@ensicaen.fr

ABSTRACT

The amount and location of acid sites (strong Brønsted and weak silanols) in zeolites are crucial for their applications. In this work we investigate the complex H-bonded silanol networks in MFI-type zeolites using solid-state NMR combined with DFT calculations. The spectral signatures are disclosed based on the experimental and theoretical correlations.

Key words: Solid-state NMR, silanol defects, Brønsted acid sites, DFT.

INTRODUCTION

The activity of zeolites resides in special hydroxyl groups present within their frameworks: the Brønsted acid sites (BAS) present at the oxygen bridge between Si and Al atoms (≡Si-OH-Al≡). Other hydroxyl groups, less acidic, exist in zeolites: the silanols, adjacent to Si atoms (≡Si-OH) inside the channels or on the solid's surface. The former ones are still a hot topic and several recent researches attempted their localization. The latter, are gaining a lot of interest lately since they permit the engineering of well-known zeolite structures to functionalize them or improve their catalytic performances. They are also identified as deactivation sites being sensitive to moisture and trappers of coke leading to low stability and short catalyst lifetime [1].

The conventional diffraction techniques being often not satisfactory to locate light atoms such as hydrogen due to their low atomic number and their high thermal vibrations [2], solid-state Nuclear Magnetic Resonance (SSNMR) can be a powerful tool to solve such a problem. Both hydroxyl groups (BAS and silanols) were the subject of several spectroscopic investigations to identify, localize or quantify them. ^{27}Al, ^{29}Si, ^{1}H SSNMR and infrared spectroscopy were the most used techniques. However, the overlapping of the corresponding signals hinders precise interpretations. The limitations encountered are intrinsic to each technique, both spectroscopies suffer from a low resolution because of the occurrence of strong couplings and hydrogen bonds [3]. Either the isotropic chemical shifts in NMR or the wavenumber frequencies of the O-H bonds in infrared spectroscopy are varying in small ranges reaching the limits nowadays to give new insights on the hydrogen environments in zeolites [4,5].

Several types of defects have been identified in the zeolite frameworks as shown in Figure 1. They include silanols coming from hydrolyzed Si–O–Si bridges; generated by missing tetrahedral framework atoms and those present on the external surface [6]. In addition, siloxy defects (SiO^-) were identified. They exist in the as-synthesized materials to balance the positive charge of the organic structure directing agents (OSDA). In these defects, either pairs or triads, the valence of the oxygen atom is approximately equal to one instead of two for Si–O–Si bridges and thus they are stabilized by a SiO^- . . .HOSi hydrogen bond [7]. Furthermore, the electronic density of the oxygen involved in a hydrogen bond depends on the O–...H donor-acceptor distance. Its length was estimated to be 1.7 Å using the empirical correlation between the OH bond length and the proton (^{1}H) NMR chemical shift (10.2 ppm). This increases the electronic density of the oxygen atom but is still not enough to neutralize the system and additional positive charges are needed [8].

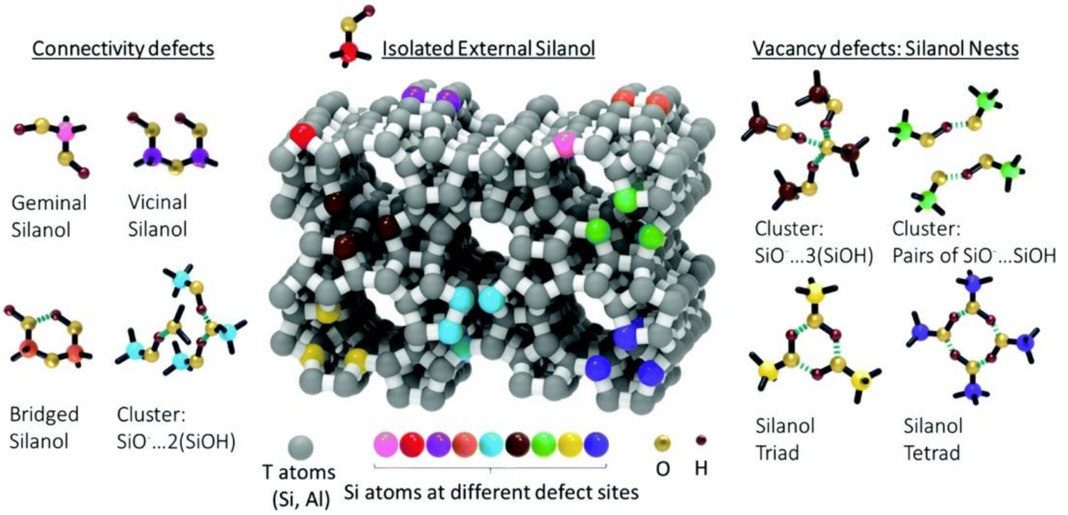

Figure 1. Schematic representation of different types of silanols grouped into three main categories: isolated external silanols, connectivity defects and vacancy defects. Green dotted lines indicate hydrogen bonding [1].

The present contribution presents the role of the OSDA in the positioning and orientation of the siloxy/silanol defects in pure silica zeolite using SSNMR and DFT calculations. Indeed, understanding the interactions between the OSDA and defects in zeolites is a necessary step toward a rational control of their distribution, and to subsequently use this knowledge for positioning catalytic sites using heteroatom substitutions.

EXPERIMENTAL

The following molar composition of the precursor suspensions were used for the synthesis of silicalite-1 samples with MFI type framework structure: 1.0 SiO2: 0.24 SDA: 20 H2O. In a typical synthesis, 5.0 g of tetraethyl orthosilicate (TEOS) was added to the corresponding weight of structural directing agents (SDA: methyltributylammonium hydroxide (MeTrBAOH) and tetrapropylammonium (TPAOH)) and 3.95 g of water under stirring at room temperature (pH =12). The obtained water-clear suspensions were stirred for 3 h at room temperature and further hydrolyzed for 4 h on an orbital shaker. The final suspensions were subjected to hydrothermal treatment at 363 K for 8 h. After crystallization, the nanometer-sized silicalite-1 crystals were purified by high-speed centrifugation (20000 rpm, 20 min). The obtained solid product was washed with hot doubly deionized water (heated at 343 K for 30 min) till the pH reaches 7.5. The nanometer-sized silicalite-1 crystals were subjected to freeze drying in order to prevent irreversible agglomeration. The freeze-dried samples were calcined at 823 K (heating rate 2 K/min) in air for 6 h. The samples synthesized with TPA and MeTrBA are abbreviated as TPA-silicalite-1 and MeTrBA-silicalite-1, respectively. One and two dimensional ^{1}H magic-angle spinning (MAS) NMR spectra were acquired at 500.07 MHz on a Bruker Avance III-HD (11.7 T), using 1.9-mm outer diameter probes zirconia rotors spun at 40 kHz, a radiofrequency power of 100 kHz and a recycle delay of 2s. The recoupling of the DQ coherence was performed following the BaBa pulse sequence. The incremented delay in the indirect dimension (δ t_1) is equal to 50 μs (i.e., two times the rotor spinning period). The DFT calculations were performed with ORCA, an Ab Initio, DFT and Semiempirical electronic structure package (vers. 4.1.2) [11], with hybrid gradient-corrected PBE0 exchange-correlation functional. Geometry optimization was performed with def2-SVP basis set with utilization of def2/J auxiliary basis.

REULTS AND DISCUSSION

The symmetry of the (MeTrBA) OSDA is changed with respect to TPA cation keeping the mass of the molecule as close as possible to the TPA, as well as the total number of carbon atoms. In parallel, pure silicate-1 (MFI) using TPA as OSDA was prepared as a reference sample. MFI was chosen as it presents two different types of channels, in which previous works have shown that alkyl chains of the OSDA may have preferential orientation and therefore, it is a good candidate to evidence possible change in the defect locations depending on the OSDA structure and symmetry [12].

The Figure 2 shows the conventional and the 2D DQ/SQ ^{1}H MAS NMR spectra of both the as-synthesised TPA-silicalite-1 and MeTrBA-silicalite-1 zeolites displaying a group of resonances between 1.0 and 4 ppm assigned to the protons of the TPA and MeTrBA cations. The isolated peak at 10.2 ppm present in both cases is attributed to the SiO^- . . . HOSi defects. In both cases, the principal information given by this experiment is the presence of the correlation (shown by the dashed lines) observed between the siloxy/silanol defects at 10.2 ppm and the protons from the terminal methyl groups in the propyl and butyl chains of the TPA and MeTrBA cations, respectively. In the particular case of MeTrBA-silicalite-1, it is interesting to note that no cross-peak resulting from the interaction between the methyl protons of the isolated methyl group (3 ppm) and the ones present in the butyl chains (1 ppm) is observed, nor between the isolated methyl group and the defects.

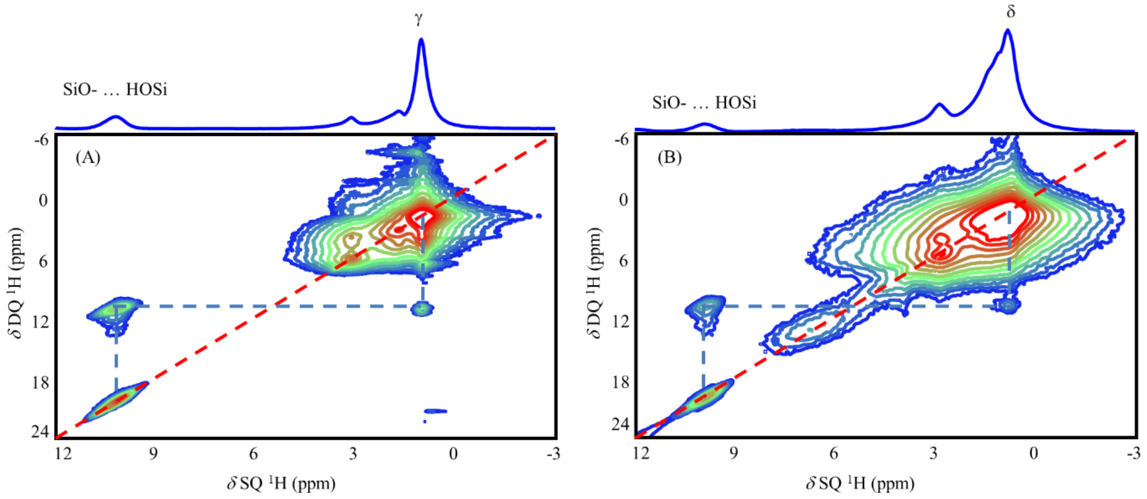

Figure 2. 1D and 2D DQ/SQ correlation ^{1}H NMR spectra of the as synthesized (left) TPA-silicalite-1 and (right) MeTrBA-silicalite-1 recorded at 500 MHz [10].

These observations can be interpreted as follows: the defects are definitely in the close vicinity of the terminal methyl groups of the longer chains (propyl or butyl) in both samples. Such a conclusion was already delivered in the case of the TPA cation. [9] However the present observations for the MeTrBA-silicalite-1 show clearly the general tendency of the siloxy/silanol defects to be always located near the end of the longer chains. Considering that the positive charge of the alkyammonium is mainly carried by the nitrogen atom, the present results show that the negative charge of the defects are situated as far as possible from the nitrogen atoms. This can be understood by considering that this arrangement is optimal to minimize the whole crystal electrostatic energy.

However, it has been shown for non-symmetric alkyl ammonium, there is a preferential orientation of the alkyl chains in the channels. For instance, the butyl chains have a preferential orientation toward the sinusoidal channels. Therefore, for TPA, with one molecule per intersection, all channels must contain a propyl chain. The fact that the silanol groups are close to the terminal methyl groups of these propyl chains show that the defects are mostly located in the middle of the channels. There is no evidence that these defects may occupy preferentially either the straight or sinusoidal channels, and therefore the defects are most likely randomly parted between the two possible positions.

The arrangement is different in the case of silicalite-1 synthesized with MeTrBA (sample MeTrBA-silicalite-1) because the butyl chains should be preferentially oriented in the sinusoidal channels, and hence the methyl is expected to point toward the linear channels. Moreover, the steric constraints must favour the location of two butyl chains in the longer sinusoidal channel, instead of the linear channels. Considering these arguments, we expect that the MeTrBA cations are ordered in the channels, with two butyl groups in the sinusoidal and one butyl and one methyl group in the linear channels. Consequently, as the defects are located close to the terminal methyl of the butyl groups, they are most probably located in the sinusoidal channels.

CONCLUSION

In conclusion, the location of the siloxy/silanol (SiO-…HOSi) may be tuned during hydrothermal synthesis by changing the symmetry of the OSDA. It was shown that preferential location of these defects is near the terminal methyl groups of the longer alkyl chains, and thus far from the nitrogen atoms. We postulate based on the preferential orientation of the alkyl groups in the various channels of the MFI structure, that in the case of the non-symmetric MeTrBA template, they are located in the sinusoidal channels, while for the symmetric TPA template they can be randomly distributed among the two types of channels. This work shows that a careful choice of the OSDA agent may be a means to induce a preferential location of the defects in the structure, which can be evidenced by 2D DQ/SQ correlation ^{1}H NMR spectroscopy. Finally, it can be anticipated that such approach might be the way to control the position of the active sites, for example, in acid zeolite catalysts.

REFERENCES

[1] I.C. Medeiros-Costa, E. Dib, N. Nesterenko, J-P. Dath, J-P. Gilson and S. Mintova, *Chem. Soc. Rev.*, 2021, Advance Article, https://doi.org/10.1039/D1CS00395J.

[2] M. Inui, T. Ikeda, T. Suzuki, K. Sugita and F. Mizukami, *Bull. Chem. Soc. Jpn.* 2009, **82**, 1160-1169.

[3] T. Steiner, *Angew. Chem. Int. Ed.* 2002, **41**, 48-76.

[4] G. Paul, C. Bisio, I. Braschi, M. Cossi, G. Gatti, E. Gianotti and L. Marchese. *Chem. Soc. Rev.*, 2018, **47**, 5684-5739.

[5] K. Hadjivanov, *Advances in Catalysis*, 2014, **57**, 99-295.

[6] J. Chezeau, L. Delmotte, J. Guth and Z. Gabelica, *Zeolites* 1991, **11**, 598-606.

[7] H. Koller, R.F. Lobo, S.L. Burkett and M.E. Davis, *J. Phys. Chem.* 1995, **99**, 12588-12596.

[8] E. Brunner and U. Sternberg, *Prog. Nucl. Magn. Reson. Spectrosc.* 1998, **32**, 21-57.

[9] E. Dib, J. Grand, S. Mintova and C. Fernandez, *Chem. Mater.*, 2015, **27**(22), 7577-7579.

[10] E. Dib, J. Grand, A. Gedeon, S. Mintova and C. Fernandez, *Micropor. Mesopor. Mater.*, 2021, **315**, 110899 (1-4).

[11] F. Neese, *Wiley Interdiscip. Rev. Comput. Mol. Sci.*, 2017, **8**, e1327, 1-6.

[12] E. Dib, A. Gimenez, T. Mineva and B. Alonso, *Dalton Trans.*, 2015, **44**, 16680–16683.

CHARACTERIZATION OF METAL SPECIES IN METAL-MODIFIED HIERARCHICAL MORDENITE

Ivana Landripet, Marko Robić, Andreas Puškarić, Josip Bronić
Department of Chemistry, Division of Materials Chemistry, Laboratory for Synthesis of New Materials, Ruđer Bošković Institute, Zagreb, Croatia
E-mail: Ivana.Landripet@irb.hr

ABSTRACT

Two methods were investigated to synthesize mesoporous mordenite. PXRD showed that the samples made by both methods are crystalline mesoporous material with MOR framework. The transition metal cations Ag and Fe were introduced by the ion exchange method. The introduction was confirmed with EDS and AAS analysis. UV–Vis spectroscopy was applied to identify the silver and iron species in samples.

Key words: zeolite, mordenite, hierarchical, wet impregnation.

INTRODUCTION

The unique physicochemical properties of the zeolites, such as their controlled acidity, adsorption capacity, ion exchange properties, thermal stability, as well as uniform channels and cavities crystallographically ordered in size and position, determine their effectiveness in catalytic processes. Mordenite is widely used in catalysis, separation, and purification because of its uniform, small pore size, and high internal surface area. Mordenite is a zeolite with two-dimensional pores, as the structure determined by Meier in 1961 showed [1]. The pore system of mordenite consists of main channels of 6.5 × 7.0 A, which are connected by tortuous pores of 2.6 × 5.7 A that form the so-called side pockets. Since the latter is too small for most molecules to enter, mordenite is generally regarded as a mono-dimensional zeolite.

The major drawback of mordenite and zeolites, in general, is the limited size of the channels and cavities and the lack of interconnectivity. This imposes diffusional limitations on reactions, limiting their activity, selectivity, and stability [2]. Despite the microporous structure, there are limitations that decrease the efficiency of the zeolite as catalysts. Such limitations can be avoided by creating mesoporous voids. Another important issue in catalysis efficiency is the number of active sites. Its number can be increased with a number of hetero T-atoms within the framework by post-synthesis treatment, such as ion exchange. Metal-modified zeolites being a very suitable substrate for selective catalytic activity.

EXPERIMENTAL

Synthesis of classical mordenite microcrystals (M-1)

Zeolite with oxide formula 20.2 SiO_2 x 4.4 Na_2O x Al_2O_3 x 173 H_2O was prepared by mixing silica and alumina alkaline solutions. The resulting gel was stirred at room temperature for 30 min. The mixture was subsequently transferred to a Teflon-lined stainless steel autoclave. The hydrothermal treatment was carried out for 5 days at 180 °C under static conditions. Autoclaves were cooled down to room temperature, and solid products were filtered off, washed thoroughly with distilled water, and dried overnight at 70 °C. The calcination of the samples was carried out at 550 °C for 10 h (2 °C min^{-1}) in the air stream. H-form of the sample was obtained by ion exchange with 0.8 M NH_4NO_3 at room temperature followed by calcination. Intracrystalline mesoporosity was developed by post-synthesis treatment with 0.2 M NaOH solution followed by ion exchange with NH_4NO_3 and calcination in a stream of air.

One-pot synthesis of mesoporous mordenite (MOR)

The second strategy of mordenite preparation with the same Si/Al ratio was the direct synthesis of hierarchical structure. It was made using a similar procedure with pore generating agent, respectively cetyltrimethylammonium bromide, CTAB. The duration of the synthesis was shortened by 1 day, and the crystallization temperature was lower by 30 °C. H-form of the sample was obtained by ion exchange with 0.8 M NH_4NO_3 at room temperature followed by calcination.

Implementation of Fe and Ag cations

Mono- and bimetallic systems of Ag, Fe, and Ag–Fe were prepared by the ion exchange method in H-form mordenite. For that purpose, slightly acidic solutions of $Fe(NO_3)_3$ and $AgNO_3$ were used. The samples of H-form mordenite were added to the preheated metal salt solution and stirred for 1 hour. After 1 hour the samples were filtered, dried, and the procedure was repeated for another 1 hour. After drying at 90 ° C, the samples were calcined at 550 °C in a stream of air.

RESULTS AND DISCUSSION

Classical mordenite microcrystals were prepared by hydrothermal synthesis. Parent material (M-1) was obtained after the introduction of mesoporous voids by post-synthesis treatment with 0.2 M NaOH solution followed by ion exchange with NH_4NO_3 and calcination. The second strategy, respectively one-pot synthesis using CTAB, resulted with slightly less crystalline material corresponds to the structure of mordenite (MOR) (Fig. 1).

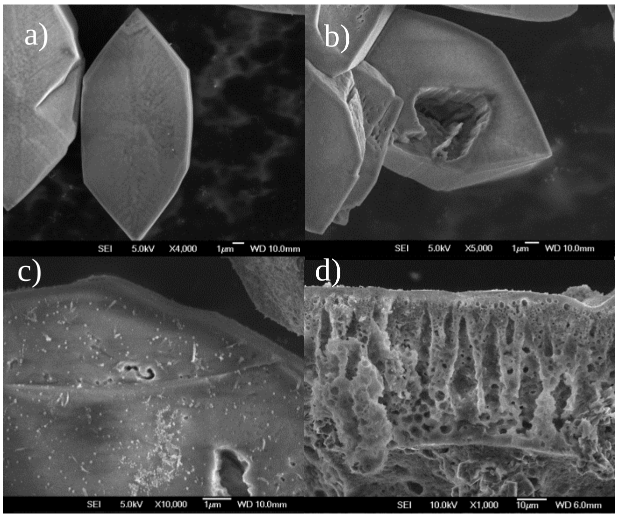

Figure 1. FE-SEM images of a) M-1, b) M-1 after treatment with 0,2 M NaOH (M-1-0.2NaOH) solution, c) surface of M-1+Fe and d) MOR.

Mono- and bimetallic systems of Ag, Fe, and Ag–Fe were prepared by the ion exchange method in H-form mordenite samples. PXRD patterns of parent materials show that the structure corresponds to the structure of mordenite (Fig. 2). Wet-impregnation treatments did not have a significant influence on the crystallinity of the samples. The exchange for metals changed only the intensity of the peaks. The missing peak (020) in the diffractogram of the samples with Ag occurs due to the displacement of H^+ cations, originally located in small mordenite channels, that occur under the action of the wet impregnation procedure. The H^+

cations leave their site, but Ag^+ cations do not replace them, preferring to settle in the main channel near the entrance to the side pocket.

The exact concentration of metals in all samples was confirmed with AAS analysis. Interesting is the fact that after all post-synthetic treatments the Si/Al ratio remained preserved.

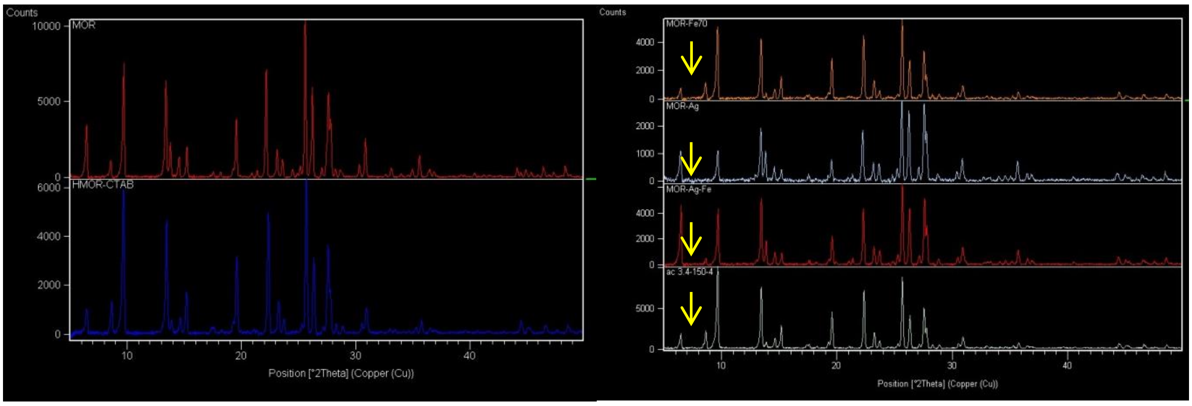

Figure 2. PXRD of parent materials M-1 (blue) and MOR (red) (left); PXRD patterns of wet impregnated MOR with Ag and Fe cations (right).

UV–Vis spectroscopy was applied to identify the silver and iron species. UV–Vis spectroscopy identify the silver and iron cationic species (Fig. 3). The peak with a maximum around 210 nm, and the shoulder around 220 nm correspond to the Ag^+ electronic transitions of isolated silver ions located on the ion exchanged sites of the mordenite framework. The other observed bands are attributed to the small silver cationic clusters. In the case of samples with iron, the spectra show a band with a maximum centered at 270 nm, which is attributed to oxygen-to-iron charge transfer of isolated Fe^{3+} ions in tetrahedral coordination. Additionally, two more contributions took place; 340 nm, which is related to octahedral Fe cations in oligomeric clusters of the Fe_xO_y type inside the mordenite channels, and 470 nm, corresponding to the Fe_2O_3 particles located on the external surface of mordenite crystals [3]. Those particles on the external surface of M-1 are visible on FE-SEM images (see Fig. 1).

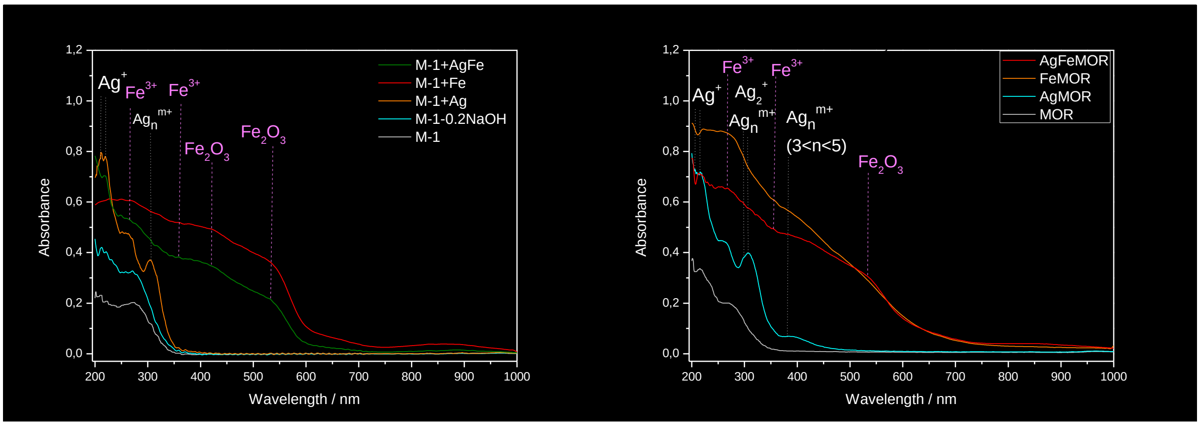

Figure 3. UV-Vis spectra of the M-1 samples (left) and MOR samples (right) in a wavelength range of 200 nm to 1000 nm

Due to the usually specific behaviour of the Ag and Fe cations under the light, photostability was confirmed by exposing the samples to radiation in the wavelength range of 200 to 1000 nm.

CONCLUSION

Samples of mordenite were prepared by a feasible method, which is suitable for application in industrial production. Introduction of mesoporous voids (hierarchical structure of the crystals) was obtained by post-synthesis treatment with 0.2 M NaOH solution or using the mesoporous template (CTAB) during catalyst synthesis. That resulted in micro- and mesoporous mordenite crystals. The second part of the post-synthesis treatment was done using wet impregnation with slightly acidic salts solutions. The content of all cations is confirmed by EDS and AAS analysis. Identification of the silver and iron species was also made using UV-Vis spectroscopy. In the M-1 samples, different morphology of the iron oxide was deposited on the crystal surface, while in the MOR samples this was not the case.

REFERENCES

[1] W.M. Meier, *Z. Kristallogr.*, 1961, **439**, 115.

[2] X. Li, R. Prinsa and J.A. van Bokhoven, *Journal of Catalysis*, 2009, **262,** 257-265.

[3] P. Sánchez-López, Y. Kotolevich, S. Miridonov, F. Chávez-Rivas, S. Fuentes and V. Petranovskii, *Catalysts*, 2019, **9**(1), 58.

ZEOLITE TEMPLATE CARBON PERFORMANCES IN CATALITIC AND ADSORPTION APPLICATIONS

Girolamo Giordano
Laboratory of Chemical Engineering, Catalysis and Sustainable Processes CECaSP_Lab
University of Calabria, Italy
E-mail: ggiordaunical@yahoo.it

Carbon-based materials synthesized in the nanochannels of powdered zeolite acting as Template (Zeolite Template Carbon ZTC) are a relatively new class of materials that are receiving a growing attention from the scientific community for their interesting properties that can be in turn tuned to obtain tuneable porosity features. Owing to their large specific surface area (up to 4000 m^2/g), nano-ordered structure, chemical stability and electric conductivity ZTC represent promising materials in different fields: from classic capacitors applications to more innovative (electro)catalytic and Carbon Capture and Storage (CCS) processes.

Providing large surfaces of the material, they can potentially guarantee high performances in all the applications based on surface interaction: storage processes with the advantage of the reversible gas adsorption phenomena and catalytic systems. This talk offers an overview about synthesis and some recent findings on those new application fields, taking into account one of the less considered aspect of ZTC: the presence of surface oxygen bonded in different ways to the carbon. Of course, these “defects” on the surface could not be avoided as it comes mostly from the synthesis/purification processes, but the content and type of carbon-oxygen bond significantly affect the surface properties. In addition, even though few examples have been published in the literature, chemical treatments can be also used to modify and tune the oxygen content, tailoring the ZTC properties to specific applications.

The talk will offer two different examples of “oxygen-modulated” ZTC applications in the general field of carbon dioxide emission reduction, either in case of Capture-and -Storage system or in the field of electrocatalytic reduction, as potential support to a high impact strategy to close the anthropogenic carbon cycle.

In the CO_2 adsorption, the high order of structural framework favourably impacts on the gas adsorption capacity. Low-pressure adsorption data revealed that two main parameters affect the performances: specific surface area and surface post-synthesis treatment governing the oxygen amount. Experimental evidences indicate that high surface area favours the CO_2 adsorption together with a high microporous fraction. In the case of surface treated ZTC, the reduction of the oxygen present on the pore surface causes a reduction of the CO_2 adsorption capacity recovered after a couple of CO_2 adsorption cycles indicating a structure stabilization, induced by CO_2, with reduction of defect groups favouring the adsorption in a complete reversible way from the third cycle on.

The study of electrocatalytic behaviour of ZTCs based electrodes in the electrocatalytic reduction of CO_2 offers a clear example of how the de-oxygenation treatment allows a significant increase of selectivity toward formate production, observing a Faradaic efficiency quadrupled in comparison with the untreated ZTCs samples.

THE HEIGHT OF THE SCHOTTKY BARRIER VERSUS THE PHOTOCATALYTIC ACTIVITY OF TiO_2+Au COMPOSITES UNDER VISIBLE-LIGHT ILLUMINATION

Gregor Žerjav, Albin Pintar
Department of Inorganic Chemistry and Technology, National Institute of Chemistry, Hajdrihova 19,
SI-1001 Ljubljana, Slovenia
E-mail: gregor.zerjav@ki.si

ABSTRACT

Composites containing different TiO_2 supports (anatase nanoparticles (TNP) and nanorods (TNR)) and 1 wt. % of Au were synthesized using wet impregnation preparation procedure. The size of formed Au ensembles in the composites was influenced by the difference in the zeta potential value (pH_{PZC}) of TiO_2 supports. The positive surface charge of TNP nanoparticles during the wet impregnation synthesis positively influenced the formation of Ti_s-O-Au(III) complex. In turn, the average Au cluster size in the TNP+Au composite was smaller (2.4 nm) than in the TNR+Au composite (9.4 nm), where the surface of the TNR nanorods was negatively charged. The UV-Vis DR spectra of composites exhibited a broad absorption peak at 550 nm, which is typical for the plasmonic behaviour of Au clusters. A detailed XPS analysis of the valence band maxima (VBM) showed that the value of Schottky barrier height (SBH) in the TNP+Au composite (0.31 eV) was almost double compared to the one in the TNR+Au composite (0.16 eV). The visible-light generated “hot electrons” in Au clusters of the TNP+Au composite need more energy and longer time to overcome the SB when injected into the TNP, compared to “hot electrons” generated in the TNR+Au composite exhibiting lower SBH. Due to this obstacle, TNP+Au “hot electrons” have a higher potential to recombine with the generated holes in Au clusters than “hot electrons” injected into the TNR support. The higher specific surface area of the TNR support presents an additional advantage, which prolongs the “lifetime” of electrons in the TNR+Au composite. The electrons can use a larger area to generate reactive oxygen species (ROS) or oxidize adsorbed substrates compared to electrons in the TNP+Au composite.

Key words: TiO_2 nanorods/nanoparticles, Au ensembles, plasmonic noble metal, photocatalysis, Schottky barrier height.

INTRODUCTION

Heterogeneous photocatalysis with a semiconductor oxide as a catalyst has been indicated as highly effective for water remediation [1]. Due to various advantages (high photocatalytic activity, stability in water, low toxicity, moderate price, etc.), titanium dioxide (TiO_2) has been identified as one of the most suitable catalysts for the heterogeneous photocatalysis aimed for water purification [2]. The drawbacks of TiO_2 are its band-gap energy of 3.0-3.4 eV (charge carriers can be generated only under UV-light illumination) and poor quantum efficiency due to charge carrier recombination [3]. One of the approaches to overcome the drawbacks of TiO_2 is to combine it with noble metal Au [4] and to use the Au plasmonic properties to trigger the catalytic activity of TiO_2 under visible-light illumination. The main mechanisms of plasmonic photocatalysis under visible-light illumination are hot electron generation and injection, plasmonic resonance energy transfer (PRET), and plasmonic heating [5]. At the junction between the Au and TiO_2 a barrier is formed, which is called the Schottky barrier (SB) [6]. Au clusters generate “hot electrons”, if illuminated with light wavelength of which is equal or greater than Au surface plasmon resonance (SPR). The generated “hot electrons” are further injected into the conduction band of TiO_2. The height of the Schottky barrier (SBH) is influencing the efficiency of the plasmon induced electron injection at the interface between the Au and TiO_2. Therefore, an in-depth understanding of the SBH is of crucial importance for the development of plasmonic photocatalysts as the plasmon-driven transfer of "hot electrons" from the noble metal to the semiconductor significantly affects the overall photocatalytic activity of a plasmonic driven photocatalyst [7].

The aim of the present study was to investigate in detail how the textural properties and the zeta potential of anatase TiO_2 supports (nanoparticles (TNP) and nanorods (TNR)) influence the optical, electronic and photocatalytic properties of plasmonic-based TiO_2+Au composites with 1 wt. % of Au loading. Besides thorough characterization of synthesized solids with several methods (SEM, SEM-EDS, TEM, XRD, N_2 physisorption analyses, UV-Vis DR, recording photoluminescence (PL) spectra of solids, electrochemical impedance spectroscopy (EIS) analysis, etc.), one of the main objectives of the research work was to use XPS technique to determine the height of SB in the prepared TiO_2+Au photocatalysts and to correlate it with their ability to generate charge carriers under visible-light illumination. Further, we conducted photocatalytic tests in the presence of examined catalysts in a batch slurry reactor under visible-light illumination and using water-dissolved bisphenols (bisphenol A (BPA), bisphenol AF (BPAF), bisphenol S (BPS) and bisphenol F (BPF)) as model organic pollutants.

RESULTS AND DISCUSSION

The results of SEM and TEM analyses reveal that an average TNP nanoparticle expresses an ellipsoid shape with a 20 nm diameter and a length of 30 nm, whereas on the other hand TNR nanoparticles express a rode-like morphology with a diameter between 8-10 nm and a length of 70-100 nm. The difference in the morphologies of the anatase TiO_2 supports was well expressed also by the results of N_2 physisorption analysis (Table 1).

Table 1. Comparison of Au particle size, specific surface area (S_{BET}), average pore diameter (d_{pore}), total pore volume (V_{pore}), anatase TiO_2 crystallite size of studied catalysts, and results of SEM-EDS elemental analysis of TiO_2+Au composites.

Catalyst	$^{a}d_{Au}$ (nm)	S_{BET} (m^2/g)	d_{pore} (nm)	V_{pore} (cm^3/g)	Anatase crystallite size (nm)	Content (wt. %)		
						Ti	O	Au
TNR	/	105	19.3	0.57	16.7		/	
TNR+Au	9.4	93	18.9	0.44	16.5	57.4	41.9	0.7
TNP	/	82	14.8	0.30	20.9		/	
TNP+Au	2.4	68	16.1	0.27	20.2	63.3	35.8	0.9

[a]Au particle size was determined by counting more than 100 particles from acquired TEM images.

Further, the TEM analysis shows that the morphology of TNP and TNR supports did not change during the deposition of Au and that the morphology of TiO_2+Au composites is dominated by the TiO_2 support. The presence of Au in the composites was confirmed by the results of SEM-EDS analysis (Table 1). The XRD patterns of prepared materials illustrated diffraction peaks indicative for anatase TiO_2 and imply that the TiO_2 supports were stable during the Au deposition procedure and calcination. Also, the values of anatase crystallite size calculated from the corresponding width of the (001) diffraction peak ($2\theta=25^o$) by means of the Scherrer formula (Table 1), show that the anatase crystallite size of the composites was not affected by the catalyst preparation procedure. Average size of Au ensembles in the composites calculated from the TEM analysis (Table 1) show that the size of Au ensembles depends on the employed TiO_2 support as the average size of Au clusters in TNP+Au sample was 2.4 nm and 9.4 nm in the TNR+Au solid. The pH_{PZC} values of bare TiO_2 supports were significantly different with the pH_{PZC} value of 2.8 for the TNR sample and 7.2 for the TNP material. The pH value of the Au precursor solution ($HAuCl_4 \times 3H_2O$) during the composite preparation procedure was 3.4, which means that the surface of TNP nanoparticles was protonated and the surface of TNR nanorods deprotonated. The positive charge of the TNP surface beneficially influences adsorption of the $[Au(OH)_3Cl]^-$ complex through a strong electrostatic attraction, compared to the negative charge of the TNR surface. UV-Vis DR spectra of bare TiO_2 supports show the typical behaviour of anatase TiO_2 with a strong absorption in the UV range (200-350 nm) of the light spectra and consequently a large band gap of 3.26 eV. The spectra of the TiO_2+Au composites display additional spectral response in the visible-light range between 500 and 600 nm attributed to the plasmonic behaviour of the Au ensembles. The difference in the size of Au clusters in the composites (Table 1) might be the reason that the TNR+Au composites expressed higher intensity in the visible-light absorbance. The recombination of photo-induced electrons and holes releases energy in the form of PL emissions, therefore the intensity of the PL signal is proportional to the electron-hole recombination rate. The decrease in the PL intensities observed in the PL spectra belonging to TiO_2+Au composites is attributed to the formation of a Schottky barrier at the TiO_2 support/Au ensemble junction, which can act as an electron sink thus suppressing the electron-hole recombination. Regarding the TiO_2+Au composites, the PL intensity of TNR+Au composite was lower than the one of TNP+Au sample, so the recombination rate of charge carriers in the TNR+Au composite is lower. The ability of prepared photocatalysts for the separation of photo-generated electron-hole pairs upon illumination with visible light was tested by the EIS measurements. The EIS results show that TiO_2+Au composites are able to generate significantly more visible-light generated charge carriers than bare TiO_2 supports, which could be due to the plasmon properties of the Au ensembles. Further, EIS measurements reveal that the TNP+Au composite is able to generate less charge carriers than the TNR+Au composite. The results of VBM measurements of the investigated materials are illustrated in Fig. 1. The VBM positions of the measured materials with respect to Fermi level (E_F) were found to be 3.07 eV for TNP, 3.09 eV for TNR, 2.76 eV for TNP+Au and 2.92 eV for TNR+Au samples, respectively. The VBM of the composites shifts toward lower binding energies as a consequence of the charge transfer and formation of a Schottky barrier height (SBH) at the junction between TiO_2 support and Au clusters. The SBH values for the TNP+Au and TNR+Au composites were found to be equal to 0.31 and 0.16 eV, respectively.

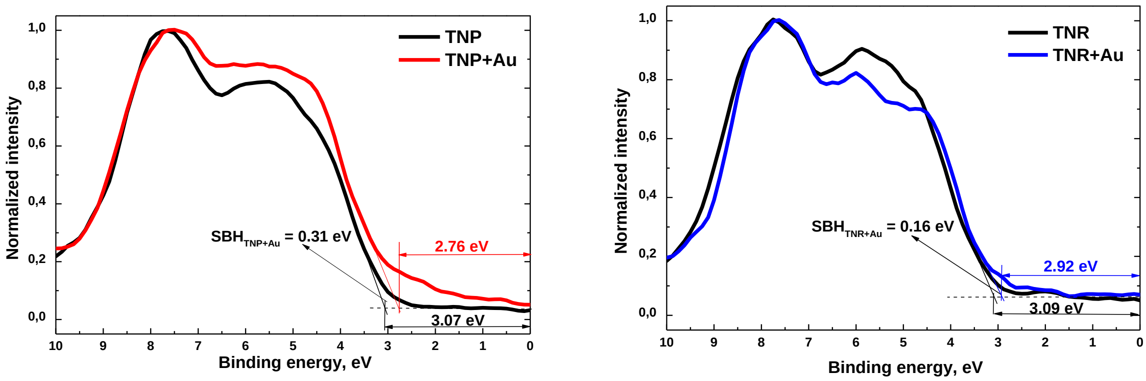

Figure 1. Determination of VBM of pure TiO_2 supports and TiO_2+Au composites by means of XPS analysis.

The prepared catalysts were investigated in a batch slurry reactor toward degradation of water-dissolved bisphenols under visible-light illumination. In the given range of operating and reaction conditions, pure TiO_2 supports show almost no or only minor ability to degrade bisphenols. However, significant decrease of concentration of model organic pollutants was obtained in the presence of TiO_2+Au composites. The results show that regardless which bisphenol analogue is used, the TNR+Au composite was able to degrade/mineralize higher amounts of bisphenols in comparison to the TNP+Au composite. This fact can be ascribed to the difference in the SBH (Fig. 1) and higher S_{BET} of the TNR+Au composite (Table 1), which makes the latter more accessible to water-dissolved molecules of organic pollutants in comparison to the TNP+Au sample. With the use of TNR+Au composite 75 % of BPA and 96 % of BPF were degraded; on the other hand, with the same composite 21 % of BPAF and 17 % of BPS were degraded after 120 min of visible-light illumination. The same trend was observed when we measured the mineralization extent (TOC_M) at the end of photocatalytic oxidation runs. Based on the measured conversions as well as extent of mineralization, the examined bisphenols can be divided into two groups: BPA and BPF on one side, and BPAF and BPS on the other. The measured differences in degradation rates of the bisphenols can be ascribed to differences in their chemical structures with the consequence that different pathways of their degradation occur. This results in different degradation products which express different resistances toward reactions with visible-light generated charge carriers and ROS.

CONCLUSION

Wet impregnation technique was used to produce TiO_2+Au composites with different TiO_2 supports (anatase nanoparticles (TNP) and nanorods (TNR)) and 1 wt. % Au loading. The results of SEM and TEM analyses show that the morphology of TNP and TNR supports did not change during the preparation procedure and that the TiO_2+Au morphologies are dominated by the morphology of TiO_2 supports. The average size of Au ensembles in the TNP+Au and TNR+Au composites was 2.4 and 9.4 nm, respectively. The Au ensembles in TiO_2+Au composites exhibited plasmonic behaviour as a broad absorption peak in the region between 500 and 600 nm was measured in the UV-Vis DR spectra. The TNR+Au composite exhibited a higher amount of visible-light generated charge carriers (EIS measurements) and lower recombination of charge carriers (PL measurements) rate than the TNP+Au composite. Detailed XPS analysis of VBM suggests that this is attributed to differences in the SB heights of the TiO_2+Au composites. The visible-light generated electrons in Au ensembles of the TNR+Au composite need lower energy to overcome the SBH of 0.16 eV, when they are injected into the valence band of TNR, compared to electrons in the TNP+Au composite, where the SBH is 0.31 eV. Another property that beneficially influences the photocatalytic activity of TNR+Au composite is its larger specific surface area. Experiments of photocatalytic oxidation of water-dissolved bisphenols over TiO_2+Au composites showed that visible-light generated charge carriers and ROS were successfully used for their oxidation and mineralization.

REFERENCES

[1] Y. Deng, R. Zhao, *Curr. Pollution Rep.*, 2015, **1**, 167-176.

[2] M.R. Hofmann, S.T. Martin, W. Choi, D.W. Bahnemann, *Chem. Rev.*, 2002, **95**, 69-96.

[3] Y. Cong, J.L. Zhang, F. Chen, M. Anpo, *J. Phys. Chem. C*, 2007, **111**, 6976-6982.

[4] D. Wang, S.C. Pillai, S.-H. Ho, J. Zeng, Y. Li, D.D. Dionysiou, *Appl. Catal. B*, 2018, **237**, 721-741.

[5] X. Chen, H.Y. Zhu, J.C. Zhao, Z.F. Zheng, X.P. Gao, *Angew. Chemie Int. Ed.*, 2008, **47**, 5353-5356.

[6] X. Chen, S. Shen, L. Guo, S.S. Mao, *Chem. Rev.*, 2010, **110**, 6503-6570.

[7] M.S. Arshad, Š. Trafela, K. Žužek Rožman, J. Kovač, P. Djinović, A. Pintar, *J. Mater. Chem. C*, 2017, **5**, 10509-10516.

THE EFFICIENCY OF NATURAL CLINOPTILOLITE FOR CIPROFLOXACIN REMOVAL FROM AQUEOUS MEDIA

Barbara Kalebić[1], Jelena Pavlović[2], Jelena Dikić[2], Aleksander Rečnik[3], Nikola Škoro[4], Nevenka Rajić[1]
[1]Faculty of Technology and Metallurgy, University og Belgrade, Karnegijeva 4, 11120 Belgrade, Serbia
[2]Innovation Centre of Faculty of Technology and Metallurgy, University of Belgrade, Karnegijeva 4, 11120 Belgrade, Serbia
[3]Jožef Stefan Institute, Jamova cesta 39, 1000 Ljubljana, Slovenia
[4]Institute of Physics, University of Belgrade, Pregrevica 118, 11080 Belgrade, Serbia
E-mail: bkalebic@tmf.bg.ac.rs

ABSTRACT

Adsorption of the antibiotic ciprofloxacin (CIP) from an aqueous solution by calcium-rich clinoptilolite (CLI) was investigated. Obtained results showed that natural CLI possesses a high adsorption efficiency in the removal of CIP at 283, 288 and 293 K and at pH= 5. Adsorption kinetics studied for the initial CIP concentrations of 15–75 mg dm^{-3} follow Lagergren's pseudo-second order equation and the adsorption is best represented by the Langmuir model. The adsorption mechanism involves strong electrostatic interactions between aluminosilicate lattice of CLI and the cationic form of CIP accompanied by an ion-exchange reaction. The CIP saturated CLI was successfully regenerated by a cold atmospheric pressure plasma treatment.

Key words: clinoptilolite, ciprofloxacin, adsorption, plasma treatment.

INTRODUCTION

The use of antibiotics in both human and veterinary medicine is constantly increasing, while water pollution by these organics is generally poorly regulated. Antibiotics present in water media have different adverse effects on environment as well as human health. They belong to organic micropollutants (OMPs) and cannot be efficiently removed from water by conventional water treatment processes. Consequently, it is of great importance to find acceptable alternative technologies for their removal from water.

CIP is widely applied antibiotic for treatment of both human and animal bacterial infections because of its excellent activity against Gram-positive and Gram-negative bacteria. Thus, it has been found in wastewater effluents in concentrations from ng to mg dm^{-3}, with extremely high concentration of up to 50 mg dm^{-3} near drug manufacturing plants [1]. Moreover, due to the CIP zwitterionic nature, the charge is strongly pH dependent.

CLI is the most abundant natural zeolite. It has been extensively studied for adsorption of inorganic pollutants from water [2,3]. Reports on usability of CLI in pharmaceuticals removal are rather scarce [4]. This could be explained by the fact that adsorption of these organics has mostly been found as an irreversible process.

This study shows an excellent adsorption efficiency of CLI in CIP removal from water media. Spent adsorbent is recovered by cold atmospheric pressure plasma treatment which is novel method in regeneration of mineral adsorbents.

EXPERIMENTAL

Clinoptilolite-rich zeolitic tuff (Z) obtained from the deposit Slanci (near Belgrade, Serbia) was used as a starting material. Rietveld analysis showed that Z contains CLI as the major mineral phase (> 80 wt.%), quartz (< 7.5 wt.%) and feldspar (< 13 wt.%). The cation exchange capacity (CEC) of the CLI determined by a standard procedure was 162 mmol M^{+}/100

g. The particle size used in the experiments was in the range of 0.063-0.125 mm for which previous experiments showed that it is optimal one.

Characterization: Rigaku SmartLab diffractometer with CuKα radiation (λ = 1.54178 Å) was used for analysis of the mineral phases present in the samples. The PXRD patterns were recorded in the 2θ range 5–65°. Elemental analysis of the CLI phase was determined by a Carl Zeiss Supra^{TM} 3VP field-emission gun scanning electron microscope (FEG-SEM) equipped with EDS detector with INCA Energy system for quantification of elements. A simultaneous thermogravimetric (TGA) and differential thermal analysis (DTA) was performed using a SDT Q-600 instrument (TA Instruments). The specific surface areas and porosity characteristics were determined by N_2 adsorption isothermally at -196 °C, using a Micrometrics ASAP 2020, and the specific surface area of sample (S_{BET}) was calculated according to the BET method. The zeta potential of CLI was measured by a Zetasizer NanoZS90 (Malvern Instruments Ltd., UK).

Adsorption tests: The adsorption tests were performed by a batch method. The adsorption capacity was studied for different initial CIP concentration (15, 25 50 and 75 mg dm^{-3}) and temperatures (283, 288 and 293 K) at pH= 5. About 0.2 g of the zeolite was suspended in 50,0 cm^3 of the certain concentration of CIP solution and left under shaking in a thermostated water bath from 5 to 60 min. Solid phase was recovered by centrifugation and the CIP concentration in filtrate was measured by an UV-VIS spectrophotometer (Perkin Elmer Lambda 365) at λ= 278 nm according to a standard procedure [5].

Adsorbent regeneration: A surface dielectric barrier discharge (SDBD) source with a segmented electrode operating in air for 20 min was used for plasma treatment of the spent CLI.

RESULTS AND DISCUSSION

The PXRD pattern (Figure 1) showed that CLI was the main mineral phase. Diffractions at 2θ = 26.6° and 27.1° correspond to the presence of quartz and feldspar, respectively, which are major sattelite phase [6].

Elemental analysis of CLI showed that the Si/Al molar ratio is 5.03 which is the common value for natural clinoptilolite. Furthermore, the specific surface area (S_{BET}) was 23.57 m^2 g^{-1} which is in accordance with reported values for S_{BET} (usually in the range 15–40 m^2 g^{-1}).

Zeta potential measurements showed that CLI has a negatively charged surface in the whole range of pH values (Figure 2).

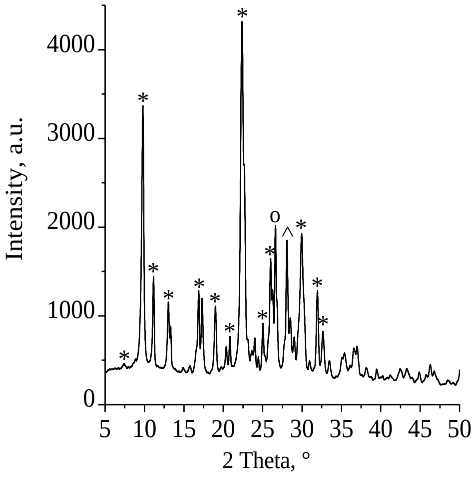

Figure 1. PXRD patterns of CLI (* – clinoptilolite, ° – quartz and ^ – feldspar).

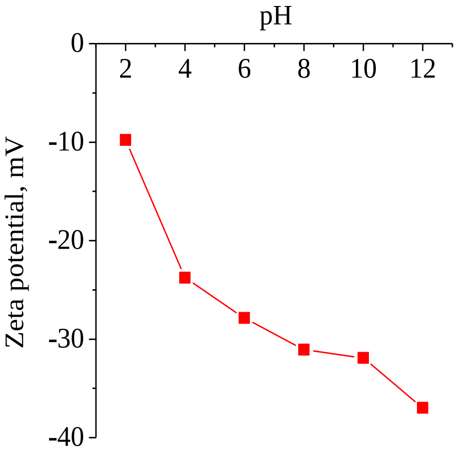

Figure 2. pH dependence of surface charging of CLI.

Since CIP molecule mainly exists as a zwitterion at neutral pH with a shift towards positively charged species at pH < 5.9 and towards anionic form at pH > 8.9, the pH of the solution strongly affects its adsorption performance [7]. Study of dependence of the adsorption capacity with pH showed that the best results can be obtained at pH= 5 (not shown). Accordingly, all experiments were done at pH= 5. Adsorption isotherms were studied at 283, 288 and 293 K. The equilibrium data were analysed by several empirical adsorption isotherm models [8]. Among the two-parameter models the Langmuir model gave the best results. The CIP uptake onto CLI increases rather sharply in the first 10 min for all studied temperatures and initial CIP concentrations. More than 80% of the maximum adsorption capacity was achieved in this 10 min period, indicating fast adsorption kinetics.

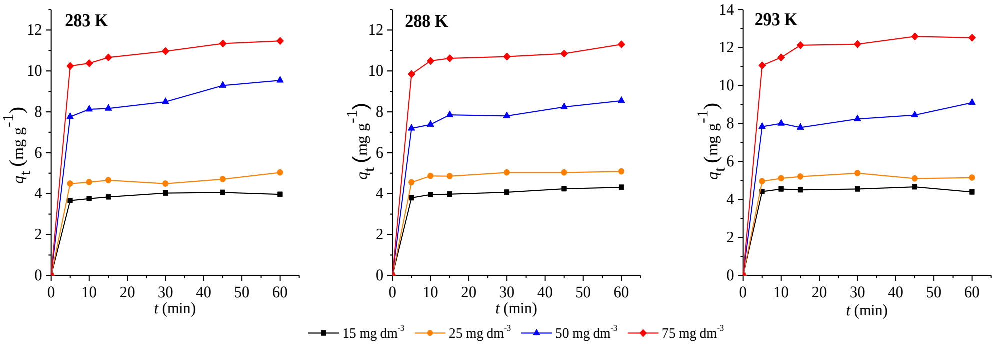

Figure 4. Adsorption kinetics for CIP on CLI for different temperatures; q_t is the amount of the adsorbed CIP (mg per 1 g of adsorbent) after time *t*.

Two reaction–based kinetic models were applied in order to describe the adsorption experimental data (Figure 4). Satisfactory fits were obtained only by the Lagergren's pseudo-second-order kinetic model (Table 1). Moreover, to investigate the influence of intra-particle diffusion on the CIP adsorption, the data were further processed by the Weber–Morris mass transfer model [9]. This did not result in agreement with experimental data suggesting that the intra-particle diffusion is not present in the adsorption.

Table 1. Rate constants for Lagergren's pseudo-second order kinetic model for the CIP adsorption on CLI (R^2 is the correlation coefficient of the linear regression).

C_0, mg CIP dm^{-3}	**CLI**			
	***T*, K**	**k_2, g mg^{-1} min^{-1}**	**q_e, mg g^{-1}**	**R^2**
15	283	0.3393	4.09	0.9999
	288	0.2490	4.28	0.9998
	293	0.2275	4.82	0.9996
25	283	0.1896	4.90	0.9988
	288	0.2900	5.13	0.9999
	293	0.4011	5.24	0.9995
50	283	0.0436	9.78	0.9983
	288	0.0703	8.63	0.9991
	293	0.0714	8.94	0.9989
75	283	0.0868	11.58	0.9997
	288	0.0886	11.28	0.9991
	293	0.0443	13.27	0.9982

C_0 – initial CIP solution concentration (mg dm^{-3}); k_2 – pseudo-second-order rate constant, g mg^{-1} min^{-1}; q_e – adsorption capacity, mg g^{-1}.

Regeneration of the adsorbent. The CIP adsorption onto CLI includes an ion exchange reaction at the CLI surface (results are not shown) which is irreversible (results are not shown). Since the adsorbent reusability is the most important issue for the operational cost of wastewater treatment based on the adsorption, we tested cold atmospheric pressure plasma for regeneration of the spent CLI. The results showed that more than 90% of the initial adsorbent capacity can be recovered in five cycles by the plasma treatment (Figure 5). This recommends cold plasma treatment as an environmentally friendly method suitable for the recycling of CIP saturated CLI.

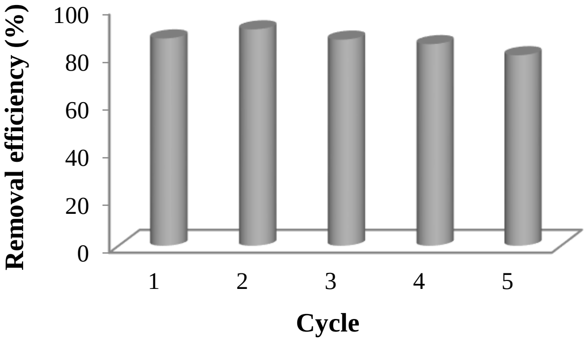

Figure 5. CLI removal efficiency through 5 adsorption cycles (C_0= 25 mg dm^{-3}; solid:liquid= 1:100; pH= 5; T= 21 °C).

CONCLUSION

The study shows that cost effective and environmentally friendly natural clinoptilolite can be a promising adsorbent for the removal of antibiotic ciprofloxacin from water media. The spent clinoptilolite can be successfully regenerated by cold atmospheric pressure plasma treatment.

ACKNOWLEDGEMENTS

The research is supported by EU Horizon 2020, Nowelties project MSCA-ITN-2018 - innovative training network (Joint PhD Laboratory for New Materials and Inventive Water Treatment Technologies. Harnessing resources effectively through innovation) [grant number 812880].

REFERENCES

[1] S. Rashit, D. Sarkar, E.J. Elzinga, P. Punamiya and R. Datta, *J. Hazard. Mater.* 2013, **246-247**, 221-226.
[2] D. Stojaković, J. Milenković, N. Daneu and N. Rajić, *Clays Clay Miner.* 2011, **59**, 277-285.
[3] N. Rajić, D. Stojanović, M. Jovanović, N. Zabukovec Logar, M. Mazaj and V. Kaučič, *Appl. Surf. Sci.* 2010, **257**, 1524-1532.
[4] B. Muir, M. Wołowiec, T. Bajda, P. Nowak and P. Czupryński, Mineralogia, 2017, **48**, 145–156.
[5] S. Neveed and N. Waheed, *Mintage J. Pharm. Med. Sci.* 2014, **3**, 10-13.
[6] H.B.I. Hawash, E. Chmielewska, Z. Netriová, J. Majzlan, H. Pálková, and R. Sokolík, *J. Environ. Chem. Eng.* 2018, **6**, 6489–6503.
[7] N. Genç and E.C. Dogan, *Desalin. Water Treat.* 2013, **53**, 1–9.
[8] K. Vijayaraghavan and Y. Yun, *Biotechnol. Adv.* 2008, **26**, 266-291.
[9] W. J. Weber Jr and J.C. Morris, in *Advances in Water Pollution Research*, Pergamon Press, New York, 1962, 231-266.

DOES BACTERIAL SURFACE HYDROPHOBICITY LEVEL INFLUENCE THEIR IMMOBILIZATION ONTO NATURAL ZEOLITE?

Jasna Hrenović, Darko Tibljaš, Svjetlana Dekić Rozman, Tomislav Ivanković
University of Zagreb, Faculty of Science, Zagreb, Croatia
E-mail: jasna.hrenovic@biol.pmf.hr

ABSTRACT

Bacterium *Acinetobacter baumannii* is nowadays an emerging hospital pathogen. From colonised or infected patients, *A. baumannii* is disseminated into the natural water environments. Due to the resistance of this bacterium to the conventional methods of water disinfection, alternative methods of *A. baumannii* removal from water are needed. There is no literature data how the hydrophobicity level of *A. baumannii* isolates influences the immobilization onto hydrophilic surface of natural zeolitized tuff (NZ). The immobilization of hydrophilic and hydrophobic isolate of *A. baumannii* onto NZ was examined. Both hydrophilic and hydrophobic isolate was successfully immobilized onto NZ, whereby hydrophobic isolate in a higher abundance than hydrophilic one. The NZ is a promising material for the capture of isolates of pathogenic bacteria *A. baumannii* from water, and could find application in water treatment technology.

Key words: *Acinetobacter baumannii*, bacteria, hydrophobic, hydrophilic, immobilization, natural zeolite.

INTRODUCTION

Bacterium *Acinetobacter baumannii* during the last 30 years developed the resistance to commonly used antimicrobial agents. Due to ability to persist in abiotic environment for months, this bacterium represents an emerging human pathogen of 21st century [1]. From colonised or infected patients, *A. baumannii* is disseminated into hospital wastewaters, urban wastewaters, wastewater treatment plants and finally into the natural environment [2,3].

A. baumannii is highly durable in the conventional methods of water disinfection such as chlorination [3]. Therefore, there is a need to find alternative methods for removal of *A. baumannii* from water. It was previously shown that *A. baumannii* could be immobilized on the particles of the natural zeolitized tuff (NZ) [4]. However, phenotypic characteristics among *A. baumannii* isolates could differ in high extent [2,3]. There is no literature data how the hydrophobicity level of bacterial surface influences the immobilization onto hydrophilic surface of NZ. When examining this issue, hydrophilic NZ could be made hydrophobic by surface modification with surfactants e.g. hexadecyltrimethylammonium bromide. Cationic surfactants used for modification act bactericidal, diminishing the answer of particle-bacteria interaction [5].

In this study a hydrophilic and hydrophobic isolate of *A. baumannii* were used to elucidate the effect of hydrophobicity level of bacterial surface on the intensity of immobilization onto hydrophilic surface of NZ.

EXPERIMENTAL

A. baumannii isolates named IN41 and IN58 were recovered from influent of the Zagreb wastewater treatment plant [3]. Isolate IN41 was resistant to carbapenems and fluoroquinolones, while isolate IN58 was sensitive to all relevant antibiotics [3]. Two examined isolates also differed in phenotypic characteristics (Table 1). Bacterial hydrophobicity was measured *via* bacterial adhesion to hydrocarbon assay [6]. Pellicle formation was determined at the air-liquid media interface [7]. Surface of colonies was inspected visually after cultivation of isolates on the solid medium.

Table 1. Characteristics of *A. baumannii* isolates used in experiment.

Isolate	Hydrophobicity (%)	Pellicle formation	Colony surface
IN41	0	none	smooth
IN58	93	huge	rough

Fresh bacterial biomass was suspended in 9 mL of autoclaved nutrient-poor commercial spring water. Into each tube, one gram of NZ was added. The NZ was obtained from the quarry located at Donje Jesenje, Croatia. The composition of NZ is: clinoptilolite (50-55%), celadonite, plagioclase feldspars and opal-CT (10-15% each), analcime and quartz in traces [8]. The NZ was crushed, sieved, and the size fraction 0.263-0.5 mm was used. Prior to its usage, dry NZ was sterilized by autoclaving. Tubes were rotated at 3 rpm at 22°C for 24h.

At the beginning of experiment, and after 24h of incubation, the number of bacteria was determined according to described protocol [4,8]. The cultivation of bacteria was performed on CHROMagar Acinetobacter at 37°C/24h. Number of bacterial colonies was expressed as logarithm of colony forming units (log CFU) per one mL of water or one gram of dry NZ.

RESULTS AND DISCUSSION

As shown in Table 1, isolate IN41 has totally hydrophilic surface while isolate IN58 has strongly hydrophobic surface. After 24h of contact with suspension of NZ in water (Fig. 1), one part of bacteria was immobilized onto NZ particles, while the other part left planktonic in water. There was no multiplication of bacteria due to the lack of nutrients in spring water. The only remarkable difference in experiment was the significantly higher immobilization of the isolate IN58 (6.9±0.07 log CFU/g) as compared to the isolate IN41 (5.2±0.17 log CFU/g). In absolute number, this means that 7.65×10^6 more CFU of isolate IN58 was captured per one gram of dry NZ.

The possible explanation for the more abundant immobilization of hydrophobic isolate IN58 onto NZ as compared to hydrophilic isolate IN41 is as follows. Hydrophobic isolate prefers the immobilization onto NZ because in this way it reduces its surface in direct contact with water. This behaviour is supported by the huge pellicle formation at the water-air contact (Table 1). Obviously, hydrophobic isolate IN58 has a tendency to escape from water. The water medium is preferable surrounding for hydrophilic isolate IN4, which therefore showed less abundant immobilization onto NZ.

The intensity of immobilization of hydrophilic isolate IN41 in this work (5.2 log CFU/g) is lower than previously reported immobilization of hydrophilic isolate of *A. baumannii* EF7 (8.0 log CFU/g) on the same NZ in the same water medium [4]. Since the immobilization of isolate EF7 was tested on the NZ with the particle size ≤ 0.122 mm, while in this study 0.263-0.5 mm fraction was used, lower intensity of immobilization of IN41 may be explained by the fact that the number of immobilized bacteria increase with the decrease of particle size [7].

In the process of preparation of biosolids it is necessary to pay attention to the particle size of chosen material and water medium used for the growth of bacteria, two parameters that mostly influence the final number of bacteria on biosolids [4,8]. However, when preparing biosolids, the hydrophilic surface of bacterial isolate would not be a guaranty for better immobilization of bacteria onto hydrophilic material.

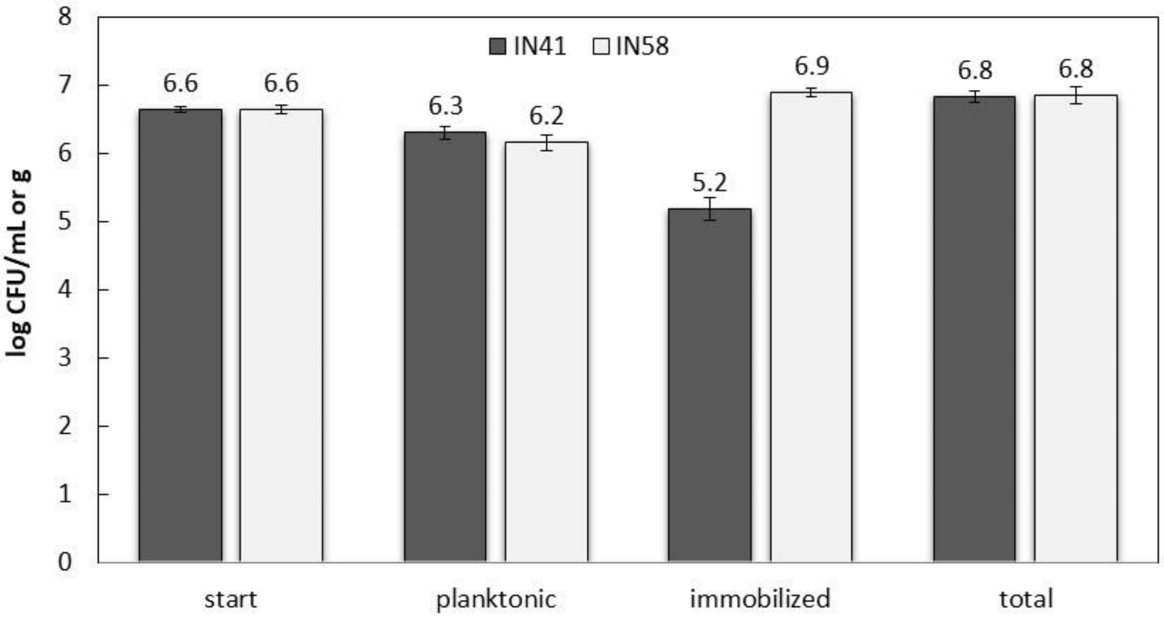

Figure 1. Numbers of hydrophilic (IN41) and hydrophobic (IN58) bacteria *A. baumannii* at the start of experiment and after 24h of contact with suspension of NZ in water (planktonic in water, immobilized onto NZ and total number in experiment).

CONCLUSION

The hydrophobicity level of bacterial surface is not a crucial factor which determines its immobilization onto hydrophilic surface of NZ. Both hydrophilic and hydrophobic bacteria could be successfully immobilized onto NZ, whereby hydrophobic bacteria in higher abundance than hydrophilic ones. The NZ is a promising material for the capture of pathogenic bacteria *A. baumannii* from water, and could find application in water treatment technology.

ACKNOWLEDGEMENTS

This work has been supported by the Croatian Science Foundation (project no. IP-2014-09-5656).

REFERENCES

[1] I. Roca, P. Espinal, X. Vila-Farres and J. Vila, *Front. Microbiol.*, 2012, **3**, 1-30.

[2] M. Šeruga Musić, J. Hrenović, I. Goić-Barišić, B. Hunjak, D. Škorić and T. Ivanković, *J. Hosp. Infect.*, 2017, **96**, 232-237.

[3] P.G. Higgins, J. Hrenović, H. Seifert and S. Dekić, *Water Res.*, 2018, **140**, 261-267.

[4] J. Hrenović, D. Tibljaš, S. Dekić and C. Venter, In Proceedings of 8th Serbian-Croatian-Slovenian Symposium on Zeolites (eds. V. Rakić, J. Hrenović, A. Ristić), 2019, 93-96.

[5] J. Hrenović, M. Rožić, L. Sekovanić and A. Anić-Vučinić, *J. Hazard. Mater.*, 2008, **156**, 576-582.

[6] M. Rosenberg, D. Gutnick, and E. Rosenberg, *FEMS Microbiol. Lett.*, 1980, **9**, 29-33.

[7] Y. Nait Chabane, S. Marti, C. Rihouey, S. Alexandre, J. Hardouin, O. Lesouhaitier, J. Vila, J.B. Kaplan, T. Jouenne and E. Dé, *PLoS ONE*, 2014, **9**, e111660.

[8] J. Hrenović, J., D. Tibljaš, Y. Orhan and H. Büyükgüngör, *Water SA*, 2005, **32**, 261-266.

NATURAL ZEOLITE AS A TOOL FOR MODELLING BACTERIAL BIOFILM DEVELOPMENT IN STATIC CONDITIONS

Tomislav Ivanković, Katarina Rotim, Jasna Hrenović
University of Zagreb, Faculty of Science, Department of Biology, Rooseveltov trg 6, 10000 Zagreb, Croatia
E-mail: tomislav.ivankovic@biol.pmf.hr

ABSTRACT

In the environment bacteria mainly exist adhered to solid surfaces in communities known as biofilms. Bacterial biofilm is a sessile community whose cells are attached to the substrate and to each other, engulfed in the matrix of extracellular polymeric substances that they have created. Currently, a five stage model for biofilm development is widely accepted for every biofilm growth, in spite the fact that it was modelled based on biofilm growth in continuous flow conditions. We hypothesize that in static conditions, which are nowadays mostly used for biofilm investigations, the five stage model is perhaps not applicable. So, we used particles of natural zeolite as a unique tool that allows simultaneous visualization and statistically satisfactory quantification of biofilm growth during 24 h. The results from testing two morphologically distinguishable bacterial strains suggested that, when grown in static conditions, five-stage model could be applicable for non-motile bacteria *Acinetobacter junii*, but not for motile bacteria *Bacillus cereus*.

Key words: motility; five-stage model; zeolite; biofilm.

INTRODUCTION

Biofilm is commonly defined as a community of microorganisms adhering to a surface engulfed in a complex matrix of self-produced extracellular polymeric substances (EPS). It can be best envisaged as a city of microbes covered by a dome. Same as a dome, the EPS protects the cell from harsh environmental conditions: antibiotics, disinfectants, or desiccation [1,2]. Same as in a city, the cells communicate with various mechanisms and even exchange genetic material enhancing the overall community fitness [3].

Recognizing the abundancy and importance of bacterial biofilms in the environment, industrial settings and medicinal surroundings, has led to vast scientific researches being conducted to investigate many phenomena linked, and arising from the biofilm. The model of bacterial biofilm growth has been one of the first items concluded from such research [4], and five-stage model is now universally accepted. However, the five-stage model has been developed from observations obtained on biofilm growth in flow systems, where biofilm is attached on solid surface and nutrient media is continuously replenished for a period of time usually counted in days [4]. On the contrary, majority of experiments on biofilm nowadays are being done in static systems that offer simplified experimental setup compared to flow systems and much faster results since the biofilms are usually grown for 24-48 h [5,6]. In addition, static systems do not replenish the nutrient media, hence the bacterial populations follow classic lag/log/static phase growth curve. Despite the obvious significant differences in experimental setup, it has become widely accepted that five-stage biofilm growth model is applicable to static conditions as well.

The goal of here presented research was to investigate whether the five-stage biofilm growth model is valid and applicable when experiments were done in static conditions. We have used the particles of natural zeolite – clinoptilolite, as a solid substrate for biofilm growth. The experimental system with zeolite particles enabled simultaneous visualization and qualitative along with quantitative analysis of bacterial biofilms, in a relatively simple and completely reliable and reproducible experimental setup.

EXPERIMENTAL

Biofilm growth of gram positive, motile bacteria with flagellar apparatus *Bacillus cereus* (4080 LBK) and gram-negative, non-motile bacteria with Type IV pili *Acinetobacter junii* (DSM 1532) was monitored in static and pseudo-flow conditions. In static conditions, a 0.5 g of natural zeolitized tuff (NZ) obtained from quarries in Donje Jesenje (Croatia) of 0.122-0.263 mm particle size was added to series of laboratory bottles already containing 50 mL of Luria Bertani liquid medium (LB; 10 g tryptone, 5 g yeast extract, 5 g NaCl, 1000 ml distilled water, pH 7.0±0.1) and bacteria at starting concentration of ~106 CFU mL^{-1} (Colony Forming Units). The bottles were set for incubation with mixing (100 rpm, Orbital Shaker, Biosan OS-10, Latvia) at 35°C. Every three hours, from one of the bottles, the media was poured out, the NZ particles were gently washed with sterile physiological solution and aseptically transferred to plastic vials containing 9 mL of fresh physiological solution. The vials were vortexed (50 Hz, Kartell, Italy) for 3 min to allow the bacterial cells to detach from the NZ. The bacteria remained as planktonic cells in the suspension. The suspension was serially diluted and inoculated onto LB agar plates, incubated for 24 h at 35°C after which the grown colonies were counted, the NZ particles were weighted and bacterial number was expressed as logCFU g^{-1} of dry NZ.

The NZ sample used in the research consisted mostly of clinoptilolite (50–55%) with major constituents being celadonite, plagioclase feldspars and opal-CT (10–15% each), whilst analcime (another zeolite group mineral) and quartz were present in traces [7].

The procedure was identical for pseudo-flow conditions, with difference that after every three hours one of the bottles was analyzed for number of bacteria attached on the NZ, and the remaining bottles were emptied of current nutrient media, the NZ particles were gently washed with sterile saline, and refilled with 50 mL of fresh sterile LB broth.

From each bottle, a few grains of NZ were placed onto microscope slides, dyed by Alcian-blue method and visually examined under the microscope (Olympus CX-21, 1000× magnification). The photos were taken using mobile phone.

All the experiments were done in duplicate. The results were statistically analyzed using Statistica software version 13.3. We used ANOVA with Duncan's post-hoc analysis and Student's *t*-test to compare independent variables. Statistical significance was set at $p<0.05$.

RESULTS AND DISCUSSION

The idea and main hypothesis of the experiment was the following; the five stage model implies clonal growth, meaning that a single cell (or aggregate of few cells) adsorbs to a solid surface and continues to grow attached to the surface, producing the EPS, and eventually forming a biofilm [8]. If this was applicable to static systems than in both growth conditions of our experiment, the static without changing media and pseudo-flow with regular removal of spent media and replenishment with fresh sterile media, the number of bacteria in the biofilm on NZ particles should be the same. The bacteria attach to surface of NZ and form biofilm regardless of the surrounding media change.

Visual observations of microscopic slides confirmed that in the case of *A. junii* the amount of bacteria attached on the NZ particles after 1 and 24 h in the experiments without (Figure 1 a and b) and with media change (Figure 1 c and d) were comparable: few cells attached on NZ after 1 h and many cells on and surrounding the NZ particle after 24 h, regardless of static or pseudo-flow conditions.

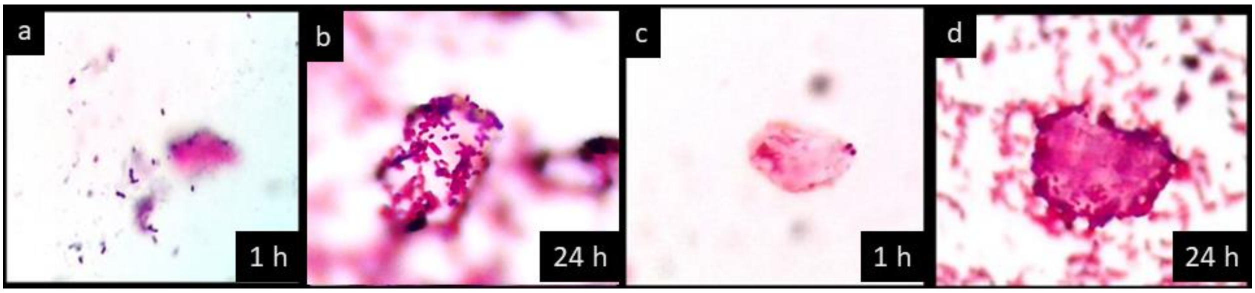

Figure 1. Cells of *A. junii* and NZ particles imaged after 1 and 24 h of experiment in static conditions without nutrient media change (a and b) and in pseudo-flow conditions with regular media change (c and d).

However, in the case of *B. cereus* the observations differed: few cells attached after 1 h in both experimental conditions (Figure 1a and c), many cells on and surrounding NZ particle after 24 h in static condition (Figure 2b) but much fewer cells on, and almost none surrounding the NZ particle in pseudo-flow condition (Figure 2d).

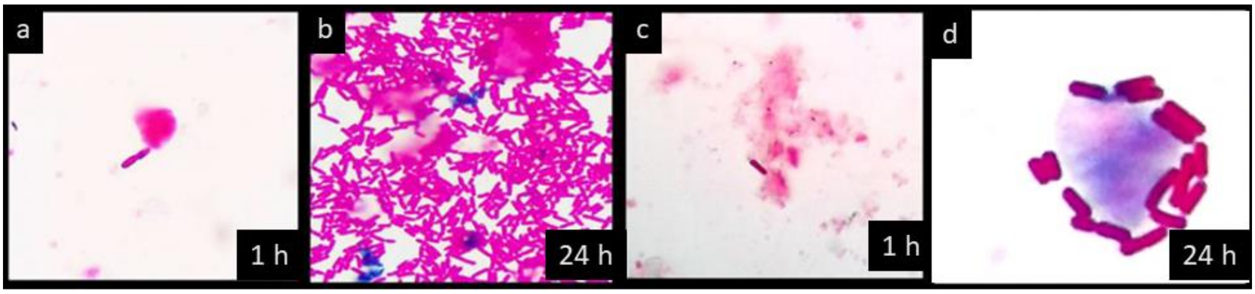

Figure 2. Cells of *B. cereus* and NZ particles imaged after 1 and 24 h of experiment in static conditions without nutrient media change (a and b) and in pseudo-flow conditions with regular media change (c and d).

The visual observations were indicative but purely qualitative and insufficient to make significant conclusions. Therefore, an analysis of bacterial numbers attached to solid particles was needed. The NZ was previously reported to be an excellent material enabling reliable and statistically reproducible counting of bacterial cells forming the biofilm on particle surfaces [7,9]. Experimental system using NZ particles as substrate for biofilm formation and quantitative analysis enabled investigation of influence of harsh environmental conditions on bacterial biofilm [10] or dynamics of biofilm formation in consortium of few bacterial species [7].

The quantification of biofilm bacteria revealed that there was no significant difference in the static and pseudo-flow experimental system with *A. junii* (Figure 3). However, significant difference occurs when static and pseudo-flow conditions were compared in the system with *B. cereus* (Figure 3). The results confirmed visual observations and showed much higher number of *B. cereus* cells in static conditions after 9 h until 24 h of growth when mature biofilm formation was expected. Most reasonable explanation would be that both bacterial species initially assume clonal growth after attachment to NZ particles, but in pseudo-flow conditions, with regular media change, motile *B. cereus* cells begin to detach from the biofilm in much higher proportion than non-motile *A. junii* cells, probably taking advantage of fresh nutrient media. In static conditions the *B. cereus* cells attach on the NZ particles not just as a result of clonal growth but also migrating from the surrounding media which after few hours becomes saturated bacterial suspension.

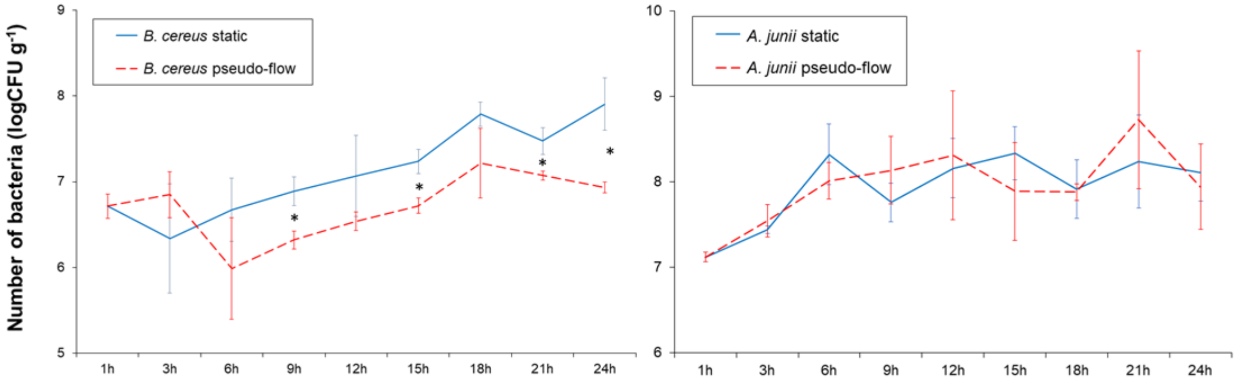

Figure 3. Number of *A. junii* and *B. cereus* attached to NZ particles after different period of incubation in static or pseudo-flow experimental conditions. * marks statistically significant difference between measurements ($p<0.05$).

CONCLUSION

The particles of NZ have shown to be an excellent tool for investigation of biofilm enabling not just qualitative but reliable and statistically reproducible quantitative analysis. Enumeration of bacterial numbers attached to the surface of NZ indicated that if bacterial biofilm was grown in static conditions, the five-stage biofilm model was applicable to *A. junii* but not to *B. cereus*. The difference is probably due to active motility by flagellar apparatus of *B. cereus*. Additional experiments with a battery of bacterial species or motile/non-motile mutants of the same bacterial species would give definite answer whether five-stage model is relevant for static biofilms.

REFERENCES

[1] L. Hall-Stoodley, J.W. Costerton and P. Stoodley, *Nat. Rev. Microbiol*. 2004, **2**, 95-108.

[2] A. Bridier, R. Briandeta, V. Thomas and F. Dubois-Brissonnet, *Biofouling* 2011, **27**, 1017-1032.

[3] V. Marx, *Nature* 2014, **511**, 493-497.

[4] K. Sauer, A.K Camper, G.D Ehrlich, J.W Costerton and D.G Davies, *J. Bacteriol*. 2002, **1**, 1140-1154.

[5] J.H. Merritt, D.E. Kadouri and G.A O'Toole, *Curr. Protoc. Microbiol*. 2005, Chapter 1:Unit 1B.1.

[6] J. Azeredo, N.F. Azevedo and R. Briandet, *Critical. Rev. Microbiol*. 2017, **43**, 313-351.

[7] J. Hrenović, D. Kovačević, T. Ivanković and D. Tibljaš, *Colloids Surf. B*. 2011, **88**, 208-214.

[8] P.R. Kendra and K. Sauer, *Nature Rev. Microbiol*. 2020, **18**, 571-586.

[9] J. Hrenović, T. Ivanković and D. Tibljaš, *J. Haz. Mat*. 2009, **166**, 1377-1382.

[10] T. Ivanković, J Hrenović and R. Matoničkin-Kepčija, *Biofouling* 2013, **29**, 641-649.

PREPARATION AND ANTIBACTERIAL ACTIVITY OF COMPOSITES BASED ON THYMOL/CARVACROL AND CLINOPTILOLITE

Jelena Dikić[1], *Ivana Lukić*[2], *Jelena Pajnik*[1], *Jelena Pavlović*[1], *Jasna Hrenović*[3], *Nevenka Rajić*[2]
[1] University of Belgrade, Innovation Center of the Faculty of Technology and Metallurgy, Belgrade, Serbia
[2] University of Belgrade, Faculty of Technology and Metallurgy, Belgrade, Serbia
[3] University of Zagreb, Faculty of Science, Division of Biology, 10000 Zagreb, Croatia
E-mail: jdikic@tmf.bg.ac.rs

ABSTRACT

Composites based on clinoptilolite and monoterpene phenols - thymol and carvacrol were prepared by supercritical solvent impregnation (SSI) at 30 MPa and 35 ºC during 18 h in supercritical carbon dioxide ($scCO_2$). The composites were characterized in detail and their antibacterial activity was tested towards two potentially pathogenic bacteria; *Escherichia coli* and *Staphylococcus aureus*.

Key words: thymol, carvacrol, antibacterial activity, clinoptilolite, supercritical solvent impregnation.

INTRODUCTION

Due to antimicrobial properties, phenols and polyphenols obtained from plant essential oils are intensively studied. Thymol [2-Isopropyl-5-methylphenol] and carvacrol [5-Isopropyl-2-methylphenol] are major components of oregano (*Origanum vulgare*) used from ancient times [1]. Both compounds exhibit antimicrobial, antioxidant, anti-inflammatory, antitumor, antimutagenic, analgesic, anti-parasitic and insecticidal properties [1,2]. The use of bioactive compounds is most favourable if they are immobilized on suitable carriers. In this work natural zeolite – clinoptilolite was tested as a carrier of thymol and carvacrol, and antibacterial activity of the prepared composites towards Gram negative *Escherichia coli* DSM 498 and Gram positive *Staphylococcus aureus* ATCC 25923 were studied.

EXPERIMENTAL

Preparation of the composites

Zeolitic tuff (Z) with about 70 wt. % of natural zeolite – clinoptilolite from Vranjska Banja deposit (Serbia) was used in experiments. Z was converted into NH_4-form (NH_4-Z) using a solution of ammonia acetate (1 mol dm^{-3}) and H-form (H-Z) using the following procedure. NH_4-Z was firstly calcined in air at 550 ºC and the calcined product was treated with 0.6 mol dm^{-3} HCl at 70 ºC. The obtained product was washed with distilled water until the negative reaction to Cl^- and dried overnight at 60 ºC to a constant mass.

Crystalline thymol and liquid carvacrol (purity > 99%, Sigma Aldrich, Germany) were impregnated onto H-Z in a high-pressure view cell using a static mode at optimized conditions (35 ºC, 30 MPa, time interval of 18 h, decompression rate of 1.5 MPa min^{-1}) using CO_2 as supercritical fluid. The obtained composites were denoted as T-Z (thymol-containing zeolite) and C-Z (carvacrol-containing zeolite).

Characterization of synthetized composites

The content of thymol and carvacrol in composites were determined by thermogravimetric analysis (TGA) using a SDT Q-600 simultaneous DSC-TGA instrument (TA Instruments), as well as by C, H, N analysis using Varian EL III C,H,N,S/O Elemental Analyzer (Elementar, Langenselbold, Hesse, Germany). Crystallinity of the samples was examined by PXRD method using Ultima IV Rigaku diffractometer equipped with Cu $K_{\alpha1,2}$

radiation using a generator voltage (40.0 kV) and a generator current (40.0 mA). The PXRD patterns were recorded in the 2θ range 5 – 45° with a scanning step of 0.02 ° and the scan rate of 5 $°\mathrm{min}^{-1}$. Specific surface area was measured by N_2 adsorption–desorption experiments (Micromeritics ASAP 2020) and calculated according to the Brunauer, Emmett, Teller (BET) method. Interactions of the phenols and zeolite lattice were studied by Fourier Transform Infrared (FTIR) Spectroscopy. The FTIR spectra were recorded in the range 4000–450 cm^{-1} with a resolution of 4 cm^{-1} at room temperature, using Nicolet iS10 (Thermo Scientific) spectrometer.

Antibacterial activity test

Antibacterial activity of the composites was tested in different water media: phosphate buffer solution (PBS), commercially available spring water (Gala, Serbia, SW), and lake water (Sava Lake, Belgrade, Serbia, SL) toward Gram negative *E. coli* DSM 498 and Gram positive *S. aureus* ATCC 25923. Firstly, bacteria were pre-grown on the Nutrient agar (NA, Torlak, Serbia) for 16 h at 37±0.1 ºC to obtain cultures in a *log* phase of growth. All water media were sterilized before the tests by autoclaving (121 ºC/20 min) and the composite samples by UV light in UV chamber for 30 min.

The experiments were performed as follows: into 10 cm^3 of bacterial biomass suspended in a sterile water media 0.1 g of each composite (T-Z or C-Z) was added, and incubated in a thermostatic water bath during 24 h at 37±0.1º C with shaking at 105 rpm. As a positive control (without antibacterial activity), the bottles with 0.1 g of H-Z in all studied media with bacteria were set up. The number of viable bacterial cells was determined at the beginning of the experiment, after 1 h (short contact) and after 24 h (long contact). After 1 and 24 h the aliquot of 0.1 cm^3 was plated by a spread plate method directly on NA and another amount of the sample (1 cm^3) was serially diluted (10^{-1}–10^{-7}). Diluted samples have also been plated onto NA and incubated for 24 h at 37±0.1º C. After incubation the bacterial colonies grown on NA were counted. The number of bacteria was reported as CFU (Colony Forming Units) per one cm^3, logarithmically transformed and the antibacterial activity was finally expressed as the percent of reduction of the log of CFU cm^{-3} according to the Equation (1). All experiments were done in triplicate.

$$Reduction\ (\%) = \frac{\log CFU\ cm^{-3}\ (t_0) - \log CFU\ cm^{-3}\ (t)}{\log CFU\ cm^{-3}\ (t_0)}\ x\ 100 \qquad (1)$$

where t_0 presents the initial number of bacteria and t is the number of bacteria after time of contact (1 or 24 h).

Desorption of thymol and carvacrol from composites

Leaching of thymol and carvacrol from the composites were studied after antibacterial activity tests. The concentration of the phenols was measured photometrically using a UV-VIS spectrophotometer Cary 100 Scan (Varian) at $\lambda_{\max}$= 274 nm.

RESULTS AND DISCUSSION

The conversion of Z into H-Z significantly increased the specific surface area of Z from 42 $\mathrm{m}^2\,\mathrm{g}^{-1}$ to 230 $\mathrm{m}^2\,\mathrm{g}^{-1}$ (H-Z) suggesting that the modification led to a partial pore opening of clinoptilolite lattice. PXRD analysis (not shown) confirmed that the modification is not accompanied by loss of zeolite crystallinity.

Thermal properties of the phenols and composites are presented in Fig.1. Thermogram of H-Z shows rather continual weight loss (10.0 wt.%) up to 350 °C. The thermal decomposition of thymol and carvacrol (not shown in the Figure) proceeds as one-step-process up to 160 °C with DTG maxima centred at 119 (thymol) and 148 °C (carvacrol). Fig. 1 shows that the composites have similar thermal behaviour: T-Z displays a strong DTG maximum at 134 and

C-Z at 135 °C, indicating that the SSI procedure successfully loaded phenols onto H-Z. Thymol and carvacrol content obtained from TGA agrees well with C, H, N analysis: 23.0 wt.% of thymol was obtained for T-Z and 19.2 wt.% of carvacrol for C-Z.

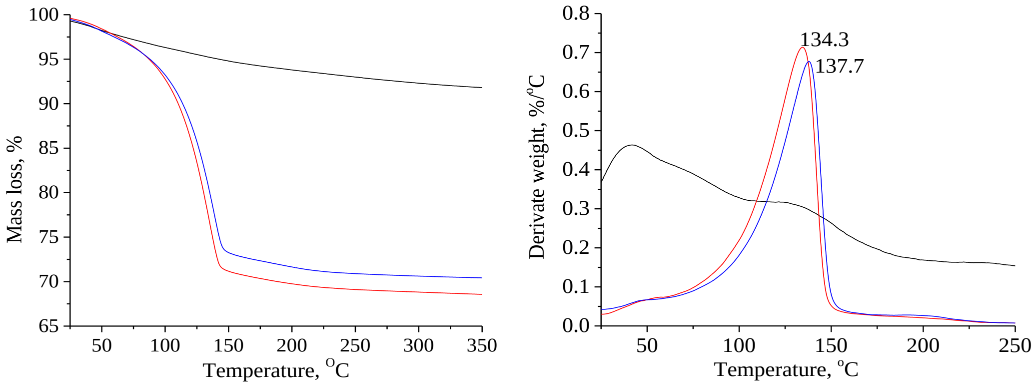

Figure 1. TG and DTG curves of H-Z (black line), T-Z (red line) and C-Z (blue line)

Fig. 2 shows FTIR spectra, which confirm the presence of the phenols on the composites. A broad band at 3580 – 3160 cm^{-1} corresponds to the phenolic –OH stretching vibrations, bands at 3000 – 2850 cm^{-1} belong to the C-H symmetric and asymmetric stretching vibration [3], while the bands between 1620 and 1417 cm^{-1} originate from C=C stretching vibrations in phenolic ring of thymol and carvacrol [4]. The bands attributed to the out-of-plane C-H wagging and bending vibrations from isoprenoids at around 804 cm^{-1} and at 945 cm^{-1}, respectively, were ascribed to phenols presented in the zeolite lattice [5]. Taking into account band positions it can be concluded that there is no significant difference between free and immobilized phenols suggesting that the interactions of the phenols and Z do not include formation of covalent bonds.

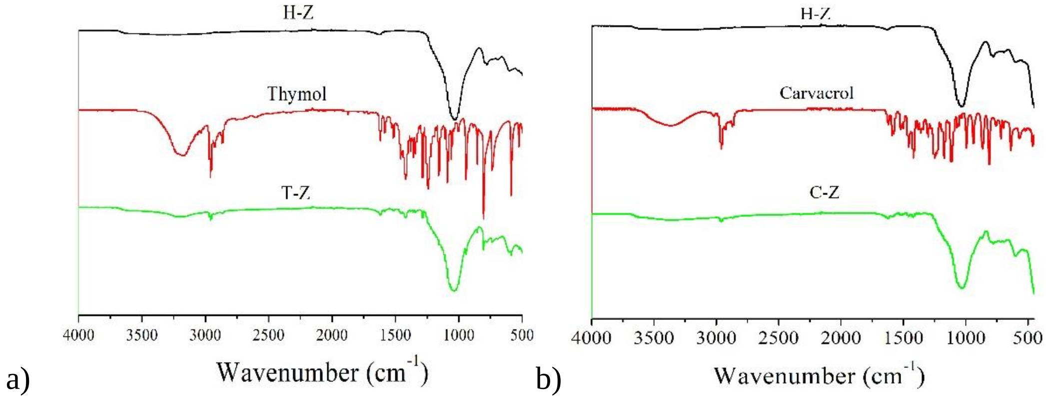

Figure 2. FTIR spectra of H-Z, thymol and T-Z (a) and H-Z, carvacrol and C-Z (b).

Antibacterial activity

Antibacterial activity was investigated toward Gram negative *E. coli* and Gram positive *S. aureus* in different water media (Table 1.). According to previous studies, H-Z did not exhibit any antibacterial activity towards examined strains (data not shown). After 1 h of contact in SL, T-Z exhibited a significant antibacterial activity toward both strains (62.6 and 72.2 % toward *E. coli* and *S. aureus*, respectively). In other water media, T-Z exhibited bactericidal effect after only 1 h of contact, except in the case of *S. aureus* in SW, where bactericidal effect appeared after 24 h. The C-Z exhibited bactericidal activity toward both examined strains in all media after 1 h of contact. Considering the obtained results, it is evident that C-Z shows better antibacterial activity than T-Z in the case of short-term exposure. This suggests that mechanism of the antibacterial action is influenced by chemical structure of bioactive compound.

Table 1. Percent of reduction in number of *E. coli* and *S. aureus* after 1 and 24h of contact with T-Z and C-Z in different water media.

Water medium	Reduction (%)							
	T-Z				C-Z			
	E. coli		*S. aureus*		*E. coli*		*S. aureus*	
	1 h	24 h	1 h	24 h	1 h	24 h	1 h	24 h
PBS	100±0	100±0	100±0	100±0	100±0	100±0	100±0	100±0
SW	100±0	100±0	70±0	100±0	100±0	100±0	100±0	100±0
SL	65±7	100±0	71±2	100±0	100±0	100±0	100±0	100±0

t_0 *E.coli* 2.1 x 10^7 CFU cm^{-3}; *S. aureus* 7.0 x 10^6 CFU cm^{-3} (experiment with thymol)
t_0 *E.coli* 7.6 x 10^6 CFU cm^{-3}; *S. aureus* 1.5 x 10^7 CFU cm^{-3}(experiment with carvacrol)

Desorption of thymol and carvacrol from the composites

Leaching of thymol and carvacrol from the T-Z and C-Z were determined in all water media after antibacterial tests (Table 2). Although antibacterial activity of C-Z is more pronounced than that of T-Z, the amount of thymol leached from T-Z is significantly higher than carvacrol leached from C-Z. This could be explained by weaker interactions between thymol and zeolite.

Table 2. Percentage of the leached thymol/carvacrol from the composites T-Z and C-Z after 24 h of the contact.

Water media	% of the leached phenols			
	E. coli	*S. aureus*	*E. coli*	*S. aureus*
	Thymol	Carvacrol	Thymol	Carvacrol
PBS	23.2	8.6	22.7	6.2
SW	26.3	7.2	26.1	8.1
SL	32.9	8.6	28.1	8.9

CONCLUSION

Components of the essential oils such as thymol and carvacrol can be successfully immobilized onto natural zeolite - clinoptilolite by the supercritical solvent impregnation. The composites that contained 23.0 wt.% of thymol and 19.2 wt.% of carvacrol showed bactericidal activity toward both Gram-negative *E. coli* and Gram-positive *S. aureus*. This suggests their potential use as disinfectant agents. It is worth noticing that the impregnation of these phenols by supercritical solvent impregnation used in this work is a novel and an environmentally friendly approach in the preparation of materials with antibacterial properties.

ACKNOWLEDGEMENTS

This work was financially supported by the Ministry of Education, Science and Technological Development of the Republic of Serbia (Contract No. 451-03-68/2020-14/200287 and 451-03-68/2020-14/200135).

REFERENCES

[1] A. Nostro and T. Papalia, *Recent Pat. Antiinfect. Drug Discov.*, 2012, **7**, 28–35.
[2] M.F.N. Meeran, H. Javed, H. Al Taee, S. Azimullah and S.K. Ojha, *Front. Pharmacol.* 2017, **8**, 1–34.
[3] C.S. Valderrama and G.C. Rojas De, *Am. J. Anal. Chem.*, 2017, **8**, 726- 741.
[4] Marchese, I.E. Orhan, M. Daglia, R. Barbieri, A. Di Lorenzo, S.F. Nabavi, O. Gortzi, M. Izadi and S.M. Nabavi, *Food Chem.*, 2016, **210**, 402-414.
[5] S. Milovanovic, G. Hollermann, C. Errenst, J. Pajnik, S. Frerich, S. Kroll, K. Rezwan, and J. Ivanovic, *Food Res. Int.*, 2018, **107**, 486-495.

COMPARISON OF COAGULATION AND ELECTROCOAGULATION WITH ADDITION OF NATURAL ZEOLITE FOR TREATMENT OF BIOWASTE COMPOST LEACHATE

Nediljka Vukojević Medvidović, Ladislav Vrsalović, Ivona Jukić, Ana-Maria Šunjić
Faculty of Chemistry and Technology, University of Split, Ruđera Boškovića 35, 21000 Split, Croatia
E-mail: nvukojev@ktf-split.hr

ABSTRACT

Even composting is recognized as an effective way of managing organic waste, it creates significant amounts of leachate which contains a variety of hazardous substances that can have potential adverse effects on the environment. This paper examines the treatment of leachate from biowaste composting by a hybrid process which integrates coagulation and electrocoagulation with addition of natural zeolite. Efficiency of each process was monitored by pH value, electrical conductivity, turbidity, chemical oxygen demand and total Kjeldahl nitrogen.

Keywords: natural zeolite, electrocoagulation, coagulation, biowaste compost leachate.

INTRODUCTION

Composting technologies are recognized as an effective way of managing organic waste because they reduce the volume and mass of the initial waste by approximately 50%. However, composting on an industrial scale creates significant amounts of leachate and contains a variety of hazardous substances that can have potential adverse effects on the environment. Therefore, they need to be treated before discharge into the sewer or natural recipient. Recently, integration of various treatment methods is highly investigated as single treatment methods are not efficient for achieving satisfactory leachate effluent quality. This paper compares coagulation and electrocoagulation with addition of natural zeolite as an integrated process for efficient treatment of biowaste compost leachate.

EXPERIMENTAL

Two biowaste compost leachate *solutions* were used for treatment. The first leachate (mark as A_o) was obtained from composting mass in an open container and the second from the rotary composter (mark as B_o). The pH, electrical conductivity, turbidity, chemical oxygen demand (COD), biological oxygen demand (BOD_5) and total Kjeldahl nitrogen (TN_K) were determined in the initial leachate.

Natural zeolite, clinoptilolite, originated from Zlatokop deposit, Vranjska Banja, Serbia, of granulation of 0.1-0.5 mm was used.

Electrocoagulation was performed in an electrochemical cell filled with 250 ml of simulated leachate solution and immersed aluminium electrodes (height: width: thickness = 5.9: 1.9: 0.6), with a distance between the electrodes of 3 cm. Electrochemical treatment was performed under the conditions of $I = 0.1$ A, $U = 29.9$ V, contact time $t = 60$ min, with gentle stirring with a magnetic stirrer, without addition of electrolyte. In the electrocoagulation experiments with addition of zeolite (marked as A_Z and B_Z), the mass of added zeolite was 5 g per 250 mL of effluent (solid to liquid ratio 20 g/L). Between each experiment, the electrodes were cleaned with distilled water and immersed into 0.1 mol/L HCl solution to remove impurities.

Coagulation is performed by addition of leachate solution and appropriate amount of coagulant $Al_2(SO_4)_3$, calculated by Faraday's law, in a glass beaker. In experiment with zeolite, 5 g of natural zeolite is added at the beginning of the process (marked as A_Z and B_Z). Coagulation was performed using the JAR test.

During electrocoagulation and coagulation with and without addition of zeolite, the pH value and electrical conductivity were monitored, and after the experiment, the pH value, electrical conductivity, turbidity, chemical oxygen demand (COD) and total Kjeldahl nitrogen (TN_K) were determined.

RESULTS AND DISCUSSION

Table 1 gives a physical-chemical analysis of leachate compared with maximal allowed values according to the Croatian Regulation [1].

Table 1. Biowaste compost leachate characterization.

Parameter	leachate A_o	leachate B_o	Natural surface waters [1]	Public sewage system [1]
pH	8.66	8.58	6.5-9.5	6.5 – 9.5
El. cond., μS/cm	838	759	-	-
Turbidity, NTU	87.5	48.5	-	-
COD, mgO_2/l	557.20	606.95	125	700
BOD_5, mgO_2/l	279.80	115.18	25	250
BOD_5/COD	0.502	0.190	-	-
TN_K, mg N/l	47.62	44.82	15*	50*

Note* - values for total nitrogen are compared since values for Kjeldahl nitrogen are not specified by Croatian Regulation [1]

The results showed that both leachates are characterized with medium organic load, ammonia concentration, conductivity and turbidity, while the pH values are within the limit values prescribed by the Croatian Regulation [1]. The value of the BOD_5/COD ratio indicates the biodegradability of leachate. This value in sample B_o is significantly lower and indicates the presence of less biodegradable organic components in leachate.

Comparison of pH and el. conductivity during leachate treatment

Both leachates were treated by coagulation and electrocoagulation, without and with the addition of zeolite. Results of monitoring of pH and el. conductivity during the process are compared in Fig. 1. and 2.

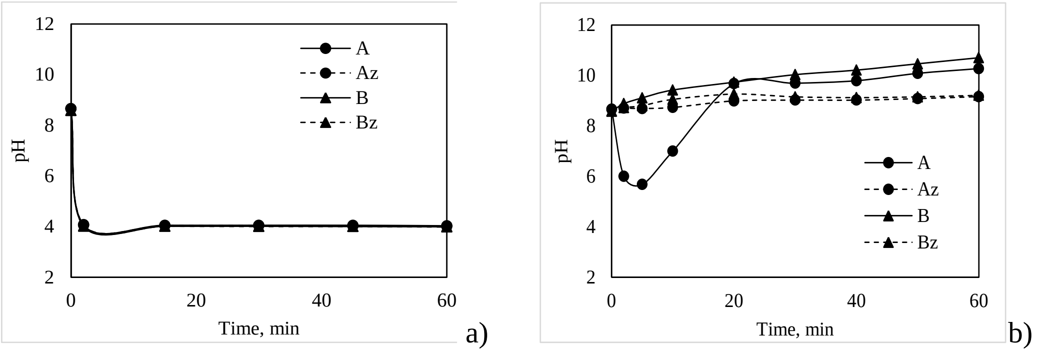

Figure 1. Comparison of pH values during leachates treatment without and with addition of zeolite by coagulation (a) and electrocoagulation (b).

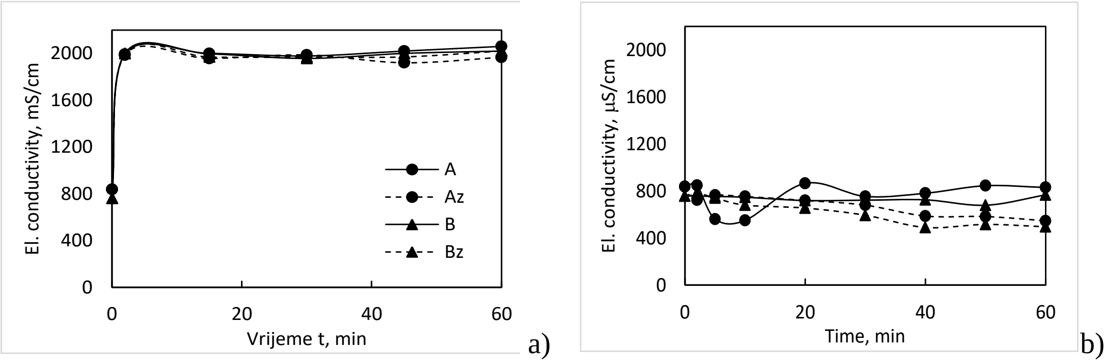

Figure 2. Comparison of el. conductivity during leachates treatment without and with addition of zeolite by coagulation (a) and electrocoagulation (b).

During coagulation, the sharp decrease in pH to values around pH~4 (Fig 1.a) and increase in el. conductivity (Fig 2.a.) are observed. This is due to addition of coagulant $Al_2(SO_4)_3$, the hydrolysis of Al^{3+} and formation of mononuclear and polynuclear hydroxo complexes according to the general reaction:

$$Me^{3+}(\mathrm{aq}) + \mathrm{n}H_2O \leftrightarrow Me(OH)_{\mathrm{n}}^{3-\mathrm{n}} + \mathrm{n}H^{+}(\mathrm{aq}) \tag{1}$$

During electrocoagulation, the pH curves show a slight increase (Fig 1b.) and slight decrease in el. conductivity (Fig 2b). This behaviour is due to the process of hydrolysis of water at the cathode, which produces OH^- ions and hydrogen gas [2]:

$$\text{Cathode:} \qquad 3H_2(l) + 3e^- \rightarrow 3/2\ H_2(g) + 3OH^- \tag{2}$$

However, the increase in pH and decrease of el. conductivity is less pronounced for samples with added zeolite (A_Z and B_Z). This is attributed to the ability of zeolite to neutralize solutions and capturing of the contaminants that contribute to el. conductivity [3]. Also, addition of zeolite particles acted abrasively on the electrodes and contributed to cleaning the electrode surface from oxides, corrosion products and organic mucous layer formed on anode.

Comparison of efficiency of process

Results of turbidity, COD and Kjeldahl nitrogen before and after leachate treatment by coagulation (C) and electrocoagulation (EC) process without and with the addition of zeolite (addition of zeolite marked as C/Z, EC/Z), are compared in Fig. 3-5. In Table 2, comparison of the removal efficiency α (%) by coagulation and electrocoagulation with and without addition of zeolite is given.

Table 2. Comparison of removal efficiency α (%) using coagulation and electrocoagulation without and with addition of zeolite.

Parameter	Removal efficiency α (%) using coagulation			
	A	B	A_z	B_z
Turbidity	92.39	97.94	92.95	93.36
COD	87.14	84.26	87.86	85.90
TK_N	85.29	34.38	97.06	53.13
	Removal efficiency α (%) during electrocoagulation			
Turbidity	78.51	73.13	99.74	99.36
COD	76.07	77.38	84.64	88.52
TK_N	41.18	31.25	82.35	81.25

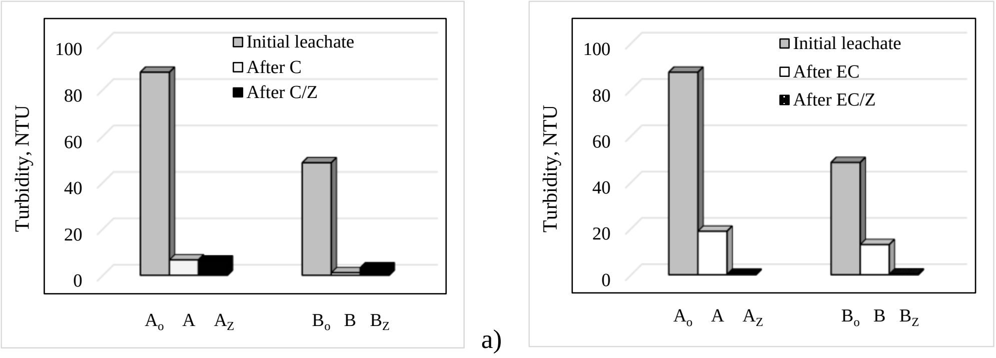

a) b)

Figure 3. Turbidity values before and after leachate treatment without and with the addition of zeolite by coagulation (a) and electrocoagulation (b).

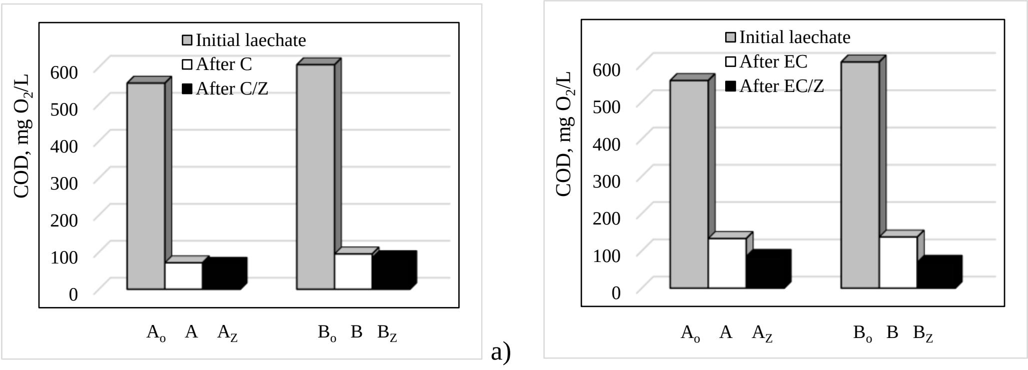

a) b)

Figure 4. The COD values before and after leachate treatment without and with the addition of zeolite by coagulation (a) and electrocoagulation (b).

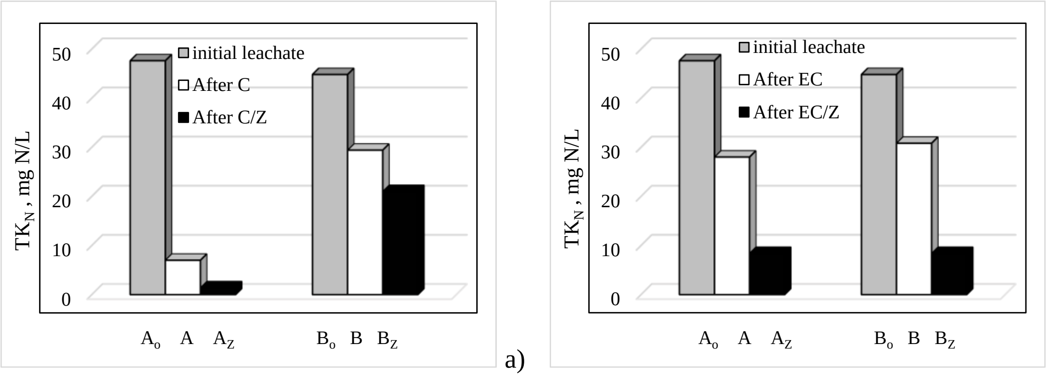

a) b)

Figure 5. Kjeldahl nitrogen before and after leachate treatment without and with the addition of zeolite by coagulation (a) and electrocoagulation (b).

CONCLUSION

Significant reduction in the turbidity, COD and Kjeldahl nitrogen by coagulation and electrocoagulation process are observed. However, significantly better results are obtained with addition of zeolite. Obtained turbidity is decreased for > 99%, COD for >84 % and total Kjeldahl nitrogen for >81%, for both samples.

REFERENCES

[1] Regulation on emission limits values in wastewater, NN 26/2020 *(in Croatian).*
[2] V. Oreščanin, R. Kollar and K. Nađ, *Hrvatske vode,* 2016, **24**, 129-142 *(in Croatian).*
[3] N. Vukojević Medvidović, Doctoral thesis, Faculty of Chemistry and Technology in Split, Split, 2007. *(in Croatian).*

ANALYSIS OF BOHART-ADAMS MODEL EQUATIONS FOR DESCRIPTION OF ADSORPTION IN FIXED BED-COLUMN

Nediljka Vukojević Medvidović, Sandra Svilović
Faculty of Chemistry and Technology, University of Split, Ruđera Boškovića 35, 21000 Split, Croatia
E-mail: nvukojev@ktf-split.hr

ABSTRACT

Bohart and Adams developed mathematical model for description of adsorption in fixed bed column. However, some researchers used the original model, some used a simplified version of the model, while others used the same equation expressed in different forms. This paper is analyzing all Bohart-Adams model equations in order to clarify their differences and similarities.

Keywords: Bohart-Adams model, adsorption, fixed-bed column, breakthrough curve, nonlinear least square methods.

INTRODUCTION

Bohart and Adam (1920) developed a model based on assumption that the adsorption rate is proportional to the residual capacity of the adsorbent and the concentration of adsorbate [1]. The original form of the Bohart-Adams (BA) model is given by Equation (1). However, in literature, one can find also Equation (2) which was obtained when the second term in the denominator (=1) was entirely negligible, except for very small values of both $k_{BA} \cdot q_{BA} \cdot H / v$ and $k_{BA} \cdot c_0 \cdot t$. Several researchers used simplified Equation (3), especially in publications related to environmental protection [2]. The nonlinear and linear forms of the BA model are compared in Table 1.

Table 1. Nonlinear and linear form of Bohart-Adams model equations.

Nonlinear form	Linear form	Eq. no.	Ref.
$\frac{c}{c_o} = \frac{\exp(k_{BA} \cdot c_o \cdot t)}{\exp(k_{BA} \cdot q_{BA} \cdot H / v) - 1 + \exp(k_{BA} \cdot c_o \cdot t)}$	$\ln(\frac{c_0}{c} - 1) = \ln\left[\exp\left(k_{BA} \cdot q_{BA} \cdot H / v\right) - 1\right] - k_{BA} \cdot c_0 \cdot t$	(1)	[1]
$\frac{c}{c_o} = \frac{1}{1 + \exp\left[\frac{k_{BA} \cdot q_{BA} \cdot H}{v} - k_{BA} \cdot c_0 \cdot t\right]}$	$\ln(\frac{c_0}{c} - 1) = k_{BA} \cdot q_{BA} \cdot H / v - k_{BA} \cdot c_0 \cdot t$	(2)	[2]
$\frac{c}{c_o} = \exp\left[k_{BA} \cdot c_0 \cdot t - \frac{k_{BA} \cdot q_{BA} \cdot H}{v}\right]$	$\ln(\frac{c_0}{c}) = k_{BA} \cdot q_{BA} \cdot H / v - k_{BA} \cdot c_0 \cdot t$	(3)	[2]

Note: c - the effluent adsorbent concentration (mmol/L), c_0 – the influent adsorbent concentration (mmol/L), t – the time (h), v – the linear flow velocity (m/h), H - the fixed bed depth (m), k_{BA} - the rate constant of the Bohart-Adams model (L /(mmol h)), q_{BA}- the adsorption capacity of Bohart-Adams model (mmol/L)

In this paper, nonlinear forms of Bohart-Adams model equations are tested on experimental breakthrough curve of zinc removal onto Na-zeolite in order to clarify their differences and similarities.

EXPERIMENTAL

The nonlinear least square method was used for testing of the model equations in the Mathcad program. The testing was performed on experimental breakthrough curve of zinc removal onto Na-zeolite, performed at three different bed depths (H = 120, 80 and 40 mm - at initial zinc concentration of 1.083 mmol/L and flowrate of 1 mL/min) [3]. The natural zeolite clinoptilolite used in this study was originated from Zlatokop deposit, Vranjska Banja, Serbia, with granulation of 0.6-0.8 mm and pre-treated into Na-form. The characterization of zeolites was previously published [4]. The parameters were calculated from the Equations (1), (2), and (3) using Solve block and Minerr as output function. Constrains for the used models could be presented as:

$$\frac{\mathrm{d}}{\mathrm{d}X}\sum_{i=1}^{z}\left[(c/c_0)_{\mathrm{exp}}-(c/c_0)_{\mathrm{m}}\right]^2=0 \qquad (4)$$

where $(c/c_0)_{\mathrm{exp}}$ is experimental c/c_0 data, $(c/c_0)_{\mathrm{m}}$ represents the right side of nonlinear form in models given by equations (1), (2) and (3), X is a parameter (k_{BA} and q_{BA}). The number of constraints is equal to the number of the parameters.

The correlation coefficient (r^2) and the root mean square error (RMSE) were used as indicators of fitting of the experimental results with the results obtained by the model.

$$\mathrm{RMSE}=\sqrt{\frac{1}{z}\sum_{i=1}^{z}\left[(c/c_0)_{\mathrm{m}}-(c/c_0)_{\mathrm{exp}}\right]^2} \qquad (5)$$

The saturation capacity of the Bohart-Adams model, q can be evaluated as follows [5]:

$$q = q_{\mathrm{BA}}\cdot BV_{\mathrm{S}}/m = q_{\mathrm{BA}}/\rho \qquad (6)$$

where q is the saturation capacity of the Bohart-Adams model (mmol/g), BV_s is the fixed bed volume (L), m - the mass of the adsorbent bed in column (g), ρ is the apparent density of the adsorbent in the packed bed.

RESULTS AND DISCUSSION

Comparison of experimental and model breakthrough curves of zinc uptake onto Na-zeolite bed depth of 120, 80 and 40 mm, obtained by different Bohart-Adams model equations are compared in Fig. 1. The parameters of the Bohart-Adams model equations have been evaluated and summarized in Table 2.

Table 2. The parameters of the Bohart-Adams model equations.

Bohart-Adams eq. no.	Bed depth, mm	k_{BA} L/(mmol h)	q_{BA} mmol/L	r^2	RMSE
(1)	120	0.184	485.818	0.993	0.033
	80	0.225	456.792	0.984	0.054
	40	0.428	456.135	0.986	0.044
(2)	120	0.184	485.818	0.993	0.033
	80	0.225	456.792	0.984	0.054
	40	0.428	456.135	0.986	0.044
(3)	120	0.049	562.092	0.924	0.083
	80	0.058	546.973	0.912	0.124
	40	0.157	525.835	0.966	0.071

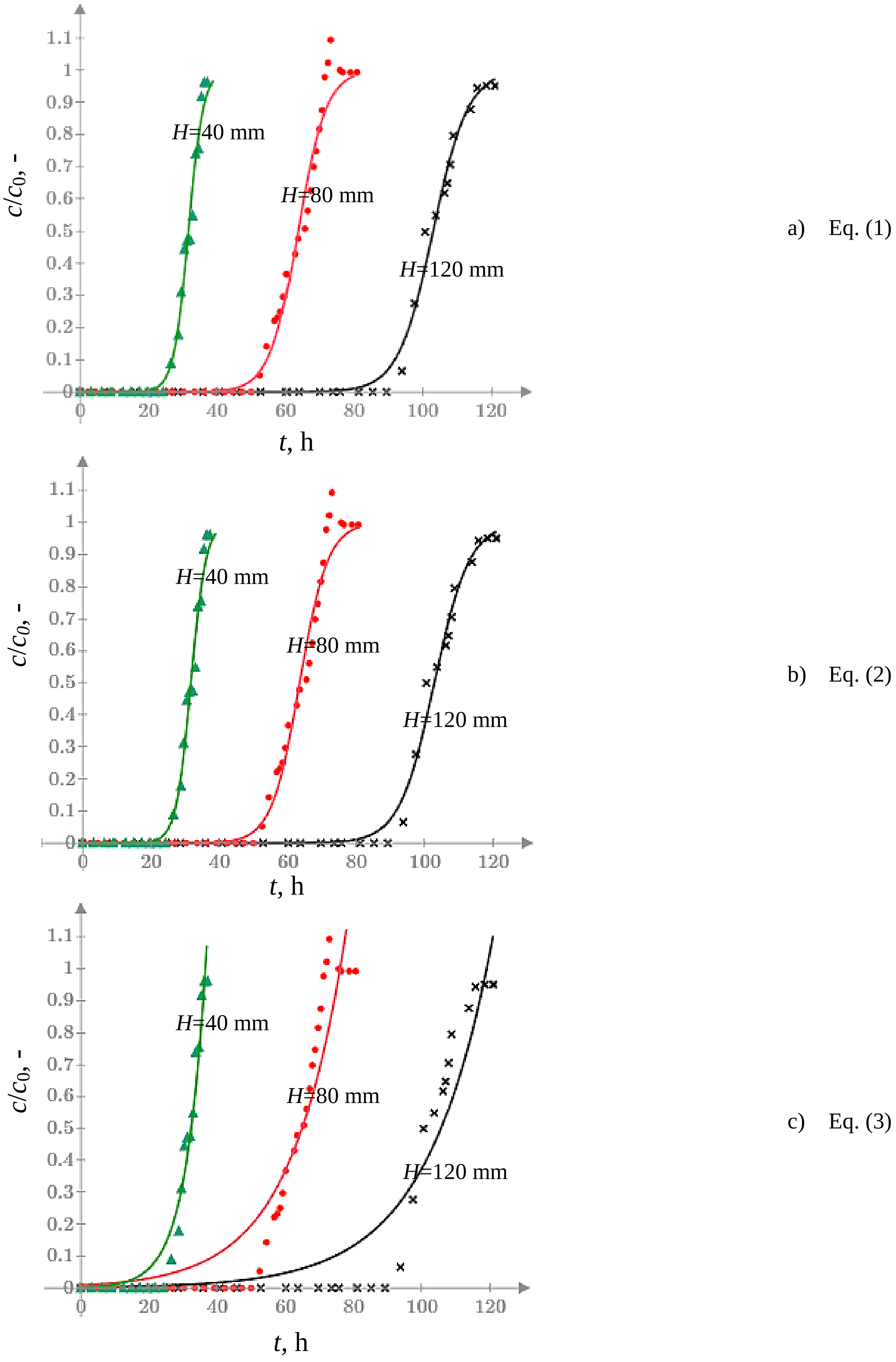

a) Eq. (1)

b) Eq. (2)

c) Eq. (3)

Figure 1. Comparison of experimental and model breakthrough curves of zinc uptake onto zeolite bed depth of 120, 80 and 40 mm, obtained by different BA model equations: a) Equation (1); b) Equation (2), c) Equation (3).

From the results in Fig 1, it is evident that experimental and model breakthrough curves obtained from Equations (1) and (2) are almost overlapping, indicating good agreement of the model equations with experimental data of zinc removal on Na-zeolite. However, model breakthrough curves obtained from Equation (3) show good agreement only in the initial part of breakthrough curve. According to Lee at al. (2015) this can be attributed to fact that

Equations (1) and (2) are convergent-type models, while Equation (3) is divergent model type [2]. Thus, Equation (3) is not suitable for the simulation of entire breakthrough curve, but only its initial part. Also, the model parameters k_{BA} and q_{BA} calculated from Equation (3) are different from those calculated from Equations (1) and (2) (see Table 2). The r^2 and RMSE values confirm better agreement of Equations (1) and (2) with experimental data.

Based on evaluated parameter q_{BA}, the saturation capacity of the Bohart-Adams model, q can be evaluated according to Equation (6). Values are compared with experimental values of breakthrough (q_B) and exhaustion capacity (q_E) in Table 3.

Table 3. Comparison of saturation capacity of the Bohart-Adams model, q with breakthrough capacity (q_B) and exhaustion capacity (q_E) experimentally obtained.

Bed depth, mm	Eq (1)	Eq (2)	Eq (3)	Experimental values [3]	
	q mmol/g	q mmol/g	q mmol/g	q_B mmol/g	q_E mmol/g
120	0.732	0.732	0.847	0.604	0.692
8	0.700	0.700	0.838	0.578	0.786
4	0.711	0.711	0.820	0.593	0.703

Better agreement of q is obtained with the experimental values of exhaustion capacity q_E. However, the values of q obtained from BA model Equation (3) are slightly overestimated, which is attributed to divergence-type model as well as exponential function type. This is in agreement with findings by Chu (2020) and Hu and Zhang (2020) [6,7].

CONCLUSION

The three different equations of Bohart-Adams model have been used in modeling of adsorption in a fixed-bed column. This paper confirms that the original form given by Equation (1) and its simplified form given by Equation (2) are totally different from Equation (3). This should be considered when choosing appropriate equation in modeling of adsorption systems.

REFERENCES

[1] G.S. Bohart and E.Q. Adams, *J. Am. Chem. Soc.* 1920, **42**, 523-544.

[2] C.G. Lee, J.H. Kim, J.K. Kang, S.B. Kim, S.J. Park, S.H. Lee and J.W. Choi, *Desalin. Water. Treat.*, 2015, **55**, 1795–1805.

[3] M. Trgo, N. Vukojević Medvidović, J. Perić and I. Nuić, in *Proceedings of International Conference on Materials, Tribology, Recycling, MATRIB 2009*, K. Grilec, G. Marić (eds.), Zagreb, Croatian Society of Materials and Tribology, 2009, 195-202 *(in Croatian).*

[4] N. Vukojević Medvidović, Doctoral thesis, Faculty of Chemistry and Technology in Split, Split, 2007. *(in Croatian).*

[5] Y. Sag and Y. Aktay, *Process Biochem.* 2001, **36**, 1187–1197.

[6] K.H. Chu, *J. Hazard. Mater.* 2020, **389**, 122025.

[7] Q. Hu and Z. Zhang, *J. Hazard. Mater.* 2020, **394**, 122508.

EQUILIBRIUM STUDY OF COPPER IONS ADSORPTION ON THE NATURAL CLINOPTILOLITE-RICH ZEOLITIC TUFF

Mario Nikola Mužek, Anđela Čović, Anita Bašić, Sandra Svilović
Faculty of Chemistry and Technology, University of Split, Ruđera Boškovića 35, 21 000 Split, Croatia
E-mail: muky@ktf-split.hr

ABSTRACT

In this study the influence of particle size on adsorption of copper ions on the natural clinoptilolite-rich zeolitic tuff was studied in batch reactor at the temperature of 25°C and with the stirring speed of 200 rpm. The appropriate amount of three different fractions (45-71 μm, 71-90 μm, and 90-125 μm) of the zeolitic tuff was placed into copper (II) nitrate solution of various concentrations and mixed until equilibrium was reached. The adsorbed amount of copper ions firstly increases with increasing of the initial copper concentration reaching its maximum at the copper concentration of 11.763 mmol dm^{-3} for all fractions of the zeolitic tuff. Langmuir and Freundlich isotherm models were used to fit the experimental adsorption data. Based on the correlation coefficient, the best fit of the experimental data was achieved with the Langmuir adsorption model, for all three particle sizes of the zeolitic tuff.

Key words: copper, natural untreated clinoptilolite-rich zeolitic tuff, adsorption isotherms, equilibrium.

INTRODUCTION

Due to rapid industrialization and globalization, the environment becomes more and more burdened by the emission of harmful substances, primarily heavy metals, especially when they are present in wastewaters. Most of them are highly soluble in water and show toxic and carcinogenic impacts on all living organisms [1]. For that very reason, it is important to reduce or, where it is possible, entirely remove heavy metals from contaminated wastewater prior to its discharge into the environment. One of the most applied treatment option is adsorption which represents a highly effective physicochemical process for removal of heavy metals from wastewater, especially at low initial metal concentrations [2-6]. Common adsorbents for removal of heavy metals are clays and zeolites.

Zeolites are microporous minerals whose structure mainly consists of alumino-silicates with SiO_4 and AlO_4 structures connected by shared oxygen atoms. Such structure generates cavities suitable for the exchange of various molecules or ions. Although natural zeolites are environmentally and economically friendly materials their effectiveness for removal of different pollutants in different technological processes mainly depends on their physicochemical properties that are closely related to their geological origin. The most widespread and studied natural zeolite is zeolite clinoptilolite due to its exceptional properties used in many industrial applications [7].

The objective of this study is to examine the effect of clinoptilolite particle sizes on the adsorption of copper ions. Experiments were performed with different initial copper concentrations and the obtained data were fitted according to two isotherm models – Langmuir and Freundlich.

EXPERIMENTAL

Starting material used in this study was the natural clinoptilolite-rich zeolitic tuff (Donje Jesenje site, Krapina, Croatia). The raw material was crushed and sieved to obtain three different particle sizes: 45-71 μm, 71-90 μm, and 90-125 μm. Solutions containing Cu ions were prepared by dissolving the appropriate amount of $Cu(NO_3)_2 \cdot 3H_2O$ (Kemika) in distilled water. The initial concentrations (3.881, 7.780, 11.763, 19.305, 30.576 and 39.390 mmol dm^{-3}) were confirmed by Perkin Elmer Lambda EZ 201 UV/VIS spectrophotometer.

The FTIR spectra of natural zeolite before and after the adsorption process was made on KBr pastille on a Shimadzu IRAffinity-1 in the range from 4 500 to 450 cm^{-1}.

The copper adsorption equilibrium studies were conducted by agitating 0.2 dm^3 of copper solutions with 1.0 g of zeolitic tuff in batch reactors at the temperature of 25°C until the equilibrium was reached. In order to determine the time needed to reach the equilibrium, kinetic experiments were performed. Appropriate amount of each solution sample was taken out from reactors at certain time interval. Results showed that equilibrium was reached after 48 h regardless on the particle size of the zeolitic tuff. The equilibrium amount of copper adsorbed on the zeolitic tuff, q_e (g $mmol^{-1}$), was calculated by the Equation (1):

$$q_\mathrm{e} = \frac{(c_0 - c_\mathrm{e}) \cdot V}{m} \qquad (1)$$

where c_0 is the initial copper concentration in the solution (mmol dm^{-3}), c_e is the equilibrium copper concentration in the solution (mmol dm^{-3}), V is the volume of copper solution in the batch reactor (dm^3), and m is the mass of the zeolitic tuff (g).

The adsorption efficiency of copper ions on the zeolitic tuff, A_eff (%), was calculated by the Equation (2):

$$A_\mathrm{eff} = \frac{c_0 - c_\mathrm{e}}{c_0} \cdot 100 \qquad (2)$$

RESULTS AND DISCUSSION

The chemical composition of zeolitic tuff is presented elsewhere [8]. The main oxide components (SiO_2 and Al_2O_3) present in the zeolitic tuff are SiO_2=64.93% and Al_2O_3=13.66%. XRD analysis showed that the zeolitic tuff contains predominantly clinoptilolite, while illite, quartz and feldspar are accessory minerals [8].

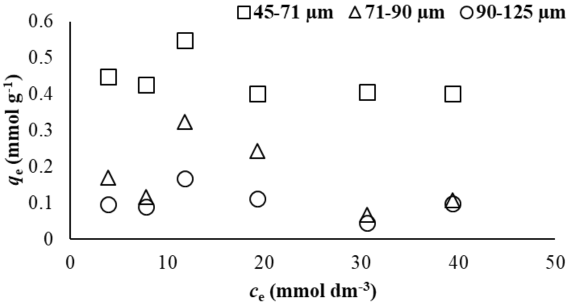

Figure 1. Equilibrium amount of copper ions adsorbed on zeolitic tuff depending on the equilibrium concentration of copper ions in solutions.

Copper adsorption isotherms of the three different fractions of the zeolitic tuff are presented in Figure 2. It is evident from Figure 1 that the adsorbed amount of copper ions increases with increase of the initial copper concentration reaching its maximum at copper concentration of 11.763 mmol dm^{-3}. After this, small decrease in copper adsorption to lower values is observed for all three particle sizes. The reason for this effect is most likely related to the presence of various impurities in the zeolitic tuff as well as to the composition and exchangeability of cations in the zeolite structure, distribution and amount of clinoptilolite in different fractions of the zeolitic tuff [9-10].

The adsorption efficiency is also determined and according to the data obtained for the adsorbed amount of copper ions on the zeolitic tuff it can be observed that it decreases as the initial concentration of copper ions in solution increases (Table 1). It is also evident that the adsorption efficiency decreases as the particle size of zeolitic tuff increases, as the result of decrease of surface area of adsorbent.

Table 1. Adsorption efficiency of zeolite clinoptilolite.

Initial concentration of copper solutions (mmol dm^{-3})	A_{eff} (%) 45-71 μm	A_{eff} (%) 71-90 μm	A_{eff} (%) 90-125 μm
3.881	57.766	21.824	11.985
7.780	27.312	7.065	5.535
11.763	23.327	12.653	5.977
19.305	10.370	5.854	2.561
30.576	6.616	1.062	0.630
39.390	5.083	1.295	1.200

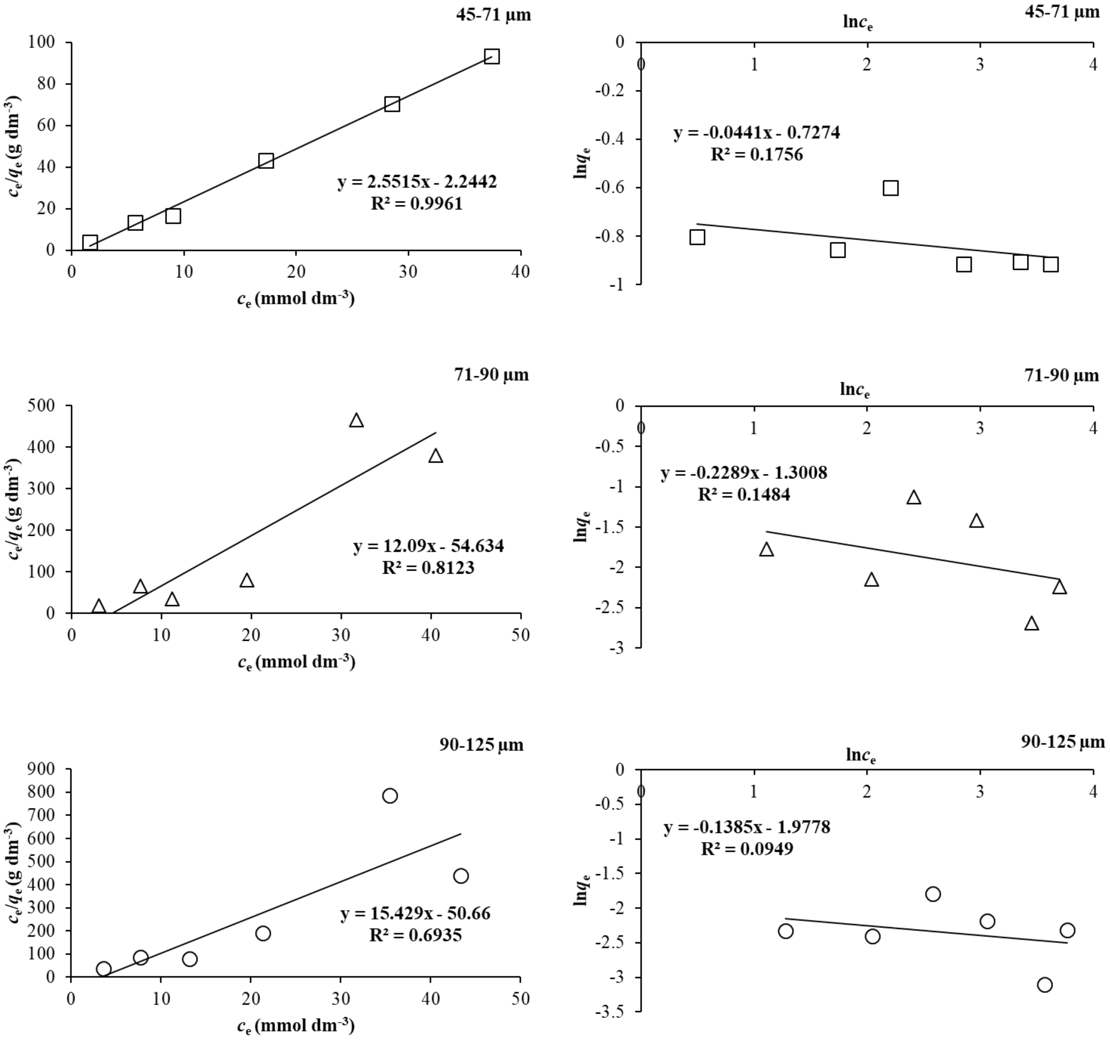

Figure 2. Correlation of experimentally obtained data (symbols) with the selected isotherm models (lines): Langmuir (left) and Freundlich (right) for various particle sizes of adsorbent used.

The experimental data were fitted to two selected isotherm models, Langmuir and Freundlich. Linear forms of both isotherms are presented in Figure 2. The Langmuir isotherm model fits the experimental data much better than the Freundlich isotherm model for all particle sizes which is confirmed with the R^2 value. From Figure 2 it is also evident that the best correlation of the Langmuir isotherm model with the experimental data is achieved when the adsorbent with a lowest particle size was used, 45-71 μm, because smaller adsorbent size offered comparatively larger available surface area for adsorption of copper ions.

In Figure 3 the FTIR spectra of the zeolitic tuff before and after the adsorption of copper ions are shown. The widest band at 1043.49 cm^{-1} is attributed to the asymmetric stretching vibrations of the Si–O–Si and Al–O–Si. The bands, located at 794.67 and 466.77 cm^{-1}, correspond to the bending of Si–O–Si and O–Si–O bonds, indicate the presence of quartz in the system. The band at 1645.28 cm^{-1}, as well as bands at 3631.96 and 3442.94 cm^{-1} corresponding to the bending vibrations of the H–O–H bond and stretching vibrations of –OH, H–O–H can also be observed. These bands indicate the presence of water trapped in the cavities within the zeolite structure [11].

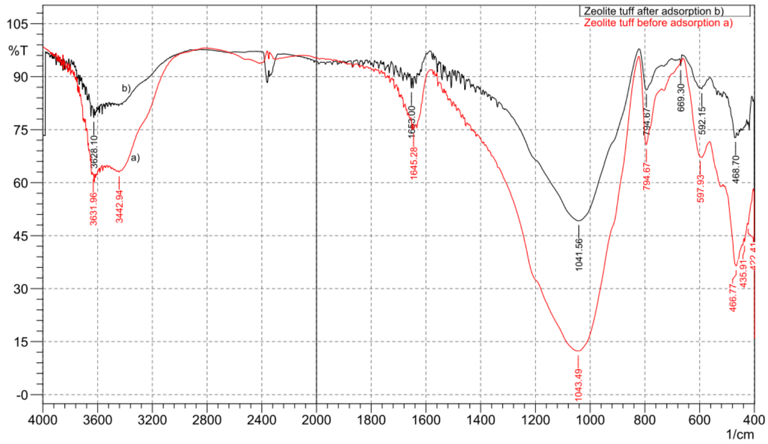

Figure 3. FTIR spectra of the zeolite tuff before and after the adsorption of copper ions.

CONCLUSION

In this study the effect of clinoptilolite particle size on the equilibrium adsorption of copper ions was investigated. The adsorbed amount of copper ions reaches its maximum at the initial copper concentration of 11.763 mmol dm^{-3}. Adsorption efficiency decreases as the particle size of zeolitic tuff increases as a result of decrease of surface area of adsorbent. FTIR spectra revealed no changes of the structure of adsorbent after adsorption of copper ions. The correlation of the data obtained with the Langmuir and Freundlich isotherm models revealed that the Langmuir isotherm model fits the experimental data better for all the particle sizes of zeolite tuff, in particular for particle size 45-71 μm.

REFERENCES

[1] P.B. Tchounwou, C.G. Yedjou, A.K. Patlolla and D.J. Sutton, *EXS*, 2012, **101**, 133-164.
[2] M.N. Mužek, S. Svilović and J. Zelić, *Desalin. Water Treat.*, 2014, **52**, 2519-2526.
[3] V. Krstić, T. Urošević and B. Pešovski, *Chem. Eng. Sci.*, 2018, **192**, 273-287.
[4] S. Svilović, M.N. Mužek, I. Nuić and P. Vučenović, *Water Sci. Technol.*, 2019, **80**, 98-108.
[5] R. Fernández-González, M.A. Martín-Lara, G. Blázquez, G. Tenorio and M. Calero, *J. Clean Prod.*, 2020, **268**, 121935.
[6] M. Bashir, S. Tyagi and A.P. Annachhatre, *Mater. Today: Proc.*, 2020, **28**, 1833-1840.
[7] A. Mastinu, A. Kumar, G. Maccarinelli, S.A. Bonini, M. Premoli, F. Aria, A. Gianoncelli and M. Memo, *Molecules*, 2019, **24**, 1517 (1-15).
[8] D. Barbir, P. Dabić and A. Lisica, *Chem. Biochem. Eng. Q.*, 2016, **30**, 401-409.
[9] M.L. Nguyen and C.C. Tanner, *New Zealand J. Agricult. Res.*, 1998, **41**, 427-446.
[10] M. Rožić, Š. Cerjan-Stefanović and L. Ćurković, *Croat. Chem. Acta*, 2002, **75**, 255-269.
[11] M.N. Mužek, S. Svilović and J. Zelić, *Sep. Sci. Technol.*, 2016, **51**, 2868-2875.

PREDICTION OF ZEOLITE BARRIER CAPABILITY IN TREATMENT OF GROUNDWATER POLLUTED BY Pb, Cd AND Zn

Ivona Nuić, Matea Šušnjara, Marina Trgo, Nediljka Vukojević Medvidović, Marin Ugrina
Faculty of Chemistry and Technology, Department of Environmental Engineering, University of Split, Ruđera Boškovića 35, 21 000 Split, Croatia
E-mail: ivona@ktf-split.hr

ABSTRACT

This paper considers the possible use of natural zeolite as filler in permeable reactive barrier (PRB). From the column experimental results, the distribution and retardation coefficients were calculated in order to evaluate the Pb, Cd and Zn distribution and immobilization within the zeolite barrier. Calculation of hydrodynamic dispersion coefficients enabled prediction of contaminants spreading in the groundwater.

Key words: natural zeolite, heavy metals, polluted groundwater, permeable reactive barrier.

INTRODUCTION

The environment pollution by heavy metals progress intensively, especially due to rapid industrialization and agricultural activities. Heavy metals are daily emitted into the air, soil and surface waters, and can endanger groundwater, which is the main source of water for human consumption. Therefore, it is necessary to develop methods of protecting water in aquifers from different types of pollution. Permeable reactive barriers (PRBs) are one of the very promising methods of groundwater protection [1]. The PRB is an underground structure located across the groundwater flow, downstream of pollution source, whose main purpose is to reduce or completely remove pollutants. Many reactive materials are used as fillers in PRB, depending on the target pollutant. Zeolites have been recognized as effective materials for the treatment of heavy metal contaminated waters [2]. In order to protect groundwater from hazardous heavy metals, prior developing a remediation plan, it is necessary to determine their mobility in the groundwater environment. The column experiments [3] are intended to simulate underground dynamic conditions and to quantify the sorption of heavy metals relative to groundwater flow. This study investigates natural zeolite clinoptilolite as possible filler material in PRB for *in situ* remediation of simulated groundwater contaminated by Pb, Cd and Zn.

EXPERIMENTAL

The column experiments were performed at 23 ± 2 °C in glass column (height, 50 cm; inside diameter, 1.2 cm) on the $H = 8$ cm high fixed bed of natural zeolite clinoptilolite (Zlatokop deposit in Serbia). An equimolar binary Pb+Zn and Cd+Zn solutions of total initial concentration ≈ 1 mmol/L, were passed through the column in down-flow mode at flow rates $Q = 1, 2, 3$ and 4 mL/min. All effluents collected at the bottom of the column were analysed for Pb, Cd and Zn concentrations by the complexometric method or the ion chromatography on the Metrohm 761 Compact IC using the Nucleosil 5SA column.

RESULTS AND DISCUSSION

The obtained column results are presented as breakthrough curves in Figure 1. All curves for both binary solutions have a characteristic S-shape, indicating the establishment of stationary conditions. With increasing in flow rate the Pb, Cd and Zn ions from the binary solutions appeared earlier at the column outlet (breakthrough point).

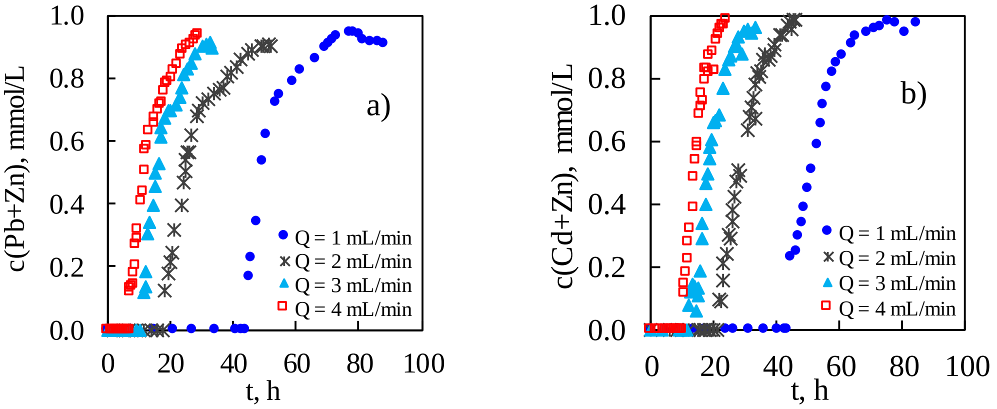

Figure 1. Breakthrough curves as total effluent concentration *vs.* retention time for a) Pb+Zn [3], and b) Cd+Zn solutions at different flow rates.

The percentage of metals uptake by the zeolite, α (%), was calculated using following equation:

$$\alpha = (\frac{c_o - c_e}{c_o}) \cdot 100 \qquad (1)$$

where c_o and c_e are initial and equilibrium metal concentrations (mmol/L) in solution. The obtained values for each metal in both binary solutions are presented in Figure 2.

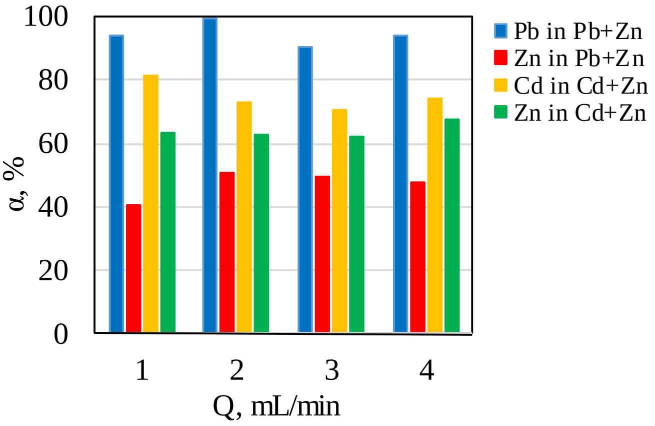

Figure 2. The uptake of each metal for both binary solutions in relation to different flow rates.

The Pb is best removed (90.1–99.4%) by the natural zeolite, compared to Cd (70.8–81.3%) and Zn (40.6–50.6% for Pb+Zn, and 62.3–67.4% for Cd+Zn). The Zn was less bound for both binary solutions, especially for the Pb+Zn. This is a consequence of competition between ions, and their hydrated ionic radius, which is lowest for the Pb, and highest for the Zn [4], making it more difficult to access zeolite binding sites.

To estimate the potential for the sorption of dissolved contaminants on the zeolite, the distribution coefficient, K_d (L/g) was calculated:

$$K_d = (\frac{c_o - c_e}{c_e}) \cdot \frac{V_e}{m} \qquad (2)$$

where V_e is the remediate volume of solution in equilibrium (L) and m is the zeolite mass (g) in the column. The ability of the zeolite in retaining contaminants is quantified by the retardation coefficient R_d (-):

$$R_d = 1 + \frac{\rho}{\varepsilon} \cdot K_d \cdot 1000 \qquad (3)$$

where ρ is the zeolite bulk density of 0.699 g/cm^3 and ε is the zeolite fixed bed porosity of 0.693. Calculated coefficients are presented in Figure 3.

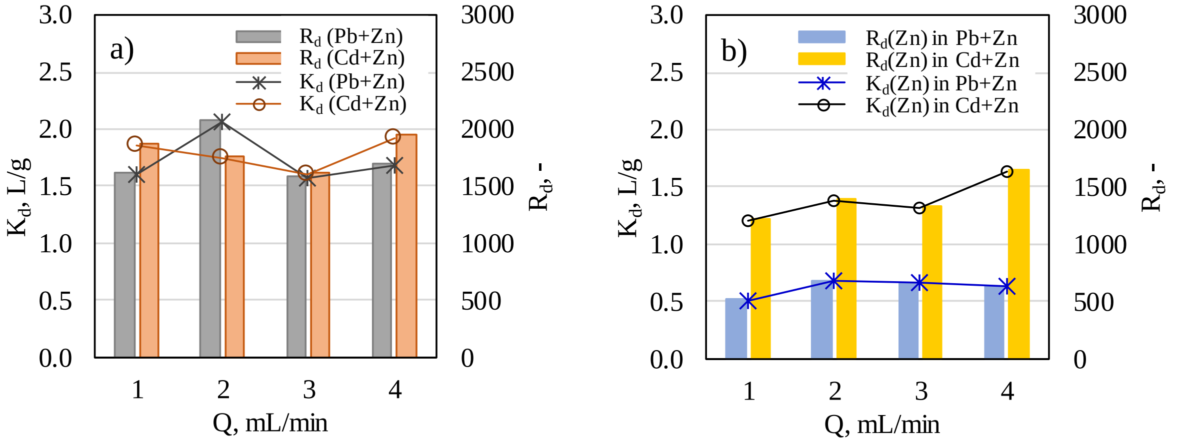

Figure 3. Distribution and retardation coefficients for a) total Pb+Zn and Cd+Zn concentration and b) Zn concentration in both binary solutions.

A higher value of K_d indicates a good distribution leading to better uptake of contaminants by the zeolite, while higher R_d points on good immobilization of the contaminants. Values of K_d and R_d in Figure 3a are very similar for both binary solutions and for all flow rates. Contrary, the differences of the K_d and R_d values of Zn (Figure 3b) in different binary solutions are quite notable. The Zn is better distributed and retained on the zeolite in case of Cd+Zn, compared to Pb+Zn system, as well as with increased flow rate. The reason for such behaviour of Zn is less pronounced competition between Cd and Zn caused by closer values of hydrated ionic radii, comparing to Pb and Zn, as well as shorter contact times. This is in line with the α values presented in Figure 2.

The degree of expansion of the contaminant in the liquid phase flowing downstream through the porous medium depends on the hydrodynamic dispersion coefficient, D_L (m^2/min) which is calculated according to the Brigham method [5] by the following equation:

$$D_L = \frac{v \cdot H}{8}\left[\left(\frac{U-1}{\sqrt{U}}\right)_{0.84} - \left(\frac{U-1}{\sqrt{U}}\right)_{0.16}\right]^2 \qquad (4)$$

where v is the mean velocity (m/min) of water through pores, $v = Q/(A\cdot\varepsilon)$, A is the cross-sectional area of the column of 1.1304 cm^2, U is the number of effluent pore volumes equals to $U = V_t/V_p = V_t/(A\cdot H\cdot\varepsilon)$, where V_t (mL) is the volume at time t. The subscripts 0.84 and 0.16 correspond to the $(U-1)/U^{1/2}$ values in $c/c_o = 0.84$ (exhaustion) and $c/c_o = 0.16$ (breakthrough), on the breakthrough curves, which are normally used as the midpoint concentration for defining the movement and velocity of the contaminant plume.

The retardation hydrodynamic dispersion coefficient D_{LR} (m^2/min) is calculated as:

$$D_{LR} = \frac{D_L}{R_d} \qquad (5)$$

Lower values of D_L and D_{LR} are preferable in order to mitigate the hydrodynamic dispersion, since it causes extra spreading of contaminants in the underground. The calculated parameters are presented in Figure 4. It can be seen that D_L and D_{LR} for Pb+Zn and Cd+Zn solutions in Figure 4a increase with increasing in flow rate, especially in case of Cd+Zn. The same happened for Zn in both binary solutions in Figure 4b, and is more pronounced for Cd+Zn.

The greater hydrated ionic radii of Cd and Zn compared to Pb preventing them binding to less accessible sites within the zeolite barrier, enhancing their spreading. Moreover, affinity of natural zeolite toward Pb is much higher than for Cd and Zn.

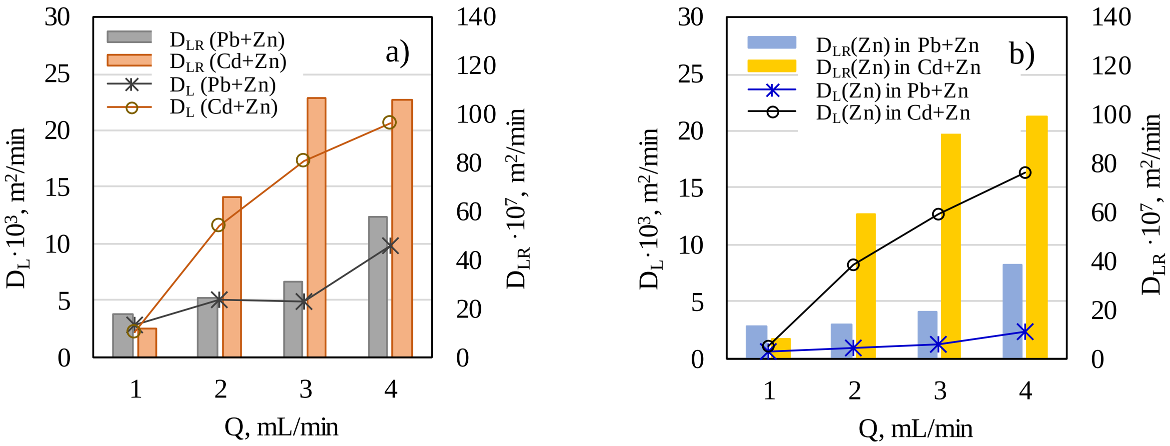

Figure 4. The hydrodynamic dispersion and retardation hydrodynamic dispersion coefficients for a) total Pb+Zn and Cd+Zn concentration and b) Zn concentration in both binary solutions.

Comparing all calculated parameters, the best distribution and retention, with minimum spreading of contaminants is achieved for the lowest flow rate of 1 mL/min in both binary solutions. This flow rate corresponds to mean velocity through the zeolite pores of v = 0.01277 m/min, which is higher than average groundwater flow rate of ≈ 0.00003 m/min [5]. This indicates that at lower flow rates than those examined, the retention of contaminants by natural zeolite barrier is even better. Otherwise, the distance within the barrier should be increased to ensure optimal contact time and longevity of the barrier.

CONCLUSION

Natural zeolite clinoptilolite showed good binding properties of Pb, Cd and Zn from binary solutions. The Pb uptake was higher than 90% for all examined flow rates, while for Cd it was in the range 70.8–81.3%. Uptake of Zn was better from binary Cd+Zn (62.3–67.4%) than from Pb+Zn solution (40.6–50.6%) due to less expressed competition between Cd and Zn compared to Pb and Zn. The retardation coefficients point on good retention of contaminants within the zeolite barrier, while hydrodynamic dispersion coefficients increase with flow rate, indicating the broadening of the contaminants plume. The best behaviour of contaminants inside the zeolite barrier was achieved at the lowest flow rate, which is closest to the real groundwater velocity comparing to other examined flow rates. These findings suggest possible application of natural zeolite as filler in PRB in treatment of groundwater contaminated with heavy metals, especially for low flow rates common in the underground environment.

REFERENCES

[1] F. Obiri-Nyarko, S.J. Grajales-Mesa, and G. Malina, *Chemosphere*, 2014, **111**, 243-259.
[2] P. Misaelides, *Micropor. Mesopor. Mat.*, 2011, **144** (1-3) 15-18.
[3] I. Nuić, M. Trgo, and N. Vukojević Medvidović, *Chem. Eng. J.*, 2016, **295**, 347-357.
[4] L. Canet, and P. Seta, *Pure Appl. Chem.*, 2001, **73** (12), 2039-2046.
[5] N. Vukojević Medvidović, I. Nuić, M. Ugrina, and M. Trgo, *Water Air Soil Pollut.*, 2018, **229**:367.

ZEOLITE SURFACE PASSIVATION: "CORE-SHELL" SYSTEMS FROM SYNTHESIS TO CATALYTIC APPLICATIONS

Massimo Migliori
Laboratory of Chemical Engineering, Catalysis and Sustainable Processes CECaSP_Lab
University of Calabria, Italy
E-mail: massimo.migliori@unical.it

Tuning the acidity of zeolite catalysts is one of the most important concerns for improving their catalytic performances. This challenging topic, studied for decades, consider that acidity in zeolites could hold either within the structure channel or at the external surface. Sometimes this classification did not receive sufficient attention leading out of the way the scientific efforts to optimize the catalyst properties. In fact, acid sites out of the surface can promote undesired reactions as the "shape selectivity" action of zeolite does not play any role, at the external surface. This is a common observation than, in the case of reactions with hydrocarbons, lead to the formation of coke species, compromising the catalyst efficiency and productivity.

Different post-synthesis techniques have been proposed to reduce the surface acidity in a controlled way and one of most stimulating is the epitaxial growth of a secondary phase of non-acidic zeolite acting as passivating layer. This leaded to the definition of the "Core-shell" systems: a class of zeolite-based materials having a non-acid shell over an active core. This technique was revealed also promising when in the case of zeolites in "hybrid" (Red-Ox/Acid) catalyst as the interaction between the two phases could affect the metal stability as negative consequence of the surface acidity (uncontrolled reactivity, water adsorption). In this concern, the option of a "phase segregation" as result of a surface passivation offers the advantage from the reduction of metal-acid sites interaction without giving up to the benefits for zeolitic support to metal catalyst (high specific surface area, microporosity, potential proximity effect between active sites).

The lecture will cover the topic of surface passivation via zeolite growth accounting for the different synthesis conditions (zeolitic or metallic core), microporous/mesoporous core structure and zeolite type, aiming at elucidating drawbacks and advantages of this approach, trying also to supply new ideas about the core-shell synthesis technique, then could be attractive for different applications.

ENVIRONMENTAL-FRIENDLY MODIFIED NATURAL ZEOLITES AS SORBENTS FOR *IN SITU* REMEDIATION OF MERCURY-CONTAMINATED SOIL IN IDRIA REGION, SLOVENIA

Marin Ugrina[1], Teja Čeru[2], Ivona Nuić[1], Marina Trgo[1], Aleksandra Daković[3]
[1]Department of Environmental Engineering, Faculty of Chemistry and Technology, University of Split, Ruđera Boškovića 35, 21 000 Split, Croatia
[2]Department of Mineral Resources and Geochemistry, Geological Survey of Slovenia, Dimičeva Ulica 14, 1000 Ljubljana, Slovenia
[3]Institute for Technology of Nuclear and Other Mineral Raw Materials, P. O. Box 390, 11 000 Belgrade, Serbia
E-mail: mugrin@ktf-split.hr

ABSTRACT

Toxicity Characteristic Leaching Procedure (TCLP) was applied to mercury-contaminated soil from the Idrija region, Slovenia to evaluate the potential soil toxicity. The TCLP test was performed with and without the addition of natural zeolite, iron(III)-modified zeolite or sulphur-impregnated zeolite. Results showed that the soil is extremely polluted and represents hazardous waste. The addition of zeolites significantly reduces the concentration of leached Hg, whereby the most satisfactory results being achieved with sulphur-impregnated zeolite, making it as a potential sorbent for *in situ* remediation of mercury-contaminated soil.

Key words: natural zeolite, iron-modified zeolite, sulphur-impregnated zeolite, leaching, mercury-contaminated soil.

INTRODUCTION

The remediation of soil in surrounding area of the Idrija mine in Slovenia is of significant interest in order to prevent spreading of pollution and negative impacts on the entire ecosystem. Investigations have shown that mentioned area is extremely polluted with mercury which is transported through watersheds to more distant areas and even to the Gulf of Trieste via the Idrijca and Soča-Isonzo rivers [1]. Although mercury is present mainly in inorganic form, it can also make complexes with organic matter which increases its mobility, or can abiotically or biotically transform into organic form. Among organic mercury compounds, methylmercury is the most toxic because it can be easily uptaken to phytoplankton, representing the starting point for its bioaccumulation and biomagnification within the food web. Therefore, there is a clear necessity to remediate this area to prevent or reduce the formation of methylmercury. For this purpose, different *in situ* and *ex situ* methods could be applied, whereby first ones based on sorption processes are more easily feasible [2]. Materials impregnated with sulfur species are most commonly used as mercury-binding sorbents due to a high affinity of sulphur for mercury, forming sparingly soluble HgS ($K_{sp} = 3.9 \cdot 10^{-53}$). It seems that natural zeolites could be good carriers for coating with iron or sulphur species due to their porous structure. Moreover, these materials are environmentally compatible since they are natural constituents of the environment. Therefore, in this paper, natural zeolites and their modified forms, iron-modified zeolite and sulphur-impregnated zeolite, are investigated as sorbents for *in situ* remediation of mercury-contaminated soils in Idrija, Slovenia.

EXPERIMENTAL

Zeolite sample preparation

Natural zeolite (NZ) clinoptilolite was collected from the Zlatokop deposit (Vranjska Banja, Serbia). The sample was milled and sieved, and a particle size fraction of 0.6 to 0.8 mm was separated. The sample was then washed in ultrapure water and dried at 60 °C. Iron-modified zeolite (FeZ) was prepared by treating NZ according to the previously published procedure [3].

Briefly, the NZ is treated separately with a 1 M $Fe(NO_3)_3 \cdot 9H_2O$ at pH = 3.6, followed with 1 M NaOH and 4% $NaNO_3$ solutions. Sulphur-impregnated zeolite (SZ) was prepared by immersing NZ in 1 M Na_2S during 4 hours at 150 °C according to a previously published procedure [4]. Systematic physico-chemical characterization of NZ, FeZ and SZ samples is described in detail in the previously published papers [3,4].

Soil sample preparation

The soil sample was taken in the area of the Idrija mine, at location of the Frbejžene trate. The sample was dried at 35 °C to a constant mass, and then ground in a ceramic mortar, homogenized and sieved through a 2 mm pore size mesh. Thereafter, the sample was additionally pulverized in an agate mill to fine grain size (< 0.075 mm) and stored in a polyethylene bag. Total Hg content in homogenized soil sample was measured after aqua regia digestion for 3h at 160 °C by using Inductively Coupled Plasma Emission Spectrometry (ICP-ES) method.

Leaching experiments according to the Toxicity Characteristic Leaching Procedure

Toxicity Characteristic Leaching Procedure (TCLP) is the most commonly used single extraction test [5]. The TCLP test involves the extraction of harmful substances from a milled sample with an extraction solution of pH values of 2.88 and 4.93 prepared according to the detailed procedure described, by mixing 1 M NaOH and/or 0.1 M glacial acetic acid. A mass of 2.5 g of a mercury-contaminated soil was leached with 50 mL of extraction solutions with and without addition of zeolites in an amount of 10–40% (w/w) relative to the mass of the soil (solid/liquid ratio is 1:20) during 18 h ± 2 h at 30 rpm. After extraction/sorption time, soil suspensions were centrifuged, the liquid phase was separated, and then the concentration of total leached soluble Hg was immediately analyzed by LECO's AMA254 Mercury Analyzer. If the concentration of leached Hg exceeds the limit value prescribed by this method (> 0.2 mg/L), waste material is classified as hazardous.

RESULTS AND DISCUSSION

The total Hg content determined in the soil sample was 1347 mg/kg, indicating that the Idrija mine site is extremely polluted and requires appropriate remediation. Therefore, the addition of different portions (10–40%) of natural or modified zeolites on the reduction of Hg mobility from the soil was compared with the raw soil at pH = 2.88 and pH = 4.93 according to the performed TCLP test.

The results of the TCLP test at two examined pHs for raw soil and treated soil with different amounts of NZ, FeZ or SZ are shown at Figure 1. From Figure 1, higher concentration of total soluble leached Hg from raw soil at pH = 4.93 (3.345 mg/L) compared to pH = 2.88 (2.178 mg/L) is observed. This finding differs from the expected, since usually at lower pH, the solubility of the metal increases. However, in a soil sample, presence of mineral components as well as organic matter, especially humic and fulvic acids, could affect the solubility of bound Hg. Unlike fulvic acids that are soluble under all pH condition, co-precipitation of humic acids at pH < 3 occurs, while increase of pH facilitates their dissolution. At pH = 2.88, dissolution of eventually present soil mineral components should also take place. However, a higher concentration of total leached Hg at pH = 4.93 indicates that dissolution of Hg from humic acids dominates. Therefore, it could be assumed that the binding of Hg to humic substances is predominant in investigated soil. This further suggests that humic acids should be the most responsible for the higher Hg retention by this soil at pH = 2.88.

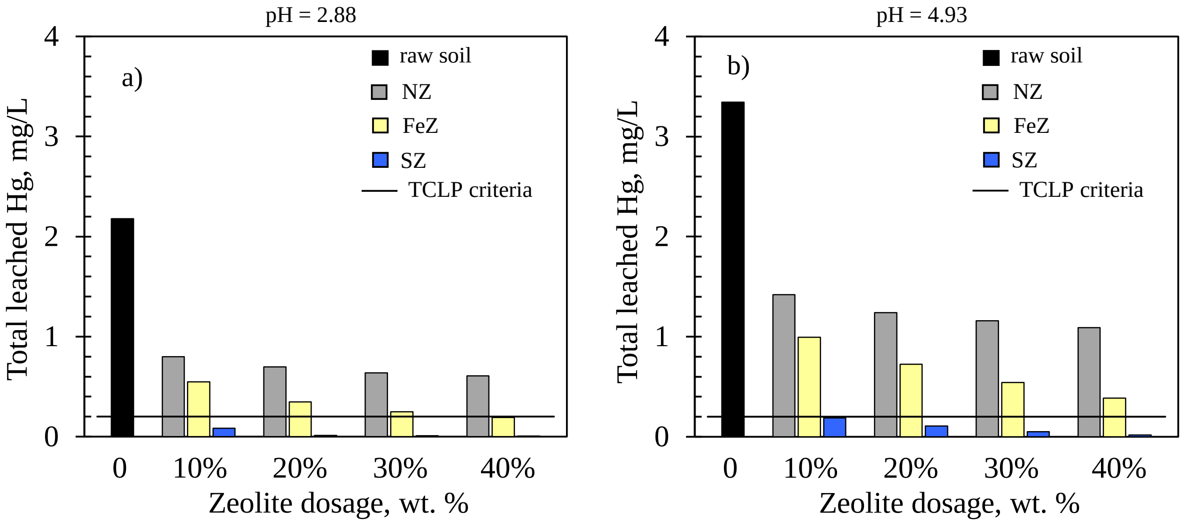

Figure 1. TCLP results of total leached Hg concentration at: a) pH=2.88 and b) pH=4.93.

In soil samples with addition of zeolites, the total soluble leached Hg concentrations not exceed 1.42 mg/L (Fig. 1a and b). With an increase in zeolite dosage, a decrease in total leached Hg is observed, which is more pronounced for the FeZ and especially for the SZ compared to the NZ. The removal efficiency of leached Hg in the zeolite-treated soil samples was calculated according to the Eq. (1) and is shown in Figure 2:

$$\text{Removal efficiency } (\%) = \frac{\left(c_{\text{Hg,raw soil}} - c_{\text{Hg,treatedsoil}}\right)}{c_{\text{Hg,raw soil}}} \cdot 100 \qquad (1)$$

where: $c_{\text{Hg, raw soil}}$ is the concentration of total leached Hg at equilibrium in raw soil sample (mg/L) while $c_{\text{Hg, treated soil}}$ is the concentration of total leached Hg at equilibrium in the soil sample treated with zeolites (mg/L).

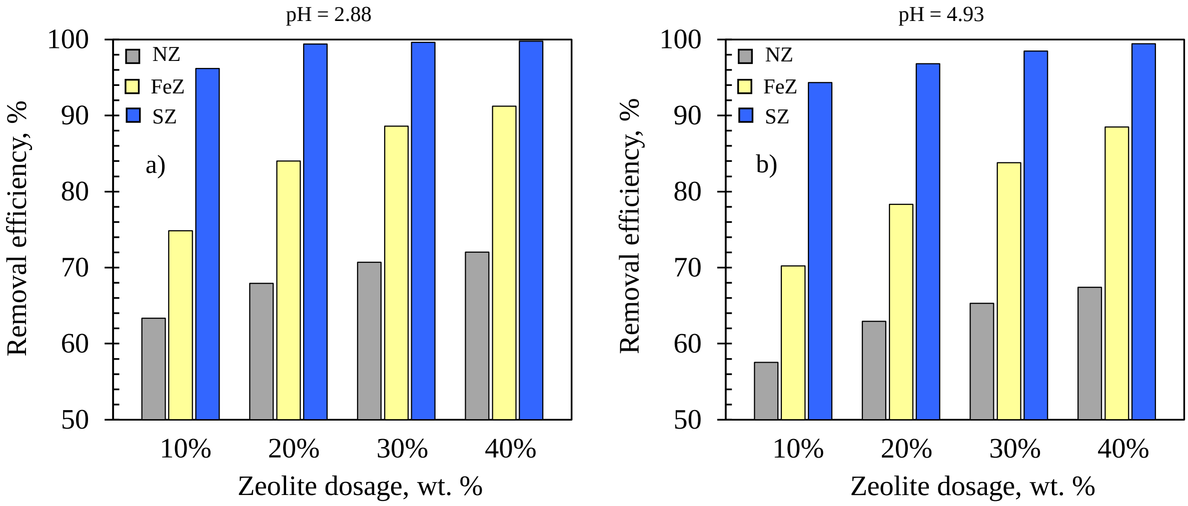

Figure 2. Removal efficiency of leached Hg by addition of different quantities of zeolites at: a) pH=2.88 and b) pH=4.93.

The removal efficiency increased with increasing in zeolite dosage at both pH values. The removal efficiency of leached Hg of 57–72% for NZ, 70–91% for FeZ and over 94% for SZ at both pHs is achieved. The most significant increase in removal efficiency with increasing zeolite dosage was observed for the FeZ, the smallest for the NZ while the SZ sample immediately achieved high efficiency even with the lowest dosage. This behavior could be attributed to the number of available active sites that differ among the zeolite samples due to the modification method.

The sorption of soluble mercury species from soil onto zeolites is presumably very complex and involves multi-sorption mechanism. The most pronounced decrease in total leached Hg in the presence of the SZ can be a consequence of the formation of sparingly soluble HgS on SZ surface, since it is well known that Hg exhibit strong affinity for sulfur species. Moreover, the formation of HgS is desirable since it is the least toxic form of mercury due to its stability, low solubility, relative immobility, which thus reduces the bioavailability of Hg for methylation in deeper soil layers. Furthermore, TCLP requires that the concentration of Hg leached from the waste material is less than 0.2 mg/L (line in Fig. 1a and b). According to the TCLP test, raw soil is an extremely hazardous waste with the concentrations of total leached Hg of 3.345 mg/L at pH = 4.93 and 2.178 mg/L at pH = 2.88. The addition of natural and especially modified zeolites significantly reduces Hg leaching by its stabilization in zeolite. At pH = 2.88, the leached Hg concentrations below the prescribed value of 0.2 mg/L, were achieved by the addition of all dosages of SZ (10–40%), and only with the highest dosage of FeZ (40%). At pH = 4.93 prescribed values was achieved only with SZ even with the smallest dosage of 10%. The stated values were not achieved with the NZ sample at both pHs. The obtained results indicate that SZ is a promising material for *in situ* remediation of contaminated soil, since its minimal dose significantly reduces Hg leaching from contaminated soil at both examined pH values.

CONCLUSION

The results clearly showed that higher pH favors Hg leaching from contaminated soil. Moreover, the tested pH of 4.93 corresponds to the real pH of rainwater, indicating that leaching of Hg in real conditions takes place continuously. Therefore, the need for topsoil remediation is necessary in order to reduce/prevent this phenomenon, and this could be achieved by applying the SZ sample.

ACKNOWLEDGMENT

This work was supported by the bilateral Croatian-Slovenian project "*Natural Modified Sorbents as Materials for Remediation of Mercury Contaminated Environment*" (2020–2023), founded by the Croatian Ministry of Science and Education and Slovenian Research Agency (ARRS) and by the Slovenian Research Agency (ARRS) in the framework of the research program Groundwater and Geochemistry (P1-0020).

REFERENCES

[1] T. Teršič, H. Biester and M. Gosar, *Geoderma*, 2014, **226-227**, 213–222.

[2] L. Wang, D. Hou, Y. Cao, Y. Sik Ok, F.M.G. Tack, J. Rinklebe and D. O'Connor, *Environ. Int.*, 2020, **134**, 105281.

[3] M. Ugrina, N. Vukojević Medvidović and A. Daković, *Desalin. Water Treat.* 2015, **53**, 3557–3569.

[4] M. Ugrina, M. Gaberšek, A. Daković and I. Nuić, *Processes*, 2021, **9**, 217.

[5] USEPA, Method 1311: *Toxicity Characteristic Leaching Procedure*, US Environmental Protection Agency, Washington, D.C., 2004.

Authors Index

We greatly appreciate the support of:

KTF
SVEUČILIŠTE U SPLITU
KEMIJSKO-TEHNOLOŠKI FAKULTET

HGK
1852
HRVATSKA
GOSPODARSKA
KOMORA

Labtim

Jasika d.o.o.
TRGOVINA I ZASTUPANJE

Statue of Grgur Ninski (Bishop Gregory of Nin), Split, sculpted by Ivan Meštrović. Gregory of Nin, 10th-century Croatian bishop who defended the usage of old Croatian language in liturgical services instead of Latin. According to tradition, after rubbing his big toe, your wish will come true…

Front-page: Panoramic view of historic old town of Split (the palace of Diocletian), waterfront, West coast and Marjan hill